LEVEL

AFWL-TR-80-104

ADA104575

PULSED DF LASER EFFECTS STUDY

R. B. Hall
W. E. Maher
D. B. Nichols

The Boeing Aerospace Company
Seattle, WA 98124

DTIC
SEP 25 1981

H

July 1981

Final Report

Approved for public release; distribution unlimited.

AIR FORCE WEAPONS LABORATORY
Air Force Systems Command
Kirtland Air Force Base, NM 87117

81 9 25 028

This final report was prepared by The Boeing Aerospace Company, Seattle, Washington, under Contract F29601-79-C-0003, Job Order 33261002, with the Air Force Weapons Laboratory, Kirtland Air Force Base, New Mexico. Dr R. R. Rudder (AREE) was the Laboratory Project Officer-in-Charge.
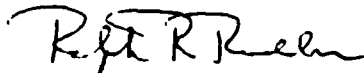
When US Government drawings, specifications, or other data are used for any purpose other than a definitely related Government procurement operation, the Government thereby incurs no responsibility nor any obligation whatsoever, and the fact that the Government may have formulated, furnished, or in any way supplied the said drawings, specifications, or other data is not to be regarded by implication or otherwise, as in any manner licensing the holder or any other person or corporation, or conveying any rights or permission to manufacture, use or sell any patented invention that may in any way be related thereto.

This report has been authored by a contractor of the United States Government. Accordingly, the United States Government retains a nonexclusive, royalty-free license to publish or reproduce the material contained herein, or allow others to do so, for the United States Government purposes.

This report has been reviewed by the Public Affairs Office and is releasable to the National Technical Information Service (NTIS). At NTIS, it will be available to the general public, including foreign nations.

If your address has changed, if you wish to be removed from our mailing list or if your organization no longer employs the addressee. please notify AFWL/AREE/Kirtland AFB, NM 87117, to help us maintain a current mailing list.

This technical report has been reviewed and is approved for publication.

RALPH R. RUDDER, PhD
Project Officer

FOR THE COMMANDER

DONALD A. CAREY
Lt Col   USAF
Chief, Effects & Vulnerability Branch

JOHN A. CARPENTER
Colonel   USAF
Chief, LEAPS Division

SECURITY CLASSIFICATION OF THIS PAGE (When Data Entered)

REPORT DOCUMENTATION PAGE	READ INSTRUCTIONS BEFORE COMPLETING FORM
1. REPORT NUMBER 18 AFWL-TR-80-104	2. GOVT ACCESSION NO. AD-A104 575	3. RECIPIENT'S CATALOG NUMBER

4. TITLE (and Subtitle) PULSED DF LASER EFFECTS STUDY.	5. TYPE OF REPORT & PERIOD COVERED Final Report.
	6. PERFORMING ORG. REPORT NUMBER

7. AUTHOR(s) R. B. Hall W. E. Maher D. B. Nichols	8. CONTRACT OR GRANT NUMBER(s) F29601-79-C-0003

9. PERFORMING ORGANIZATION NAME AND ADDRESS The Boeing Aerospace Company Seattle, WA 98124	10. PROGRAM ELEMENT, PROJECT, TASK AREA & WORK UNIT NUMBERS 33269 002/62601F

11. CONTROLLING OFFICE NAME AND ADDRESS Air Force Weapons Laboratory (AREE) Kirtland Air Force Base, NM 87117	12. REPORT DATE July 1981
	13. NUMBER OF PAGES 104

14. MONITORING AGENCY NAME & ADDRESS(if different from Controlling Office)	15. SECURITY CLASS. (of this report) UNCLASSIFIED
	15a. DECLASSIFICATION/DOWNGRADING SCHEDULE

16. DISTRIBUTION STATEMENT (of this Report)

Approved for public release; distribution unlimited.

17. DISTRIBUTION STATEMENT (of the abstract entered in Block 20, if different from Report)

18. SUPPLEMENTARY NOTES

19. KEY WORDS (Continue on reverse side if necessary and identify by block number)

Pulsed DF Laser	Impulse Damage
Laser Effects	Mass Loss
Laser Interaction	Aluminum
Thermal Coupling	Fiberglass

20. ABSTRACT (Continue on reverse side if necessary and identify by block number)

This study of DF laser interaction with materials investigated the amount of energy coupled to targets. Large focal spot dimensions were obtained with the Boeing photo-initiated 50-1 pulsed chemical laser with a stable resonator. Effects experiments emphasized metallic targets, especially aluminum. The single pulse coupling results yielded absorbed fluence values greater than those obtained with comparable energies at 10.6 μm wavelength. Ambient pressure and angle of incidence were varied.

Continued

DD FORM 1473
1 JAN 73

Item 20 continued.

Research results also showed multiple-pulse effect at DF wavelength. Multiple-pulse thermal coupling experiments with aluminum demonstrated that, after 10 shots on the same spot, the coupled fluence per pulse doubled. Because of target melting and vaporization, both the intrinsic absorptivity and the plasma enhanced coupled fluence of succeeding pulses is greatly increased. In general, the multiple pulse effect is intensity-dependent and is small at either low or high intensities.

Energy deposition was tested for uniformity by measuring the rises in temperature at five locations within the focal spot with an array of thermo-couples. The coupled fluence was obtained as a function of incident fluence for a pulse length of 2.0 μs as well as the normal 3.5 μs pulse length. Mass loss and impulse measurements in Cordopreg fiberglass targets were made. Optimized CO_2 and DF laser coupling were compared, and a repetitively-pulsed scenario was analyzed.

Accession For

NTIS GRA&I

DTIC TAB

Unannounced

Justification

By

Distribution/

Availability Codes

Dist   Avail and/or   Special

A

PREFACE

CONTENTS

ILLUSTRATIONS

ILLUSTRATIONS (continued)

ILLUSTRATIONS (continued)

ILLUSTRATIONS (continued)

I. INTRODUCTION

The main goal of this study of DF laser interaction with materials was to determine the amount of energy coupled to targets. Interest centered on effects on metallic targets. Effects experiments with aluminum materials received the greatest overall effort. The single-pulse coupling results yield absorbed fluence values greater than that obtained, with comparable energies, at 10.6 μm wavelength. In addition, however, this study has shown a significant multiple-pulse effect at DF wavelength. Because of target melting and vaporization both the intrinsic absorptivity and the plasma-enhanced coupled fluence of succeeding pulses is greatly increased.

Section II describes the Boeing photoinitiated 50 liter pulsed chemical laser (PHOCL-50) (Ref. 1) and the beam profile obtained with a stable resonator. With this configuration large focal spot dimensions are obtained. This capability to make large spots in the far field with a beam path length which would fit within the laboratory was an important asset.

Section III describes the results of single-pulse coupling experiments to metallic targets. Coupled fluence results are given for several targets, including aluminum (2024-T3), titanium (6A14V), steel (4130), and stainless steel (304). The coupled fluence is determined for pressures of 1.0, 0.5, 0.25 atm and at 0.1 torr. Because of the practical importance of large angles of incidence, the coupled fluence was determined as a function of θ for θ as large as 87.5°.

---

1. M. F. Weisbach, V. R. Buonadonna, C. J. Artura, W. B. Shepherd, J. E. Shrader, and J. D. McClure (Boeing Aerospace Co.), and R. L. Taylor, P. F. Lewis, and J. F. Cronin (PSI), PHOCL-50: A 50 Liter Photoinitiated Chemical Laser, Boeing Document D180-24898-1,1978.

These measurements were all obtained with single thermocouples that determine the absorbed fluence. To define the value of this kind of central measurement, the energy deposition was tested for uniformity by measuring the rises in temperature at five locations with an array of thermocouples.

For an investigation of some aspects of the pulse-length dependence of absorbed fluence, an experimental set-up was designed in which the incident laser pulse could be cut off at an arbitrary time after the beginning of the pulse. With this set-up, the coupled fluence was obtained as a function of incident fluence for a pulse length of 2.0 µs compared to the normal 3.5 µs pulse length.

Section IV describes the results of multiple-pulse thermal coupling experiments with aluminum. After 10 shots on the same spot, it was found that the coupled fluence per pulse doubled. Further measurements at several incident irradiances show that the multiple-pulse effect is decreased at both low and excessively high intensities.

An analysis of these results indicates that combined low and high irradiance strategy may be useful in a repetitively-pulsed scenario. Under these conditions the overall efficiency with which energy is absorbed at a metallic target can be increased by first emitting high irradiance pulses (to roughen the surface) followed by sub-plasma threshold pulses.

Section V develops an optimization model for single pulse laser interactions. Using this approach the wavelength and pulse length were varied and comparisons of optimized CO_2 and optimized DF laser coupling were made.

The Appendix describes the results of mass loss and impulse measurements (at DF wavelength) on Cordopreg fiberglass targets.

10

II. DESCRIPTION OF LASER FACILITIES

2.1 THE PHOCL-50 LASER

To obtain large focal spot dimensions with laboratory-sized focussing optics, PHOCL-50 was redesigned to operate with a stable resonator. The laser itself, shown in Figure 1, has an overall length between mirrors of 3.5 m with a cross-section of 20 x 20 cm. In particular, a 4 mrad full beam divergence was planned so that large spot sizes could be obtained with mirrors of moderate focal length. The conditions which were desired included $\hat{\tau} = \frac{ct_p}{r}$ (c is sound speed in plasma, t_p is pulse length, r is laser focal spot radius) values near or below unity in order to perform experiments in a regime with large spot interactions. (Ref. 2) This would allow scaling to scenarios of interest to the Air Force. With pulse length at half maximum of about 3 μs and a plasma sound speed of about 6.6×10^5 cm s^{-1} (Ref. 3), a focal spot radius of 2.0 cm would give $\hat{\tau} = 1$. This led to a reasonable laboratory setup, with a 10 m focal length mirror appropriate for the desired spot size given the divergence anticipated.

The new resonator design was also intended to best utilize the lower gain per unit length present in DF as compared with hydrogen fluoride (HF). The resonator built for these experiments used a four-fold stable resonator configuration using a long radius-of-curvature mirror and a flat output coupler as shown in Figure 2. There was a high sensitivity to alignment settings

---

2. A.N. Pirri, R.G. Root, and P.K.S. Wu, Analytical Laser/Material Interaction Investigations, PSI TR-104, 1977.

3. R.G. Root, A.N. Pirri, P.S.K. Wu, and H. Gelman, Analysis of Laser-Target Interaction, PSI TR-170, 1979.
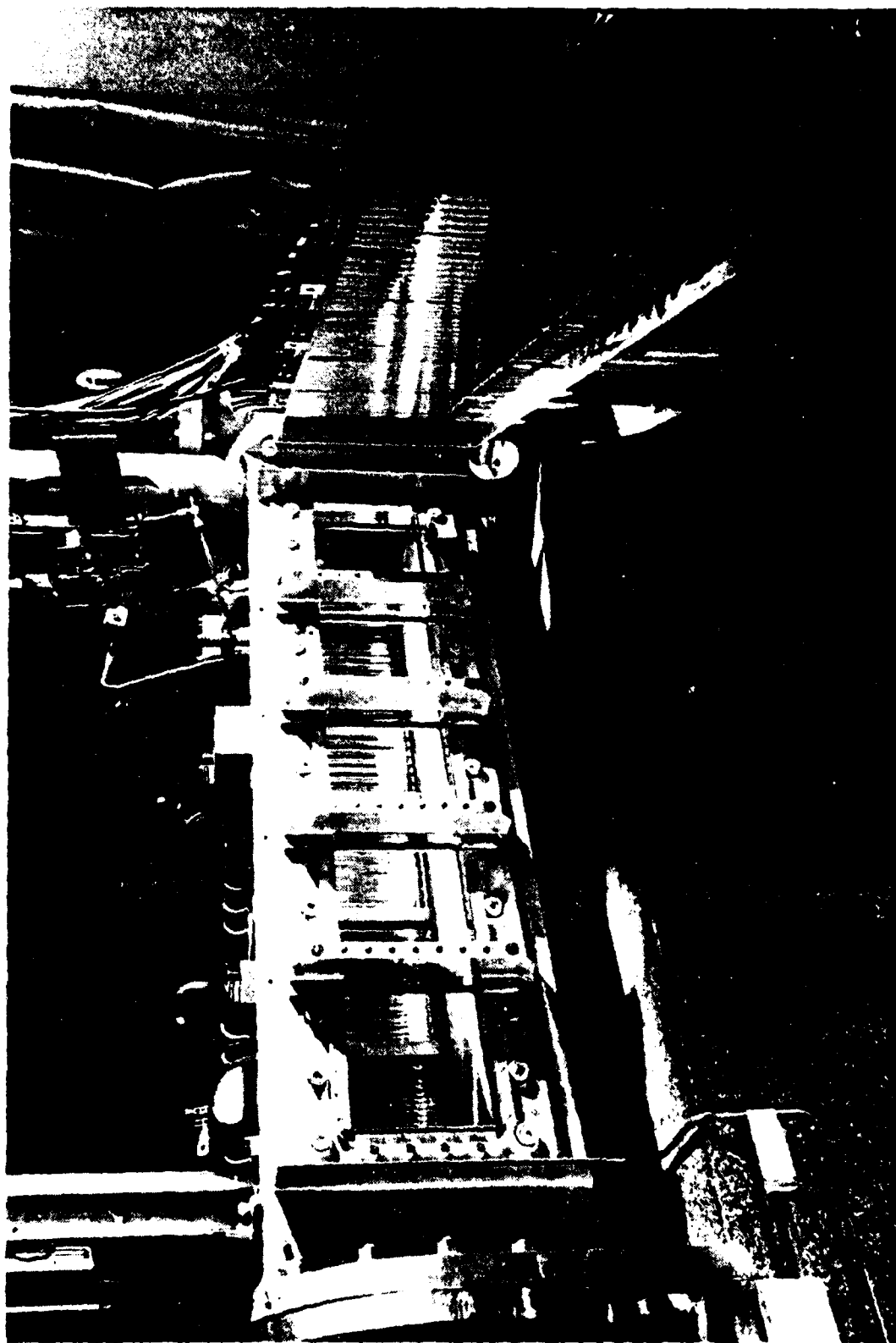
Figure 1. PHOCL-50 laser with one flashbank open showing reactor space.

FLAT
MIRRORS

REACTOR CONTAINING LASER GASES
D_2, F_2, He or Ar, and O_2

FLASH LAMPS

WINDOWS FOR FLASH LAMPS' UV LIGHT

SAPPHIRE OUTPUT COUPLER

25 m FOCAL LENGTH CONCAVE MIRROR

GATE
VALVES
SEPARATING
REACTOR FROM
OPTICS SECTIONS

OPTICS SECTIONS
PROTECTED BY
BUFFER GAS

OUTPUT BEAM

FLAT
MIRRORS
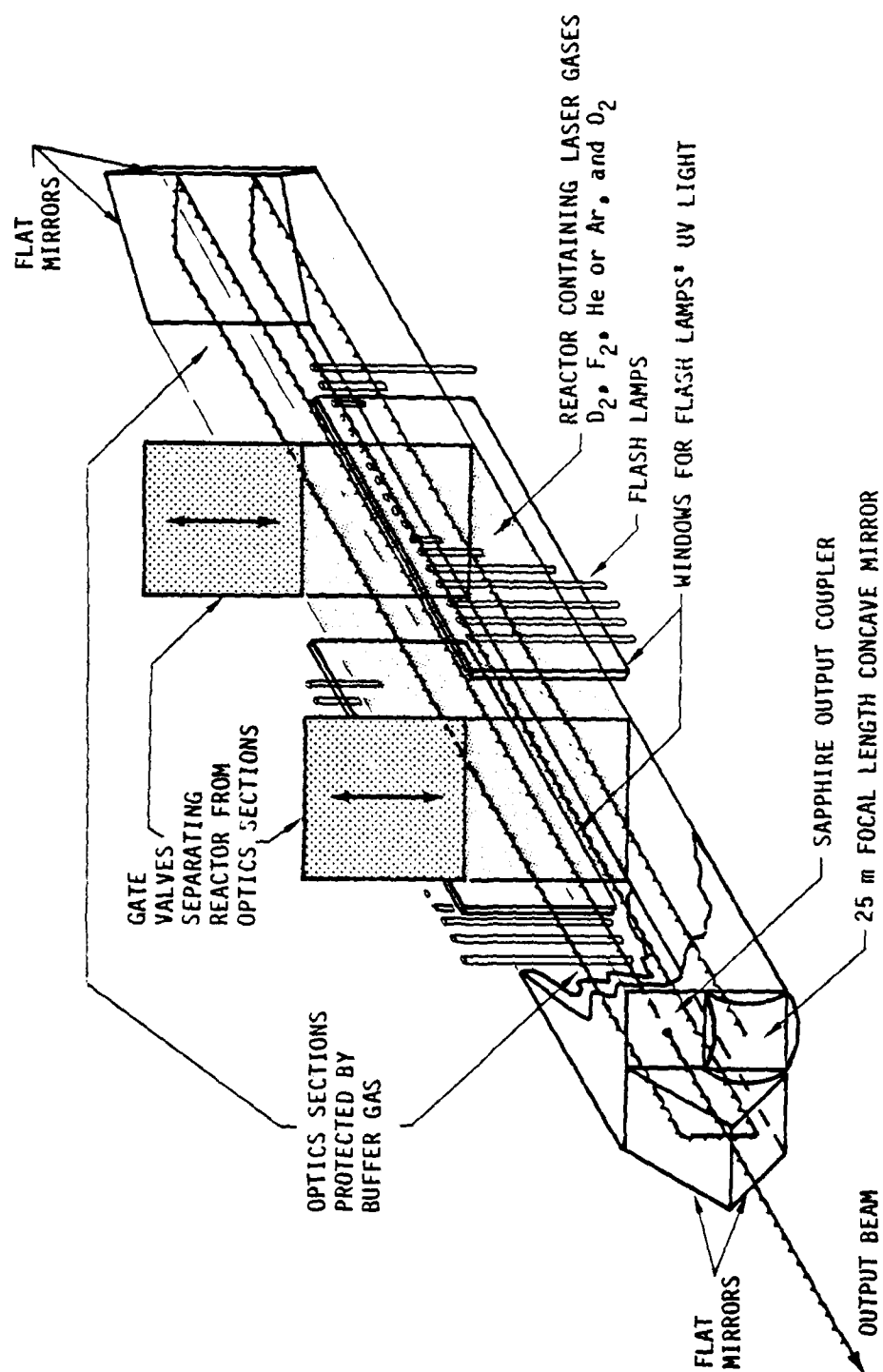
Figure 2. Schematic view of PHOCL-50 laser.

13

because of the 14 m total distance between the ends of the resonator and because of the 13 reflections encountered in one transit of the cavity.

Uncoated copper mirrors furnished by AFWL were used for this resonator and were located in the end sections. Before each shot these were prefilled with static-pressure-matched buffer gas. These buffered sections were opened to the reactor just before the reaction was initiated, so that buffer gas stayed between the mirrors and the reactive gases. However, over the 8 mo. in which these experiments took place, the mirrors became severely tarnished and the output energy dropped.

Normally, laser operation was maintained at 2% D_2, 10% F_2, 86.5% diluent, and 1.5% O_2. Diluents were either Ar or He, with slightly higher energy for He. Usually the 40 reaction-initiating flash lamps were operated at 35 kV. Under constant operating conditions, the laser pulse length stayed almost constant with only about 10% of the shots having abnormalities. In addition, the output energy, for these constant operating conditions, stayed nearly constant over any short term period.

The output coupler was a square wedge of sapphire with a 0.3 mrad. angle and a square 10 cm wide clear aperture. In the near field the spatial intensity profile was almost uniform, as seen in Figure 3. Beam profile measurements which were made at greater and greater distances from the laser revealed that the divergence was more pronounced in the vertical direction with noticeable hot areas in the form of parallel horizontal lines above the main beam. This was probably due to reflections from the top and bottom of the reactor supporting parasitic modes.

14

Figure 3. PHOCL-50 near-field intensity pattern.

2.2 BEAM DIAGNOSTICS

Figure 4 shows the diagnostic set-up for determining both energy and pulse shape. At the output of the laser but before diagnostics, the energy can be attenuated by insertion of attenuators in the beam. For the experiments reported here, up to 90% attenuation of the laser output was obtained with very little change in the temporal or spatial properties of the beam. Attenuators were Teflon and Tedlar sheets.

After leaving the laser and attenuation region the laser beam was incident on an optical wedge. The entire beam passed through this wedge and the reflections produced at the front and rear surfaces were each 2.4% of the incident beam. One of these reflections was sent to the calorimeter and the fixed reflection fraction provided a means to measure the total beam energy. As indicated in Figure 4, the pulse shape was determined by use of a Gold-doped Germanium detector placed to observe scattering from the calorimeter or by use of the second reflected beam from the wedge.

To do focal plane diagnostics at fluence levels low enough to be usable, it was necessary to use a much weaker representation of the high energy main beam. As shown in Figure 5 the second surface reflection from the wedge made these diagnostic measurements possible. As indicated, a flat copper mirror directed this beam to the same focussing optics as used in the laser effects experiments. This flat mirror was located to the rear and side of the wedge from where the beam could be reflected past the outside of the wedge, hitting the same spot on the focussing mirror as the main beam, but with a difference in incident angle. The two beams reflected from it and were focussed at points separated by the initial angular difference. In this way a focal spot identical to, but 1/40 as intense as the main beam focal spot

16
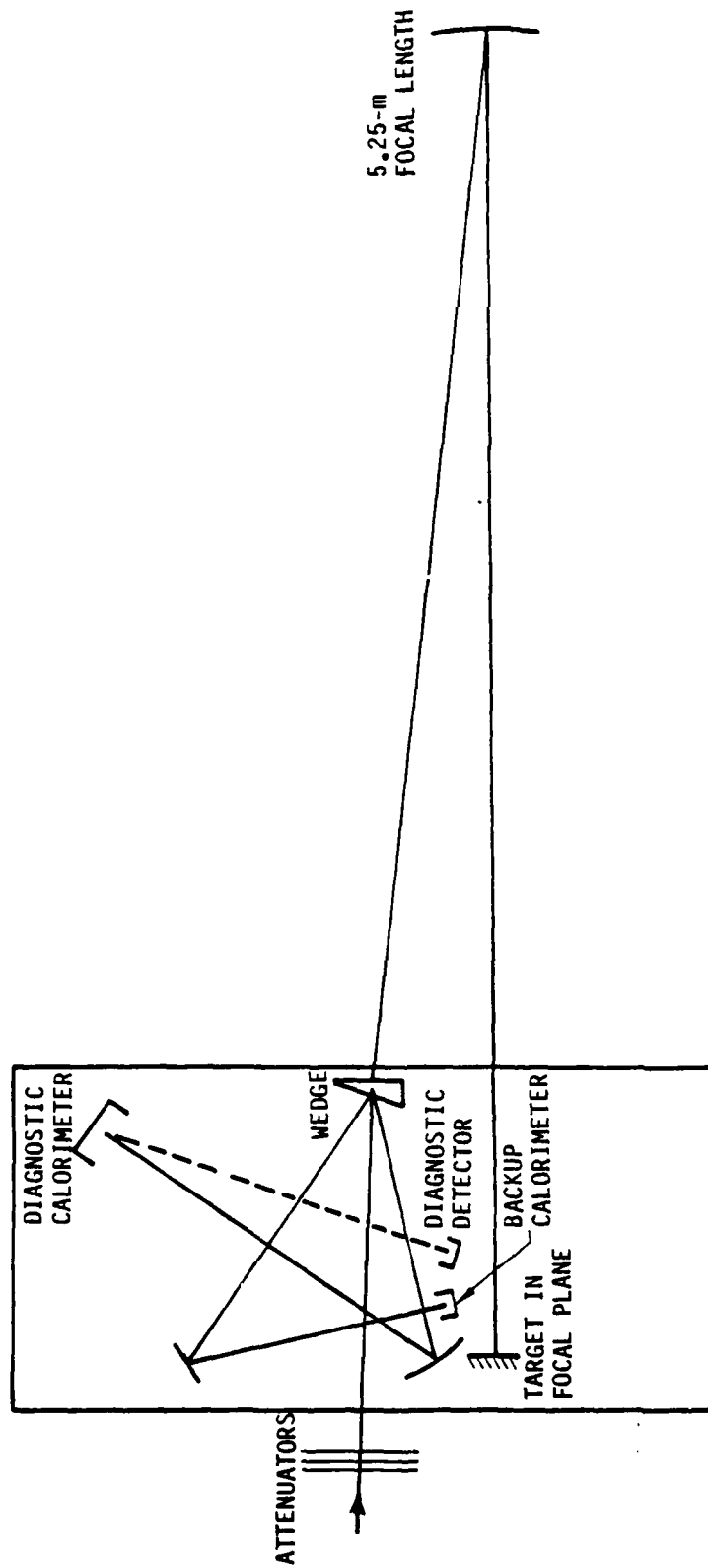
Figure 4. Schematic diagram of laser beam diagnostics arrangement.

17

5.25-m FOCAL LENGTH

DIAGNOSTIC CALORIMETER

WEDGE

DIAGNOSTIC DETECTOR

TARGET IN FOCAL PLANE

DIAGNOSTIC POSITION IN FOCAL PLANE

ATTENUATORS
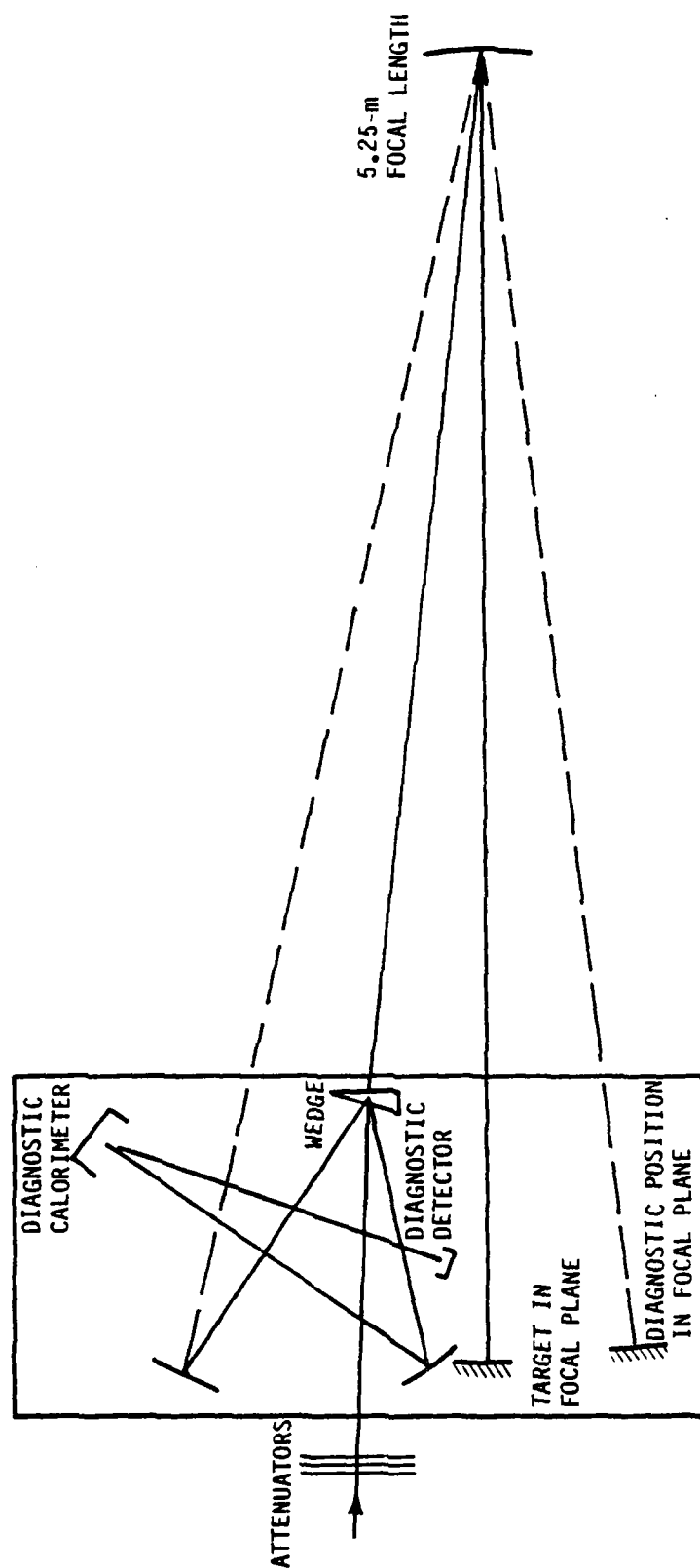
Figure 5. Alternate beam arrangements.

18

was formed which could be scanned or otherwise utilized. The carbon block calorimeters built by Boeing (Ref. 1) were susceptible to damage above 8-10 J/cm^2 so this less intense focal spot allowed operation at 5 J/cm^2 with a square 2 cm wide spot.

The front and rear reflections from the wedge were both used at times for calorimetric measurements. Calorimeters were placed at both beams for calorimeter comparisons using two carbon calorimeters or either one for comparison with the Scientech Model 364 and to reduce total uncertainties. Ordinarily only one beam was used for calorimetric data. Care was taken to avoid geometrical arrangements where any portion of the original beam which was scattered by the attenuation sheets could reach a calorimeter.

A gold-doped germanium infrared (IR) detector was positioned where it could see the front of one calorimeter and so that some of the diffusely reflected beam power from the calorimeter absorption surface would reach it. This provided a good temporal signal as it averaged over the entire beam. A record of the pulse shape was kept for every laser pulse used in an experimental measurement. An average pulse shape is shown in Figure 6. The triangular approximation given in Figure 6 has a full width at half maximum (FWHM) of 3.60 µs with a temporal peak occurring at 1.45 µs. Occasionally (in 10% of all shots), pulses were found to deviate significantly from the average pulses. These abnormal shots varied in pulse width from 2.6 to 4.6 µs and with spikes less than 1.4 times the nominal maximum power.

All of the laser effects experiments were done in the far-field (focal plane) of spherical focusing mirrors. The focused beam was off-axis by no more than 7° (i.e., there was a 14° angle between the beam arriving at the
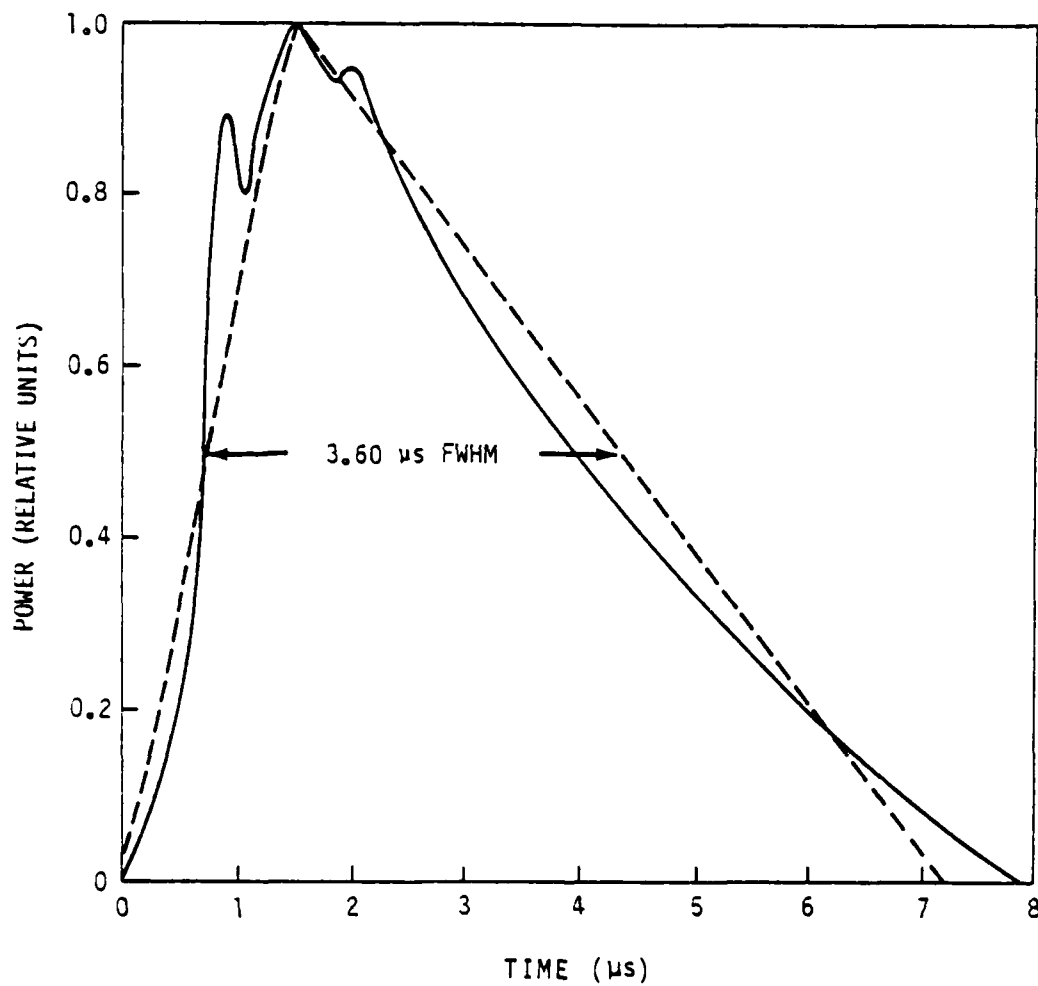
Figure 6. Temporal shape of DF laser beam.

focusing mirror and the beam leaving it). By keeping the attenuator sheets, vacuum chamber windows, and targets slightly tilted, reflective feedback into the laser was reduced along with the generation of any spurious modes. A coaxial HeNe laser beam followed the path of the DF beam to provide easy preliminary alignment. Dispersion in the wedge, however, created an angular divergence between the two beams for which corrections were necessary. Actual DF laser beam burn patterns were used, in fact, for final alignment.

The far-field spatial profile was determined by measurements on the focal spot from a 5.25 m focal length mirror. This was done using the beam reflected from the front of the wedge so that the resulting incident fluence was low and no damage to calorimeters would occur. Spatial profile information obtained in this way is applicable for any far-field spot in the main beam. The incident fluence distribution was first sampled using a series of concentric square apertures with sides 2, 3, 4, and 5 cm. The results of these measurements are shown in Figure 7 where one notes only a small amount of energy was found outside of the 4 cm boundary.

A more detailed fluence profile was obtained by scanning in both the vertical and horizontal directions using a 3 mm diameter aperture and bore-sighted calorimeter combination. The results, shown in Figure 8, were obtained using the laboratory arrangement shown in Figure 9. At the left rear of the table was the scanning calorimeter with the 3 mm aperture. The high energy beam with this focal length had an approximate focal area of 4 cm^2 and the damaged spot was observed on a 10 x 10 cm aluminum target. The detector observed the diagnostic calorimeter (not visible) in order to determine pulse shape.
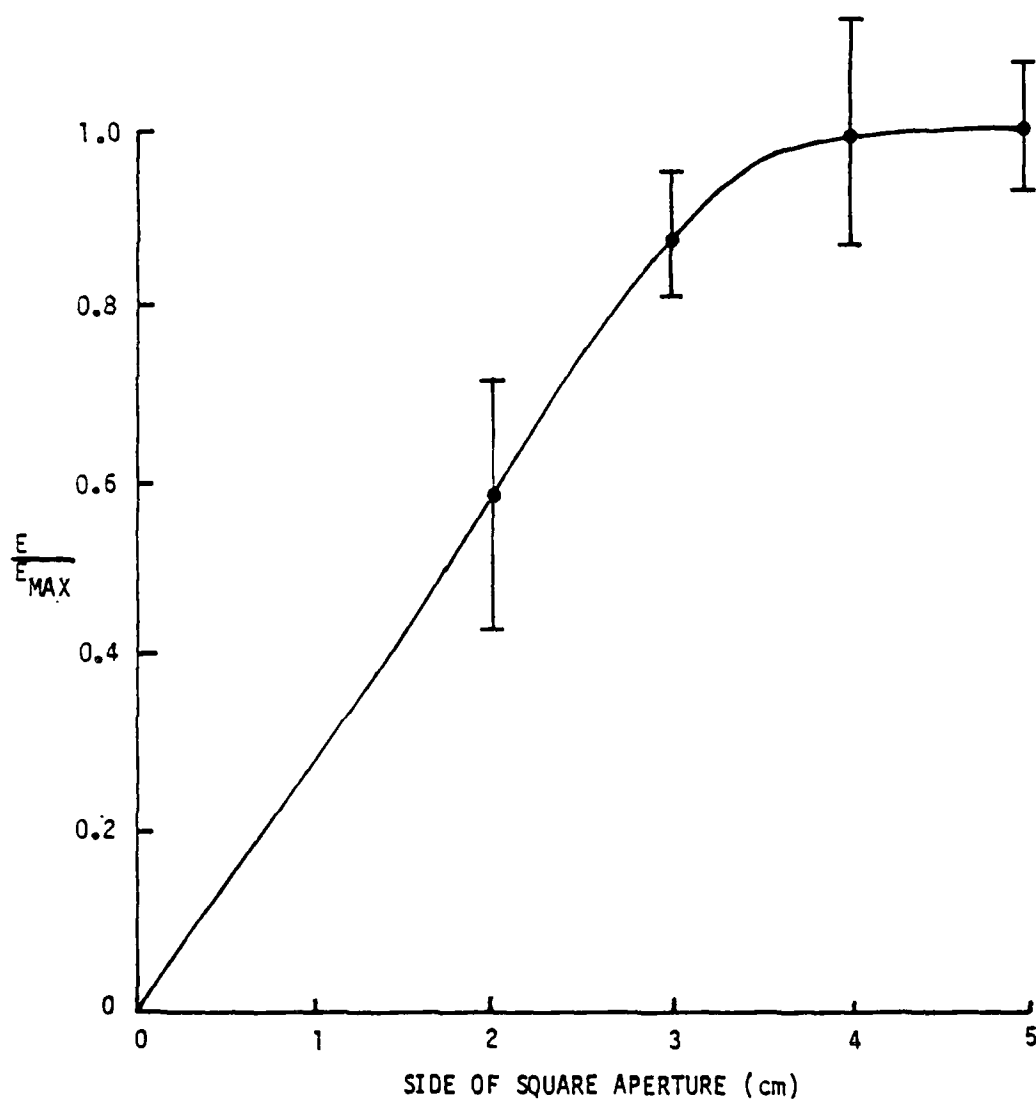
Figure 7. Measurements of focused beam profiles using nested square apertures.
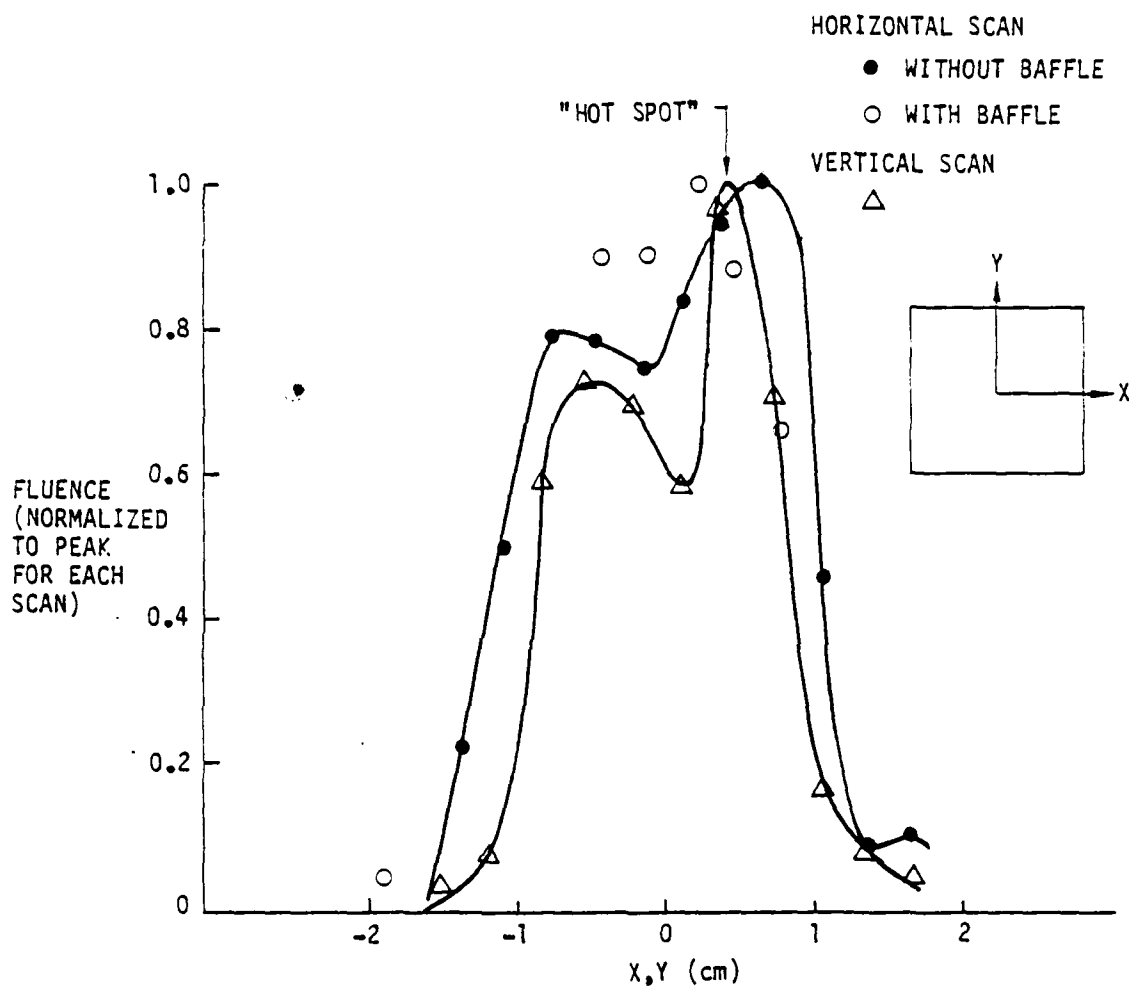
Figure 8. Profiles of focused beam using vertical and horizontal scans.

SCANNING CALORIMETER

LASER TARGET

DETECTOR

LASER OUTPUT WINDOW

FLAT
COPPER
MIRROR

OPTICAL
WEDGE
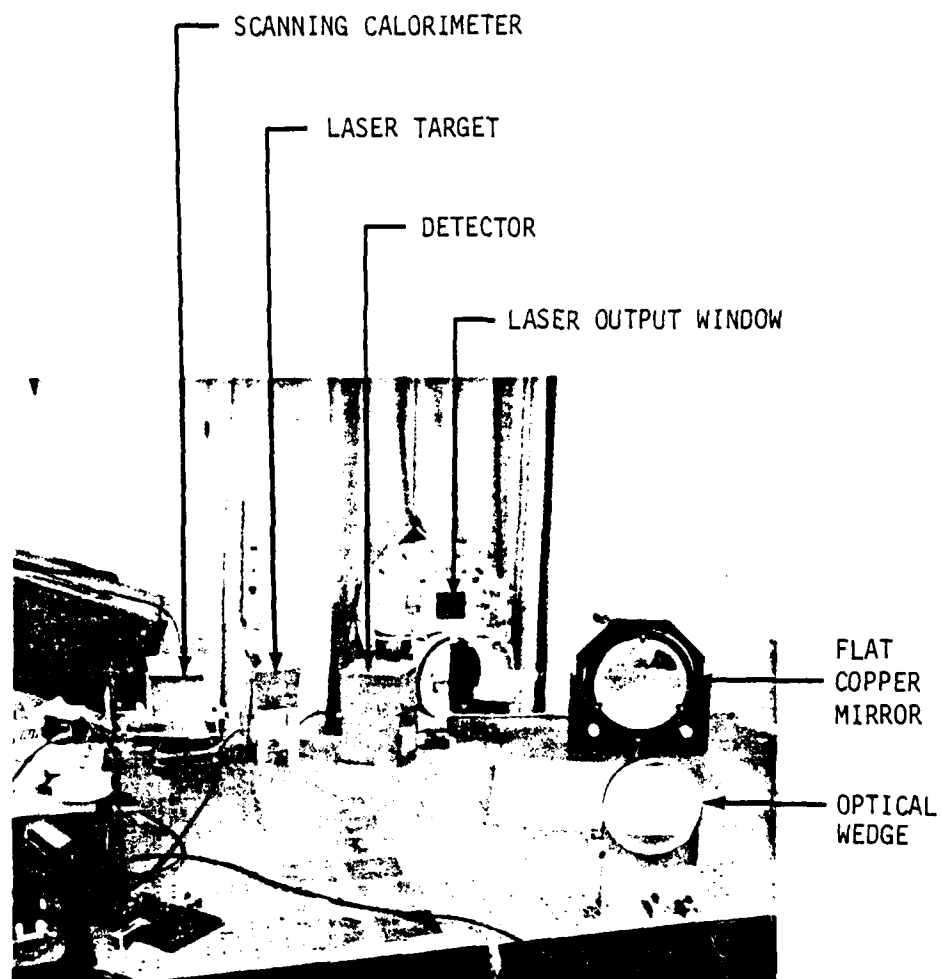
Figure 9. Diagnostic setup.

The measured spatial fluence profiles given in Figure 9 can be closely approximated by the functions

$$e = \frac{1}{1 + (\frac{x}{x_0})^6} \qquad (1)$$

where x_0 = 1.032 cm and 0.86 cm respectively for the horizontal and vertical directions. Equation 1, shown in Figure 10, is adequate for defining the fluence profile; however, it does not (obviously) indicate the hot spot visible in the measured data. The definite integrals of the functions of Equation 1 in the x and y directions are 2.16 cm and 1.79 cm respectively.

The amount of energy outside of any boundary may be calculated from Equation 1. For a square aperture 2 cm on a side one finds almost exactly one percent of the total energy defined by Equation 1 lies outside that area. However, the "nested aperture" measurement indicated in Figure 8 indicates that 44 percent of the total incident energy was found outside the 2 cm aperture boundary. This indicates that a large fraction of the total energy existed as a low-intensity "halo" surrounding the central high intensity zone. Taking this correction into account leads to

$$e_0 = 0.146 \text{ J/cm}^2 \qquad (2)$$

for f = 5.25 meters. For a mirror of arbitrary focal length one obtains

$$e_0 = 4.02 \text{ E/f}^2 \text{ J/cm}^2 \qquad (3)$$

The level indicated in Equation 3 is the average peak value of the fluence. However, the "hot spot" shown in Figure 3 has a magnitude 1.67 times greater.

(HORIZONTAL)

$$e = 1 / \left(1 + \left[\frac{x}{1.032}\right]^6\right)$$

(VERTICAL)

$$e = 1 / \left(1 + \left[\frac{y}{.86}\right]^6\right)$$
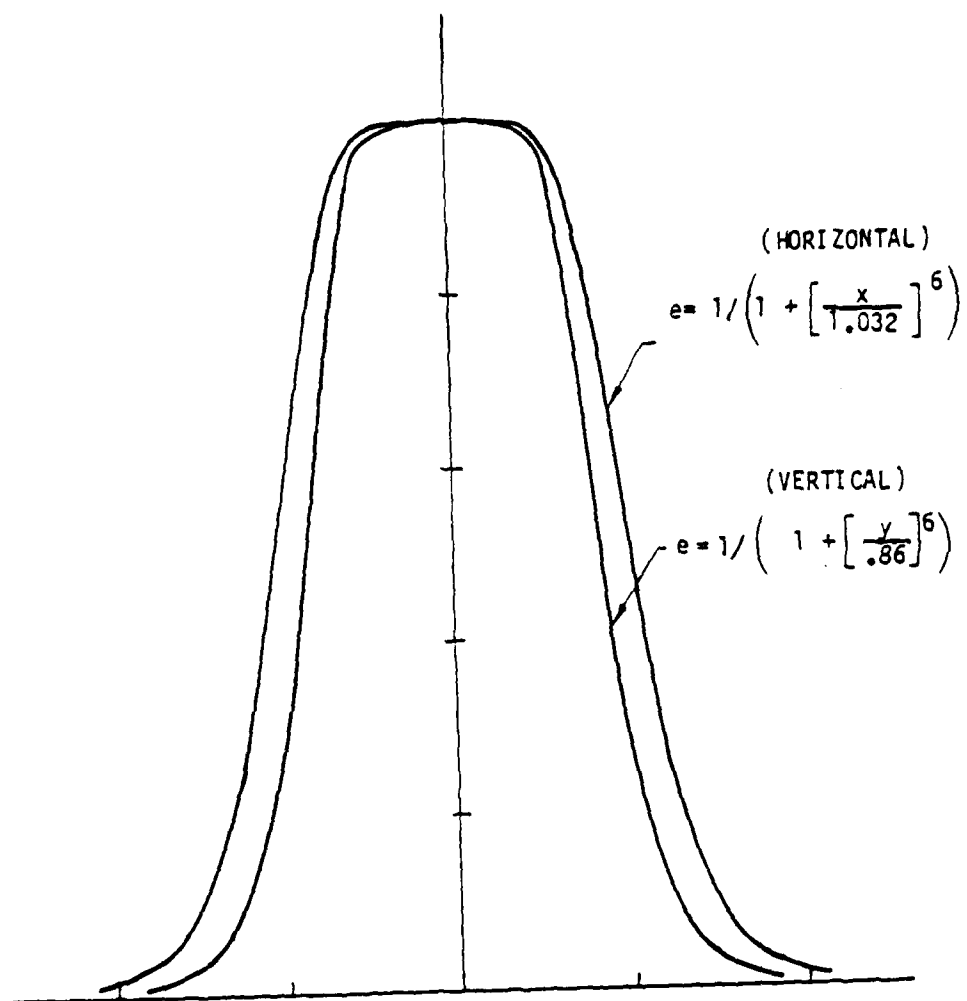
Figure 10. Analytic approximations to focused beam profiles.

26

At high intensities, the damage profiles on an aluminum target can aid in determining the details of the incident fluence distribution. These constant fluence contours were obtained from a large number of laser shots with varying incident laser energy. The resulting relative fluence profile for the 5.25 m focal length mirror is shown in Figure 11. Although an exact comparison with scans of Figure 8 isn't possible, there are strong similarities. However, quantitative comparisons between the hot spot at the top of the pattern and the center spot with this data has a ratio of 1/.85 = 1.18, not nearly as large as 1.67 ratio seen in the data in Figure 8.

Similar burn patterns were used to check the depth of field of the focal spot. Using an approximation, one can estimate that the axial distance x from the focal spot to a point where the spot area has increased by 10% is $x = 0.46 \frac{f^2 \Delta\theta}{d}$ where the focal length is F, the full beam divergence angle is $\Delta\theta$, and the beam diameter at the focusing mirror is d. For a laser beam of 4.8 mrad divergence and a focal length of 5.25 m one finds x = 60 cm. Burn measurements on aluminum began to show deviations from the nominal focal spot burn pattern at about 50 cm from the focal spot. Since all measured focal distances were determined with better than 1 cm accuracy, the above fluence estimates are valid for all reported data.
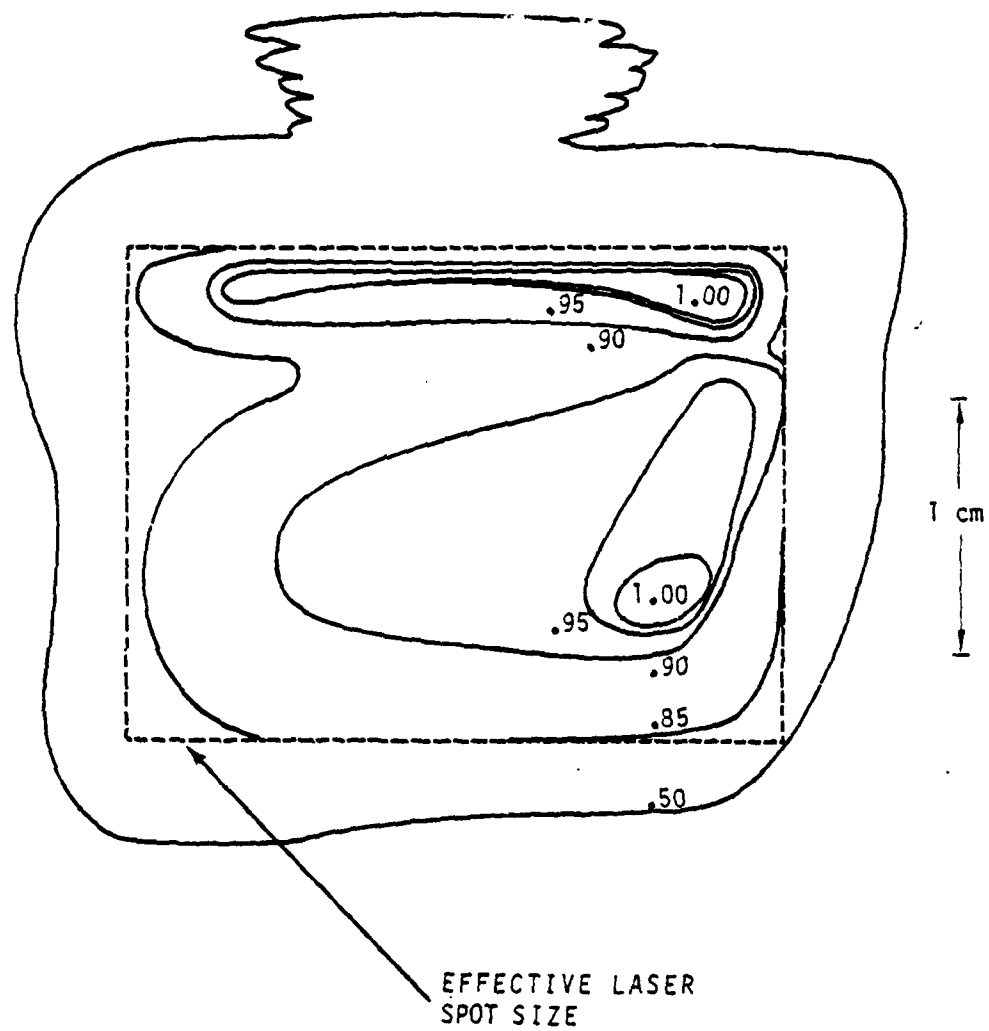
Figure 11. Normalized intensity contours from damage measurements on aluminum.

III. SINGLE-PULSE COUPLING TO METALS

As is well known, the fraction of incident laser energy actually absorbed at a metal surface depends on many parameters. At low intensities the intrinsic coupling coefficient depends on target material characteristics including resistivity and surface preparation. At CO_2 wavelengths, for example, the absorptivity of as-received aluminum alloy is approximately 2%. At 3.8 μm wavelength the corresponding absorptivity is between 5 and 8%. If 2024-T3 aluminum alloy target materials is roughened the measured absorptivity can reach 30%.

At high intensities, non-linear interactions can dominate the observed coupling. These effects occur because of: (1) temperature-dependent resistivities, (2) vaporization and melting of the target, and (3) plasma-related effects. The present study concentrates on the metal target coupling that occurs in air when plasmas are generated at the target surface. Surface defects, which are vaporized with relatively low fluence, can cause an air breakdown to occur near the target surface. At atmospheric pressure, the laser absorption length in the resulting plasma is small. Since nearly all the incident energy is absorbed in the resulting plasma, a laser-supported absorption wave is produced. This wave travels away from the target surface with a plasma temperature about 40,000 K. (Ref. 3). The resulting emission of radiation at UV and visible wavelengths is great enough to produce a large amount of coupled energy to the target surface. This occurs because of the much greater absorptivity at these wavelengths than at the laser wavelength itself. On the other hand, targets which have a high intrinsic absorptivity

(such as steel, glass, fiberglass, and titanium) may have about the same plasma coupling as the targets of low intrinsic absorptivity, and hence not have any big increase in coupling when a plasma is present.

In this section, the single pulse coupling of metal targets is presented. In all cases, the fluence at the center of the focussed laser beam is determined by measuring the peak temperature rise of the target iself. From this temperature and the known heat capacity of the target, the absorbed fluence is found. The chromel-alumel thermocouple with a wire diameter of 0.0127 cm were spotwelded to the target and produced a voltage rise time of several milliseconds which depends both on the thermocouple and target thickness. Under these conditions, the effect of radial heat flow in the target is negligible and the thermocouple voltage is proportional to the local absorbed fluence.

In all single-pulse experiments, the targets were cleaned with methanol and only one shot per target was used. Sets of targets prepared in this way produced data for plasma ignition time and for coupled fluence with considerable scatter for nearly identical laser pulses.

3.1 SINGLE-PULSE COUPLING TO 2024-T3 ALUMINUM AT ONE ATMOSPHERE

With the experimental configuration shown in Figure 5, a series of coupling measurements was made with varying laser energy delivered to the target. With a mirror focal length of 5.25 m, the "average" peak fluence at the focus is defined by Equation 2.

The corresponding temporal peak in the spatially averaged peak irradiance q_M occurs at a time of 1.45 μs after the laser start.

$$q_M = \frac{e_o}{t_p} \text{ W/cm}^2 \tag{4}$$

where the pulse length (FWHM) is 3.60 μs.

At this pulse length and with an approximate spot of 1 cm radius the value of $\hat{\tau}$ is

$$\hat{\tau} = \frac{ct_p}{r} \approx 2.4 \tag{5}$$

where c is the plasma sound speed of approximately 6.6×10^5 cm/s. The value of $\hat{\tau}$ defines the reduction in plasma coupling caused by radial expansion which, in turn, leads to a reduction in plasma temperature. Figure 12 shows the thermal coupling data (absorbed fluence) plotted as a function of the total incident energy or the incident fluence (on the upper scale).

The data are divided into two regions. For average peak fluences below about 36 J/cm^2 the absorbed fluence is proportional to the incident fluence with an absorptivity of 6.8%. For $e_i > 36$ J/cm^2, plasma is ignited and there is an abrupt increase in coupled energy to the target. For greater incident fluences, however, the absorbed fluence actually decreases gradually. In fact, the coupled energy crosses the intrinsic coupling slope at about 68 J/cm^2 incident fluence.

With the scatter of data actually observed, no clearly-defined curve of absorbed fluence versus laser energy can be defined. The straight-line curve is drawn merely to guide the eye. The curve labeled "Model Results" uses the analytical results of Section V. In that section an irradiance and pulse-length dependent plasma absorptivity is defined which assumes ignition always

31
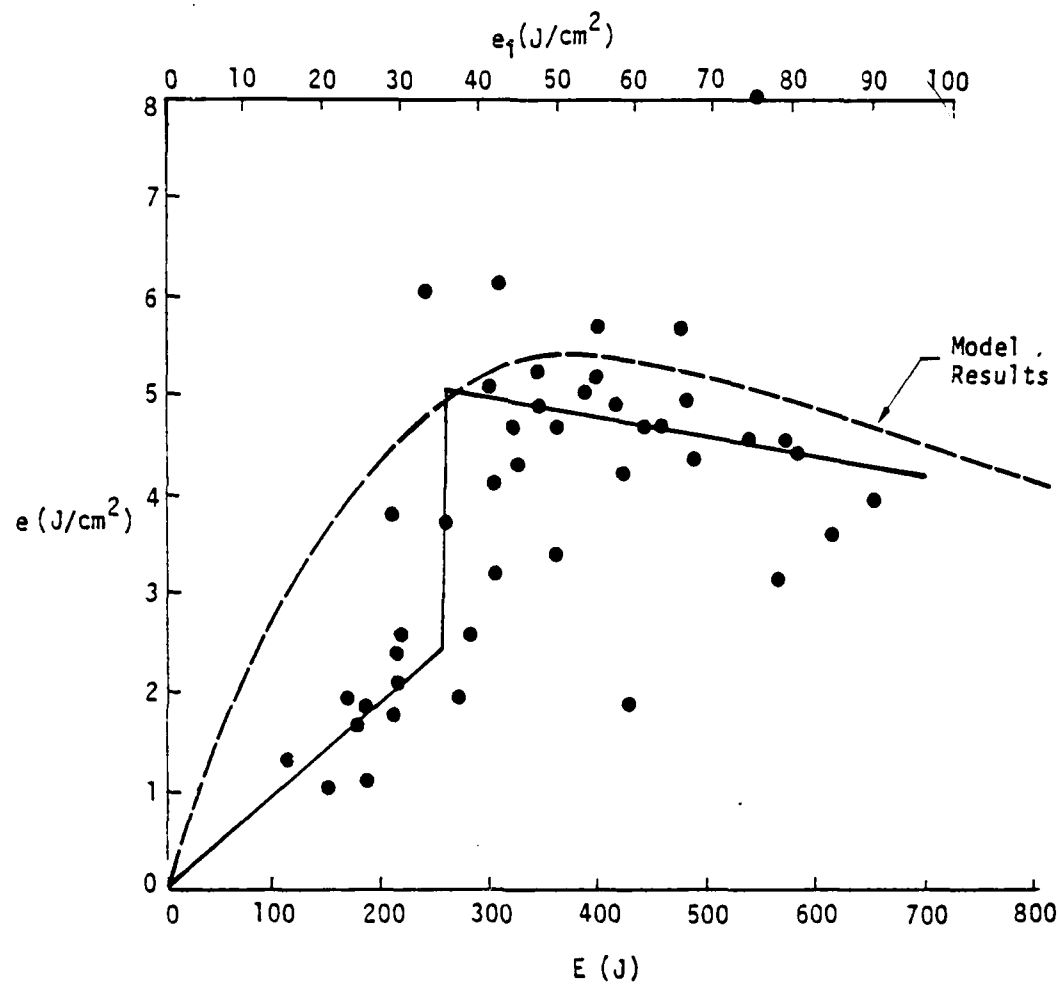
Figure 12. Thermal coupling of 2024-T3 aluminum to single DF pulses for
τ = 2.4, α_0 = 0.068.

occurs. The analytical curve below plasma threshold obviously has no
significance.

The data of Figure 12 were taken with a mirror of focal length 5.25 m.
A second set of data were taken with a 2.9 m focal length mirror which
produced a spot with a side of 1.1 cm. Since the corresponding value of $\hat{r}$ is
4.2 (instead of 2.4), the model in Section V predicts that the coupled fluence,
for a given incident fluence, would be reduced by approximately two-thirds
However, as shown by the results of Figure 13, there appears to be little
difference in the absorbed fluence. Part of this discrepancy may be due to
the data scatter. Part of this discrepancy may be from the model prediction
which is likely to be in error for large $\hat{r}$. Even further complications in
analyzing these data arise from the fact that the effective pulse length
is not constant. It is longer at high incident fluence where ignition occurs
promptly and shorter near threshold where late ignition occurs. This can be
seen in Figure 14 where the plasma ignition time is plotted versus the incident
laser energy for the same conditions as Figure 12 (5.25 m focal length).

Near threshold, the plasma is ignited only late in the pulse. From this
data, an empirical equation describing the ignition time delay (as measured
from the laser peak power) can be written as

$$t_d = 7.2 \exp \left(-\sqrt{\frac{e-40.2}{13.1}} \right) - 1.5 \ \mu s \qquad (6)$$

where e is the incident fluence indicated by Equation 2.

From this data and the pulse shape of Figure 6, one can determine the
fluence coupled to the target before plasma ignition. This result is
indicated in Figure 15 where it is obvious, by comparison to Figure 12, that

33
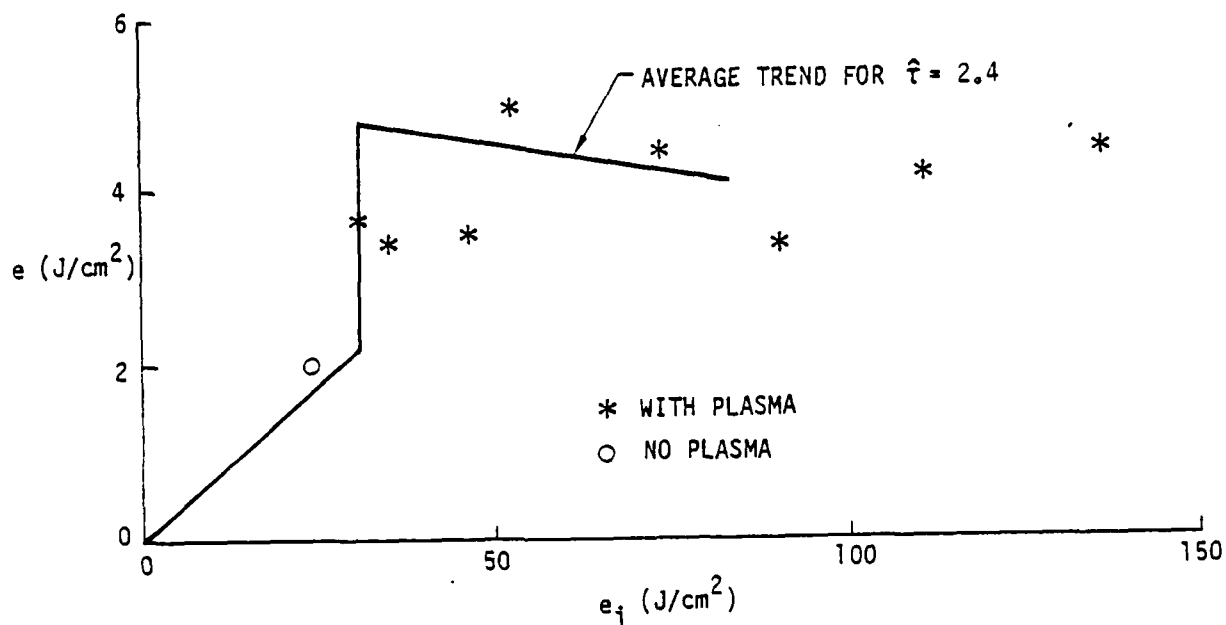
Figure 13. Thermal coupling of 2024-T3 aluminum to single DF pulses for $\hat{\tau}$ = 4.2 compared to average trend for $\hat{\tau}$ = 2.4.

34
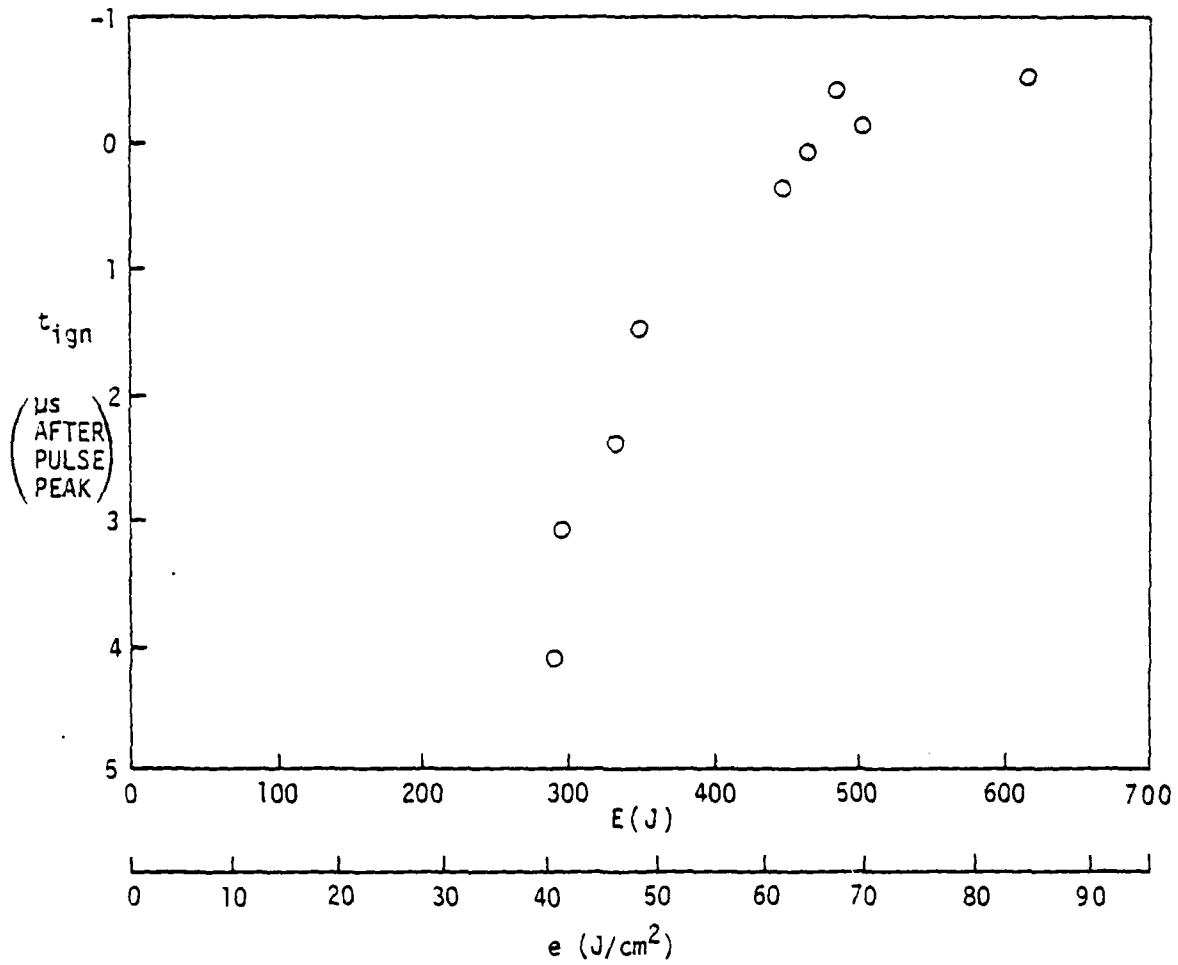
Figure 14. Plasma ignition time as a function of energy in DF laser beam incident on 2024-T3 aluminum.
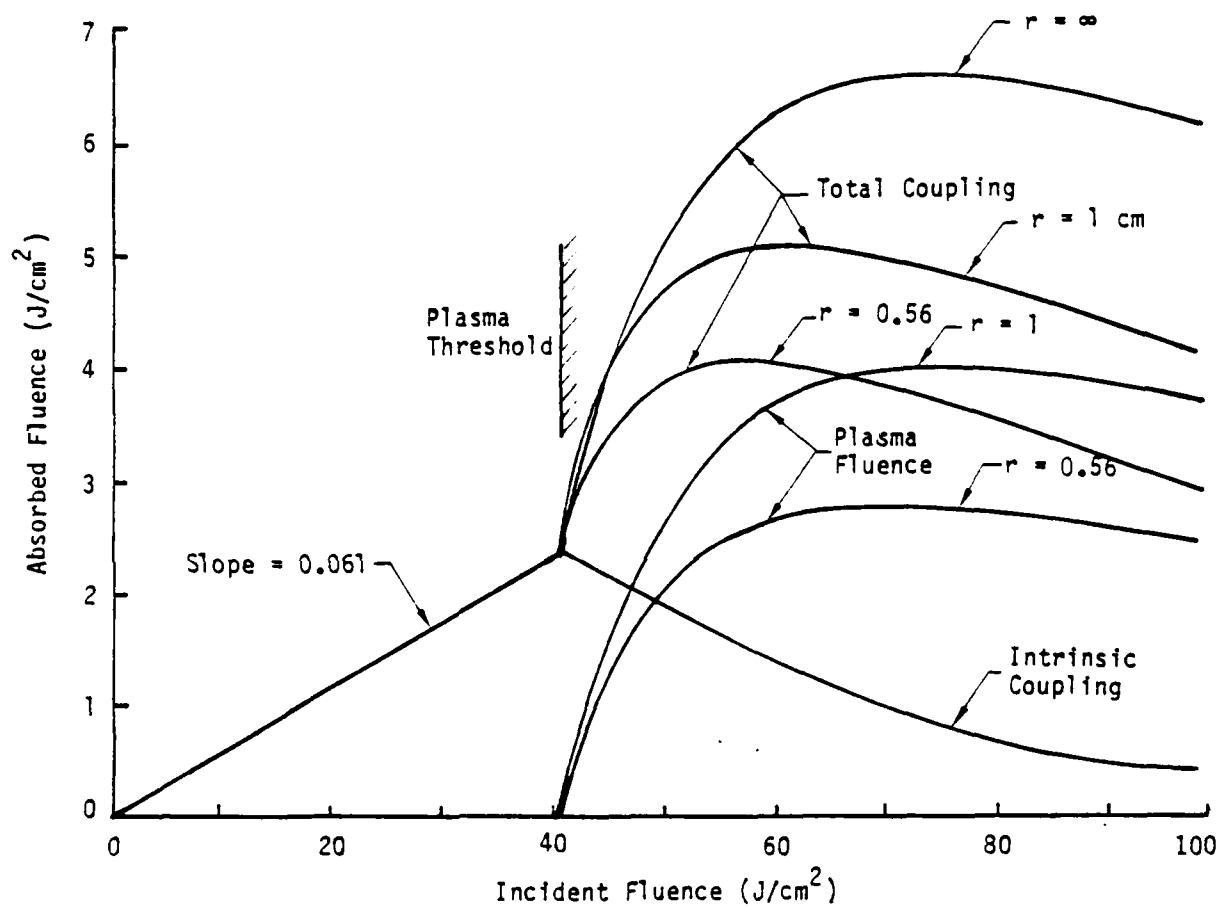
Figure 15. Intrinsic and plasma-enhanced coupling. The intrinsic coupling behavior is determined from the time to ignition. The plasma fluence is calculated from the model results using the reduced pulse length.

the intrinsically coupled fluence is an important part of the total coupled fluence. Also shown on Figure 15 is the total expected coupled fluence for three spot radii of 0.56, 1.0, and ∞ cm. The plasma fluence was computed using the plasma absorptivity discussed in Section V.

$$\alpha_p = 0.33 \; f(\hat{t}) \; \exp - (q/q^\star) \tag{7}$$

where

$$q^\star = \frac{10}{r^{1/4}} \; \sqrt{\frac{10.6}{\lambda}} \; MW/cm^2 \tag{8}$$

This α_o coefficient of 0.33 must be understood as applying to a formulation of α_p where the intrinsic part is not included. In Section V the value used for α_o is 0.40 because it is for the entire coupling. The effective pulse length t_{peff} was chosen as the FWHM of the incident laser pulse after the plasma was ignited. Thus, for $t_d > 0$,

$$t_{peff} = (7.2 - t_d)/2 \quad . \tag{9}$$

and the value of laser irradiance q used in Equation 7 occurs at the time of ignition. For $t_d < 0$

$$t_{peff} = (2.85 - t_d)/2 \tag{10}$$

and q is the maximum value of irradiance defined by Equation 4.

The coefficient 0.33 in Equation 7 was chosen empirically in order to best match the data of Figure 12.

Using the above definition of effective pulse length, the plasma coupled fluence near threshold is very small. In addition, the predicted difference

37

between the nominal $\hat{\tau}$ = 2.4 and 4.2 data of Figures 12 and 13 are only different by 20%. This occurs because the effective plasma pulse lengths are considerably shorter than that of the incident pulse. The total coupled fluence is given by

$$e_{abs} = 0.061\ e_i + \alpha_p\ (e-e_i) \qquad (11)$$

At the present time, a full comparison of Equation 7 with experiment is incomplete. As will be noted, from comparison with Section IV, there is a discrepancy between the numerical coefficients defining the coupling coefficients. The results of Section V include the coupled fluence originating over the entire pulse width. Equation 7 and the results shown in Figure 15 include, separately, the coupled fluences below and above plasma threshold.

3.2 SINGLE-PULSE COUPLING TO 2024-T3 ALUMINUM AT REDUCED PRESSURE

Because of possible applications at high altitude, a limited number of coupling experiments was carried out at low pressures. The targets were placed inside a 1-m diameter vacuum chamber with a 6.4 cm diam. CaF_2 window as shown in Figure 16. In order to compare this low-pressure data with the 1-atm data of Figures 13 and 14 an additional energy calibration was carried out on the vacuum side of the window.

The results for both 0.5 and 0.25 atm are essentially identical and are shown in Figure 17 for a spot diameter of 1.1 cm. These results are hardly distinguishable from the 1-atm coupling results of Figure 13. The lowest pressure at which thermal coupling to aluminum alloy targets was measured was 100 μm (the air density is a factor of 7600 times less than atmospheric). At this low pressure, the atmosphere appears to play a greatly reduced role in
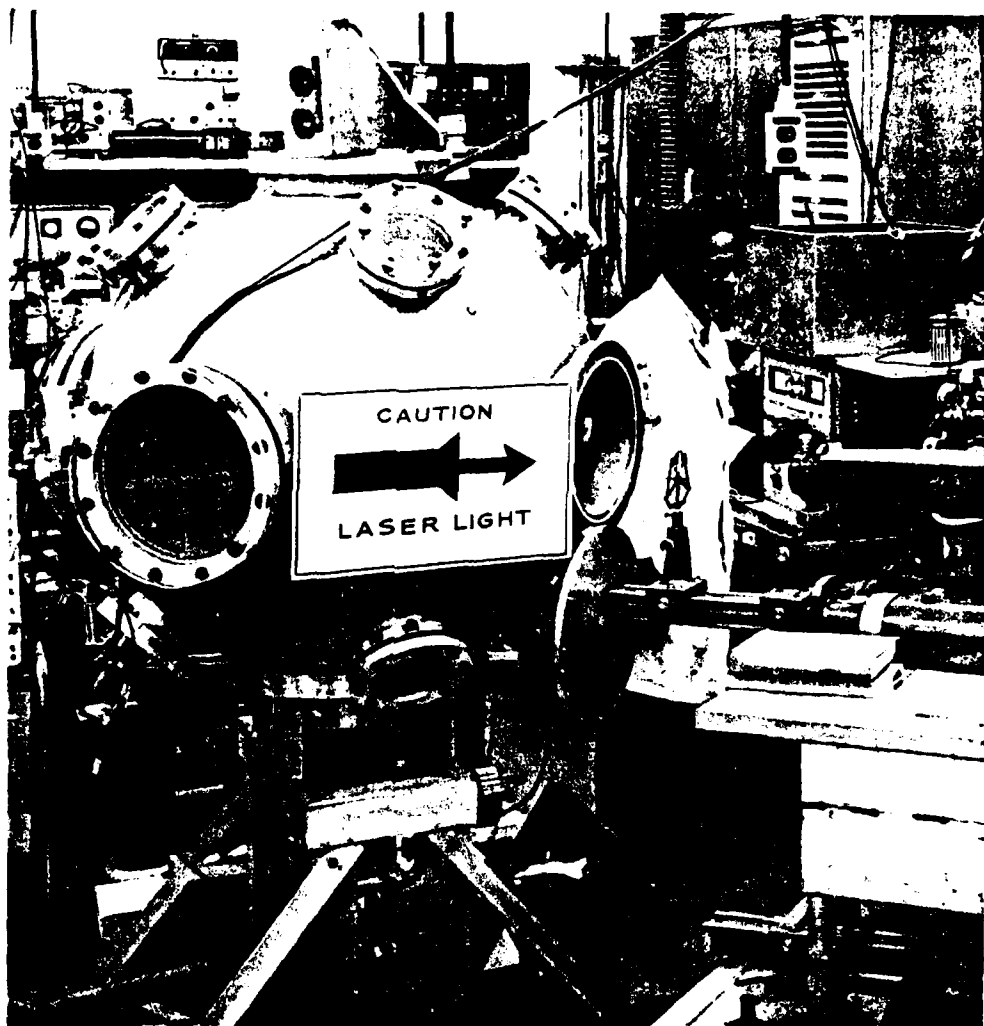
Figure 16. 1-m diameter vacuum sphere.
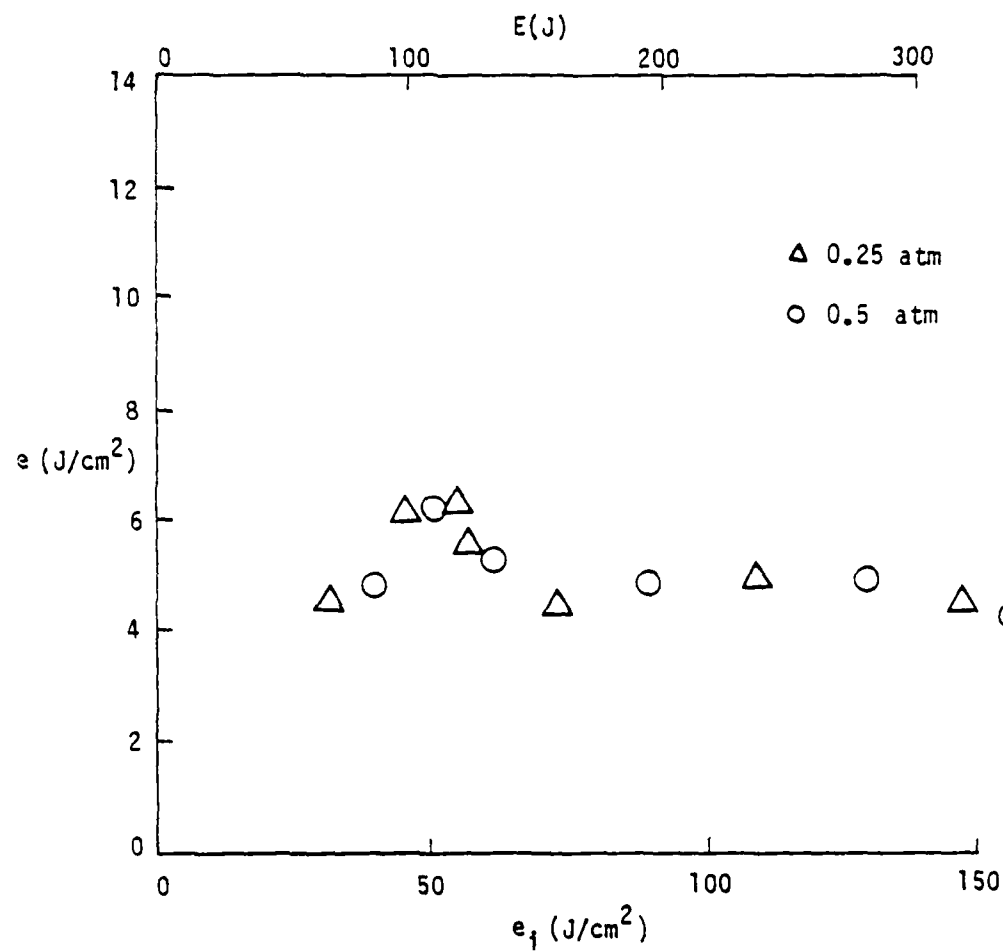
Figure 17. Single pulse thermal coupling to 2024-T3 aluminum at 0.5 and 0.25 atm.

coupling energy to the target as can be seen in Figure 18. For this pulse
length, the coupling still appears to be intrinsic below 40 J/cm^2 while
above this value there is an abrupt rise in coupling coefficient. It is
believed that this overall dependence of coupled energy on incident fluence
could be explained by the temperature dependence of the intrinsic coupling
coefficient taking into account vaporization losses.

The average behavior of the coupled fluence as a function of incident
fluence is shown in Figure 19 for the various values of atmospheric pressure.
Only the low pressure coupling at 0.1 torr is unique in that the absorbed
fluence continually increases, at least to the highest irradiances utilized.
Near atmospheric pressure ($p > \frac{1}{4}$ atm), however the coupled fluence gradually
decreases as the incident irradiance increases.

3.3 SINGLE-PULSE COUPLING TO OTHER METALS

To evaluate the role of high-reflectivity targets such as aluminum in
defining coupling behavior a series of measurements was made with lower
reflectivity metals. The results for titanium (6A14V), steel (4130), and
stainless steel (304) are given in Figures 20, 21, and 22, respectively. The
value of α_0 indicated on each figure is an average value of absorptivity as
deduced from the straight-line approximation to the results. It is of interest
to note that, not only is the coupling coefficient higher than for aluminum
(as expected), but that its magnitude does not change drastically when plasma
is ignited. Those experiments where plasma was ignited are shown by asterisks.
This characteristic is especially evident with titanium (see Fig. 20)
where the near-straight-line trend continues for an incident fluence 2.5
times that required for plasma ignition.
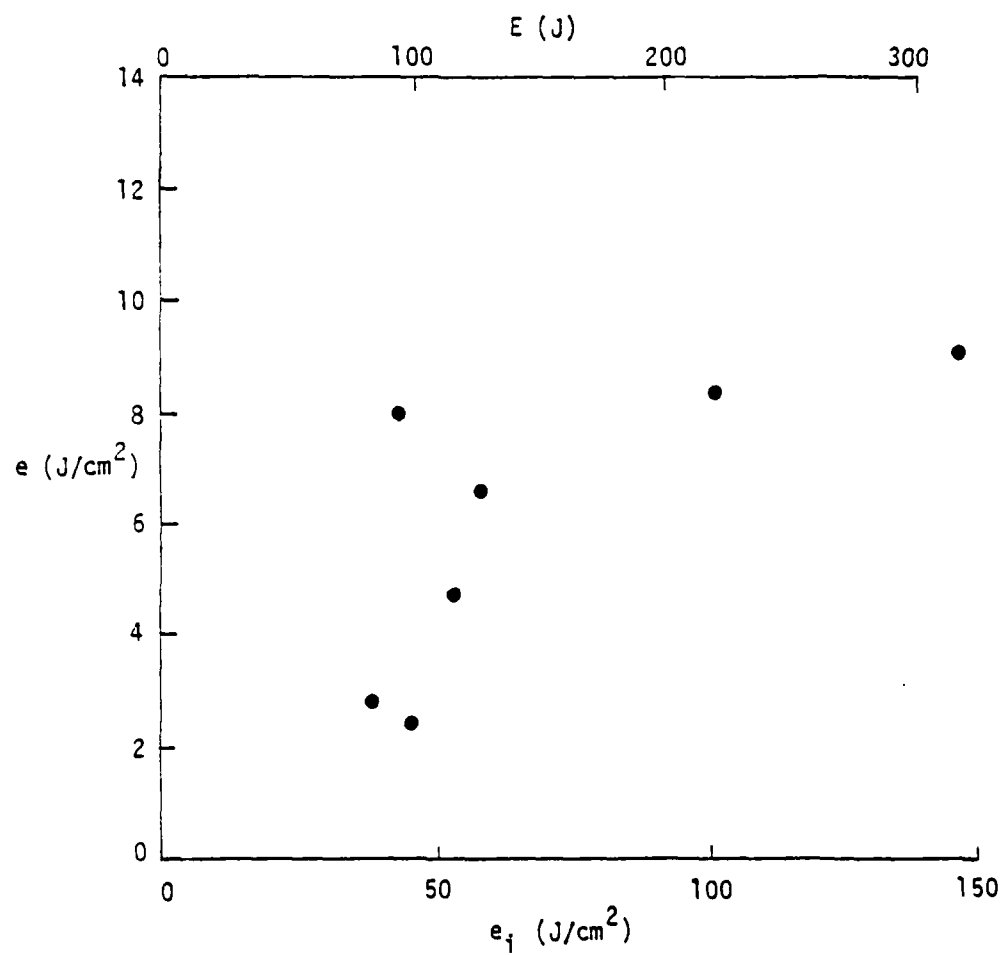
Figure 18. Single pulse thermal coupling to 2024-T3 aluminum at P of 100 μm.
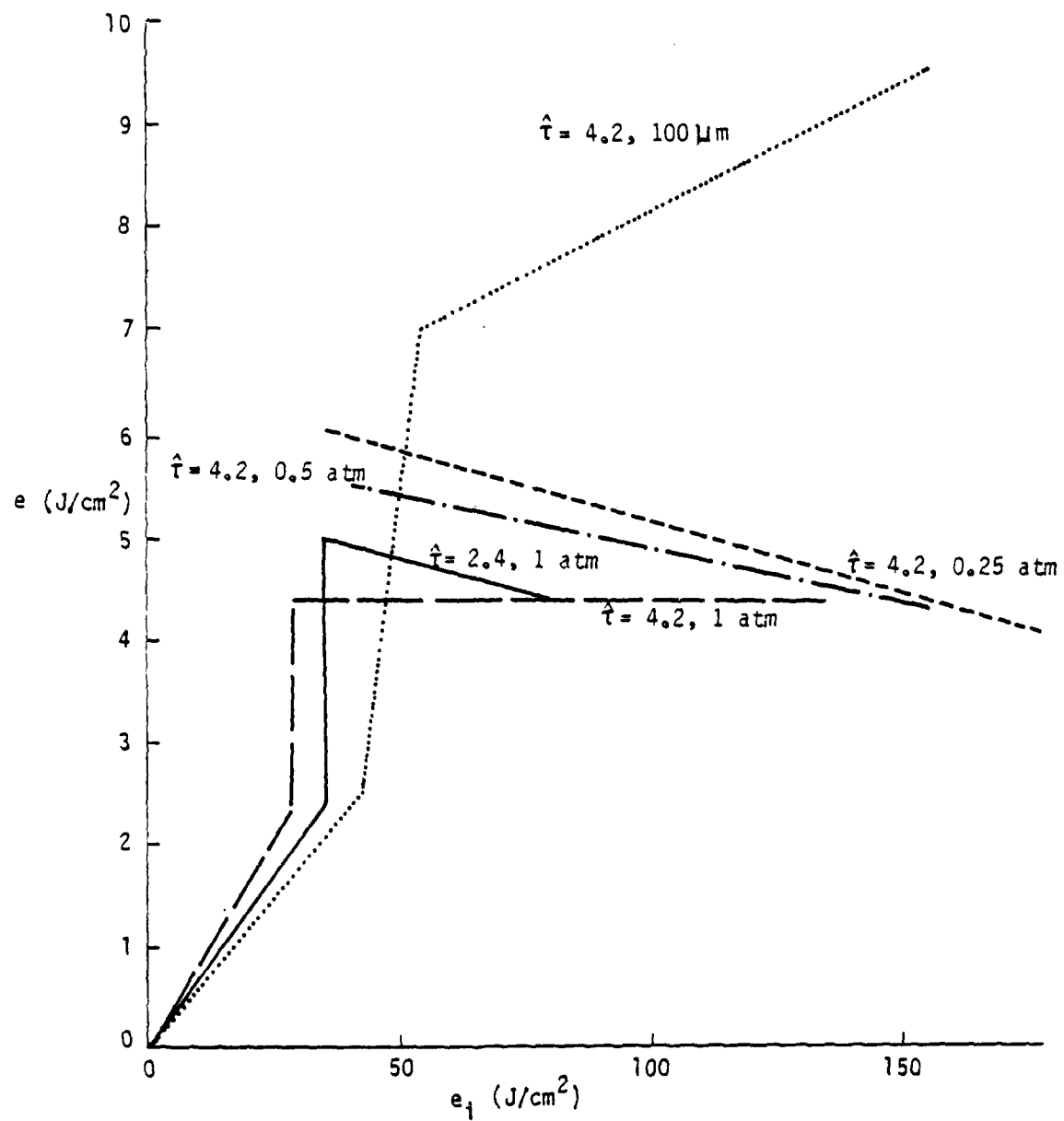
Figure 19. Comparison of average trends of single pulse thermal coupling to 2024-T3 aluminum with pressure as a parameter (all with $\hat{\tau}$ = 4.2, except as noted).
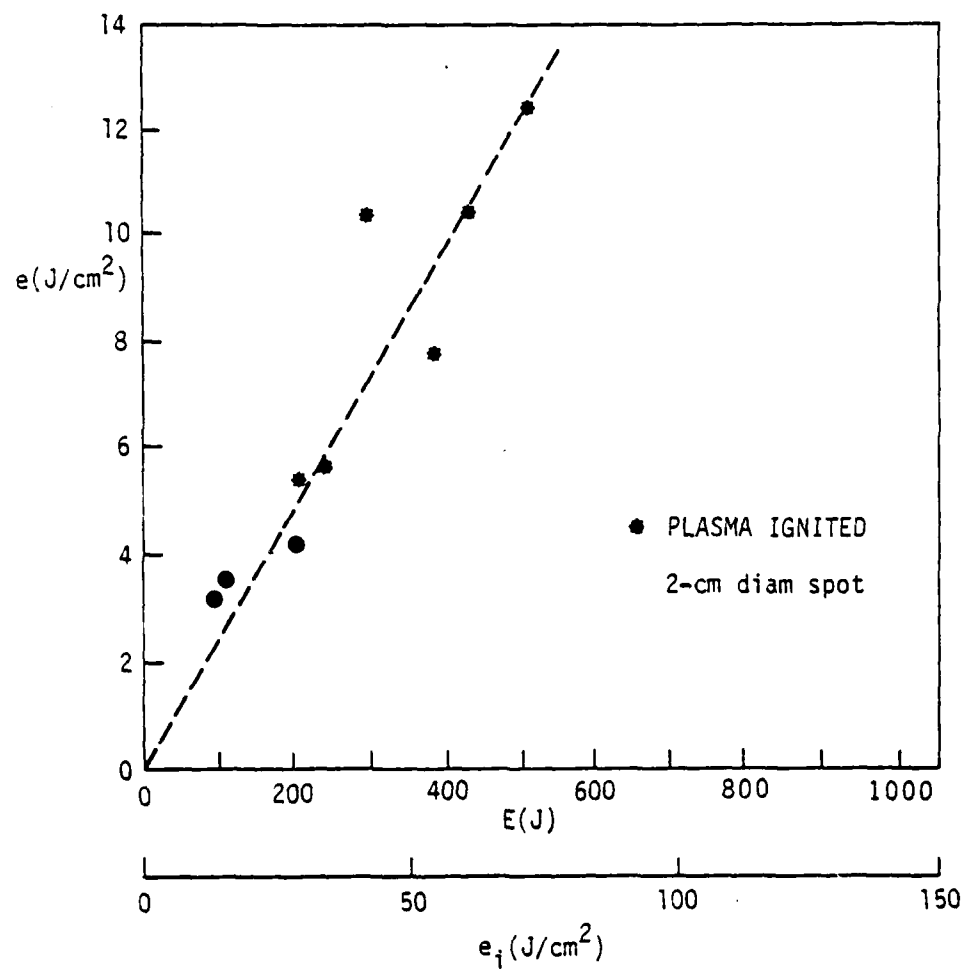
Figure 20. Coupled fluence for titanium (6Al 4V) at 1 atm.
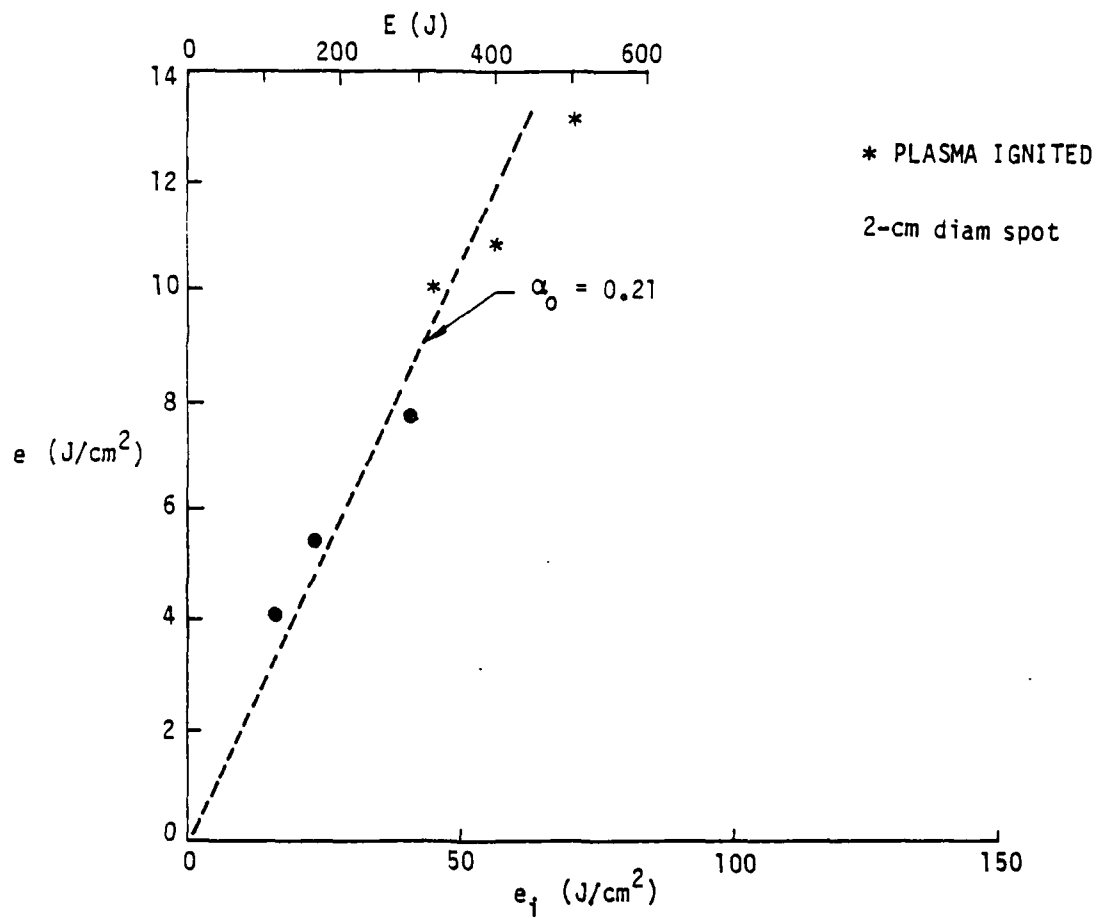
Figure 21. Coupled fluence for steel (4130) at 1 atm.
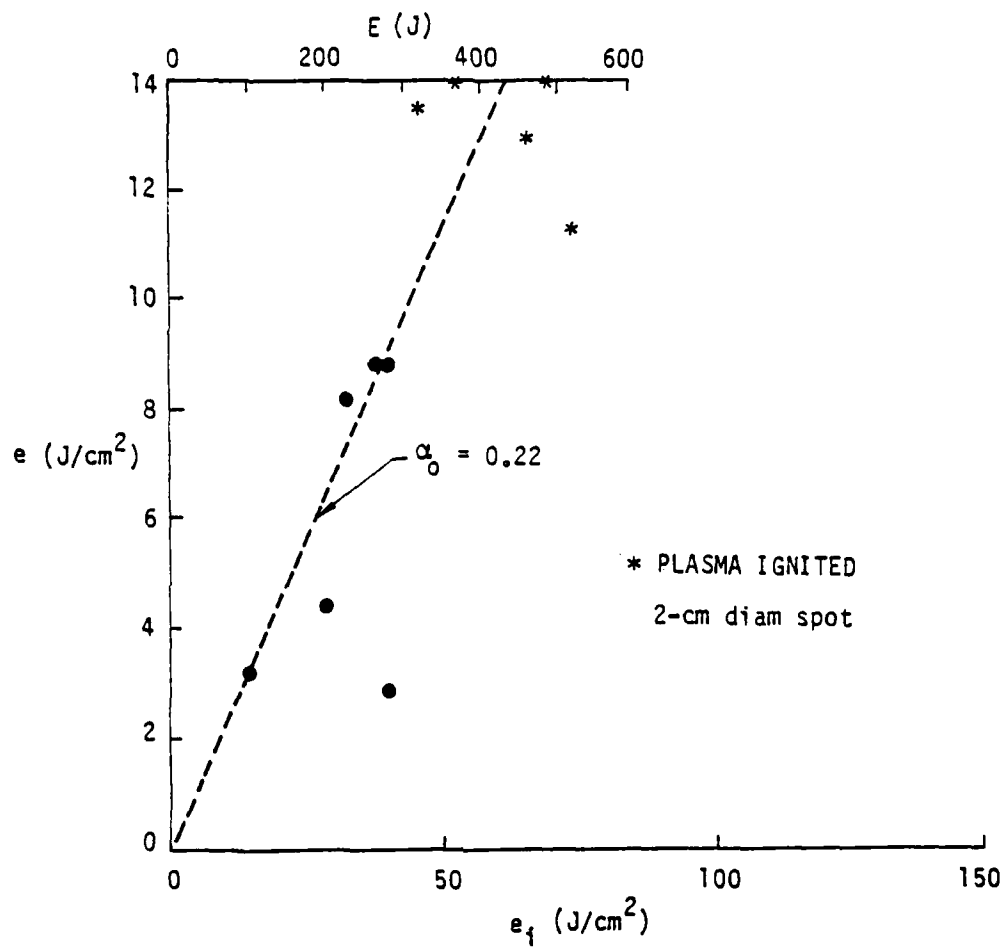
Figure 22. Coupled fluence for stainless steel (304) at 1 atm.

For pressures of 0.25 atm or greater one expects little dependence of the coupled fluence on pressure. This can be seen from the data summary (for aluminum) of Figure 19. An additional series of coupled-fluence measurements with a smaller spot size and 0.25 atm pressure was carried out for the above described titanium, steel, and stainless steel targets in order to determine any spot-size dependence. The results are given in Figures 23, 24, and 25. At the higher irradiances achievable with these smaller-spot experiments, one observes the expected gradual decrease in coupled fluence as the incident fluence increases. However, it is of interest that the coupled fluence maxima are roughly two times greater for these materials (titanium, steel, and stainless steel) than for aluminum.

3.4 SINGLE-PULSE COUPLING AT OBLIQUE ANGLES

Because real interaction scenarios often involve incident angles far from normal, a series of such laser coupling experiments was made with aluminum 2024. At oblique incidence angles θ the normal irradiance is reduced by a cos θ factor. However, since ignition results from vaporization of small micron-sized imperfections such as local laminae, the actual peak irradiance should largely control when plasma is produced. Thus, both ignition fluence and irradiance at oblique angles should not increase as rapidly as $(\cos \theta)^{-1}$.

At these oblique angles, the actual spot size on the target becomes elliptical. In the experiments reported here, the targets were made two (or more) times as long as the length of the laser spot. For example, when θ = 87.5°, a nominal 2 x 2 cm spot is transformed into an ellipse with dimensions of 2 x 46 cm. With optics of 5.25 m focal length, the depth of field exceeds 46 cm so that only small errors in knowing the angle of incidence over the laser spot occur. A more serious error arises in mounting these flexible
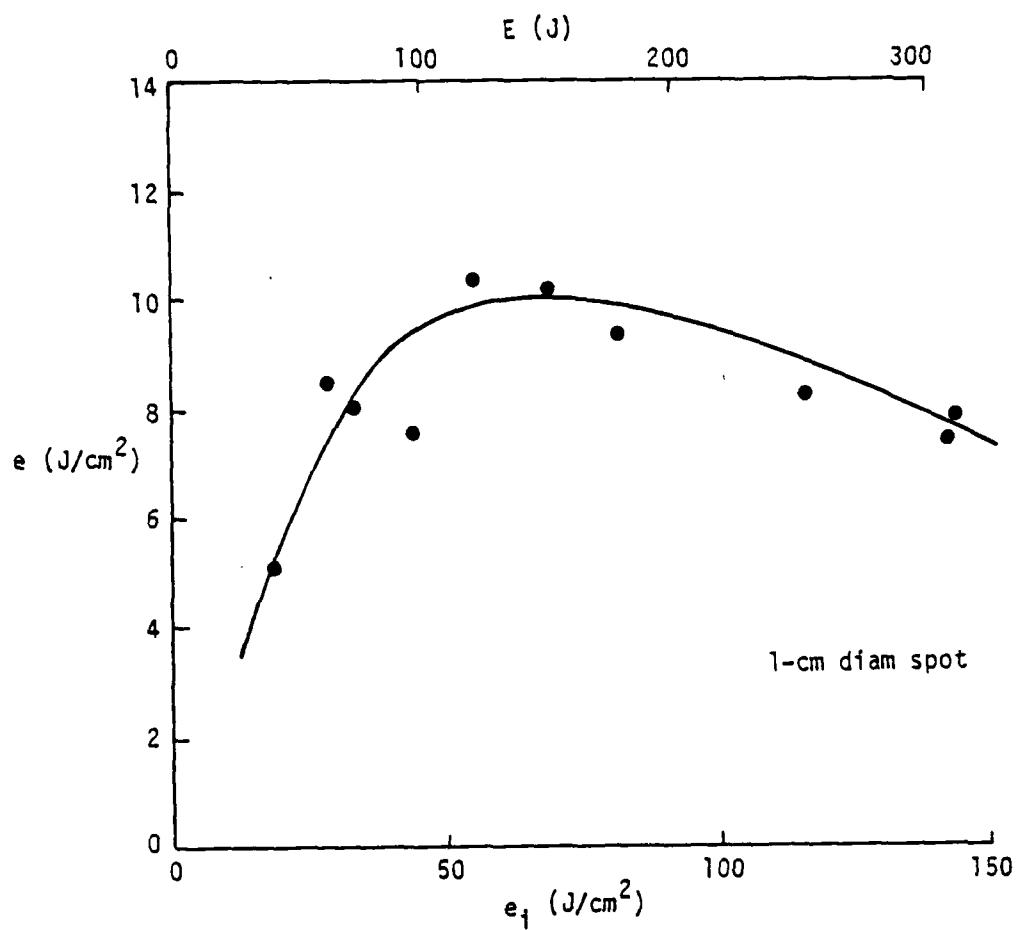
Figure 23. Coupled fluence for titanium (6Al 4V) at 0.25 atm.
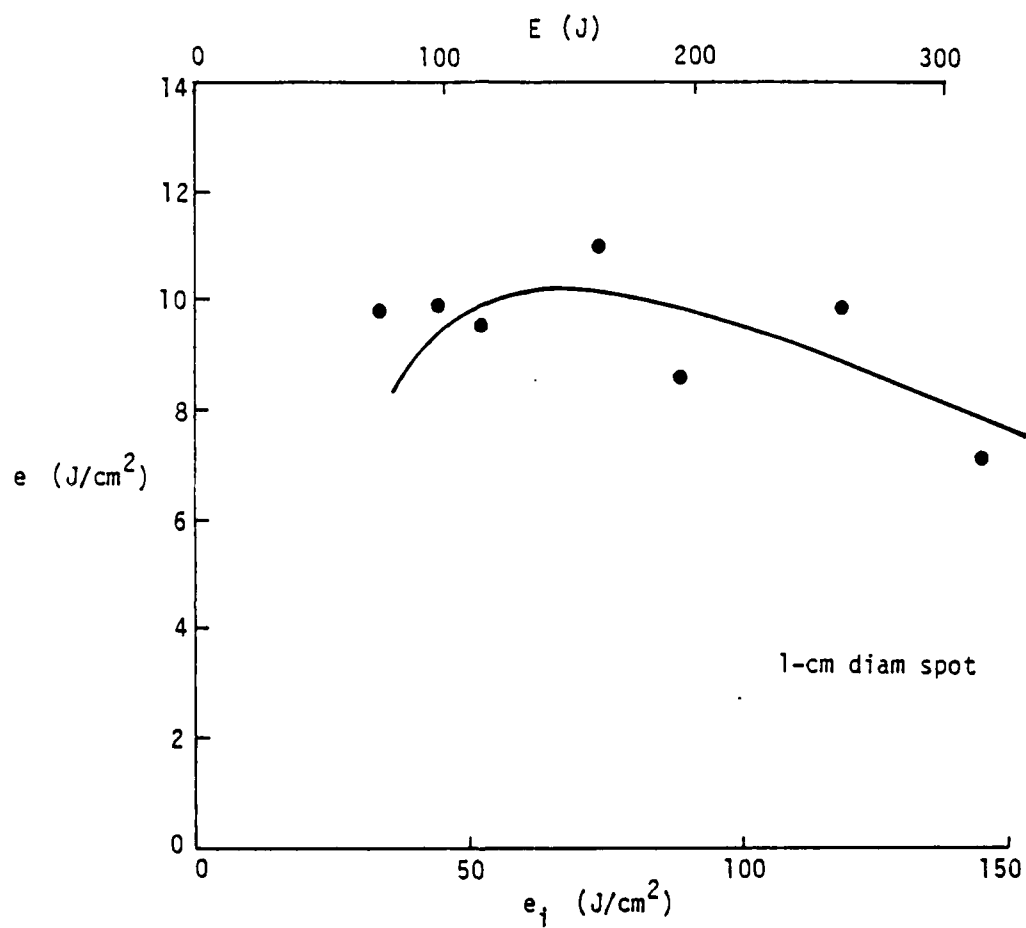
Figure 24. Coupled fluence for steel (4130) at 0.25 atm.
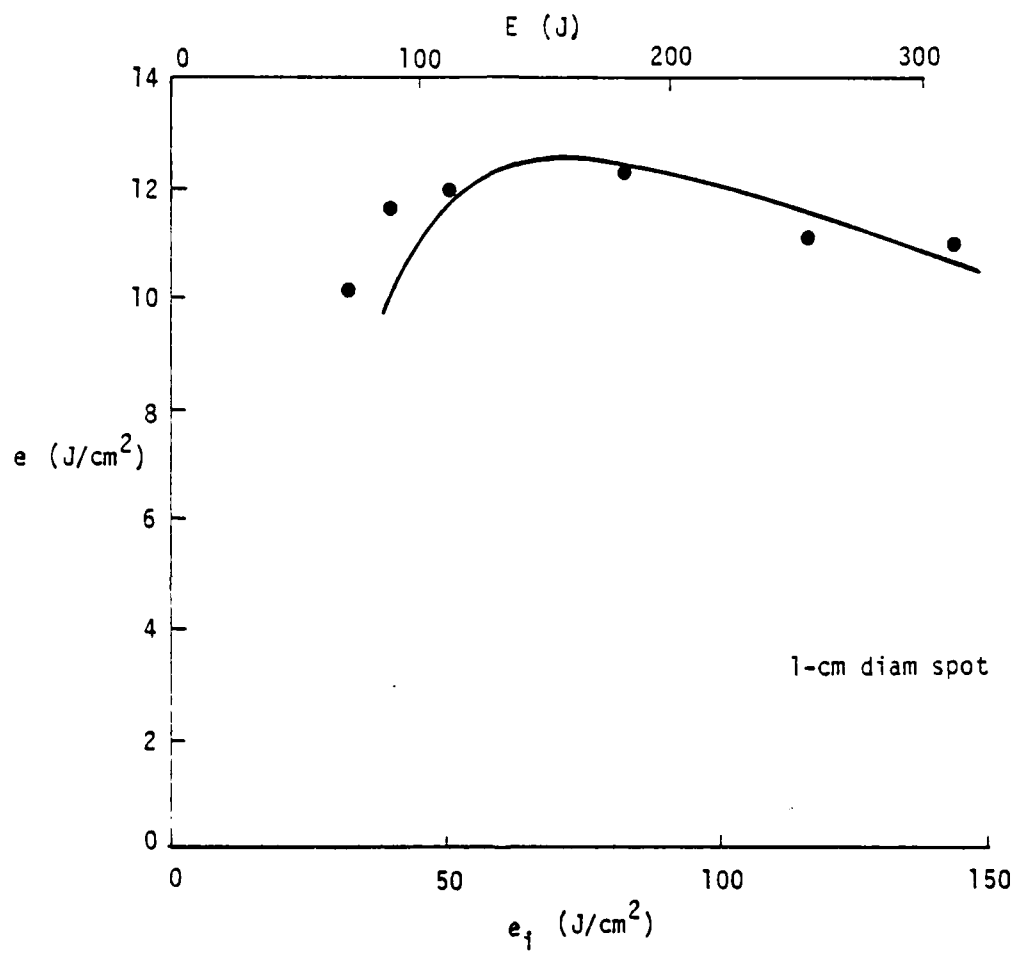
Figure 25. Coupled fluence for stainless steel (304) at 0.25 atm.

long thin targets. We estimate this error to be $\pm 0.5°$ at $\theta = 87.5°$.

The fluence coupled to these targets was determined as a function of incident angle θ at a (nominally) fixed total incident energy. The central coupling coefficient was determined at the center of the laser spot by measuring the absorbed fluence and then dividing by the incident normal fluence.

The results, shown in Figure 26, are well fit by

$$\alpha \approx .75 \; \alpha_0 / \sqrt{\cos \theta} \qquad (12)$$

where $\alpha_0 \simeq .073$ is the plasma-enhanced absorptivity at an incident fluence of 63 J/cm^2 corresponding to an incident energy of 461 J. This is consistent with the normal incidence data of Figure 12. The actual incident energy on any shot in Figure 26 varied from this value by less than 5%.

In Figure 26, at the most grazing angle ($\theta = 87.5°$), no visible plasma was ignited where the normal incident fluence was only 2.85 J/cm^2. The measured absorptivity under this condition is approximately twice that deduced from sub-threshold normal-incidence measurements, however. At this time no explanation of this discrepancy is offered. The highest plasma-enhanced absorptivity occurs at $\theta \sim 85°$ where only a maximum of 1.1 J/cm^2 was absorbed. At $\theta = 60°$, the absorptivity has dropped to ~ 0.07 but the absorbed fluence is 2.3 J/cm^2.

The empirical equation describing the results given in Figure 26 is valid only for $\cos \theta < 0.5$. In order to fit the normal incidence absorptivity, the actual value of α for $.5 < \cos \theta < 1$ must be nearly constant. The plasmas ignited when the incidence angles are large do not completely fill the spot

51
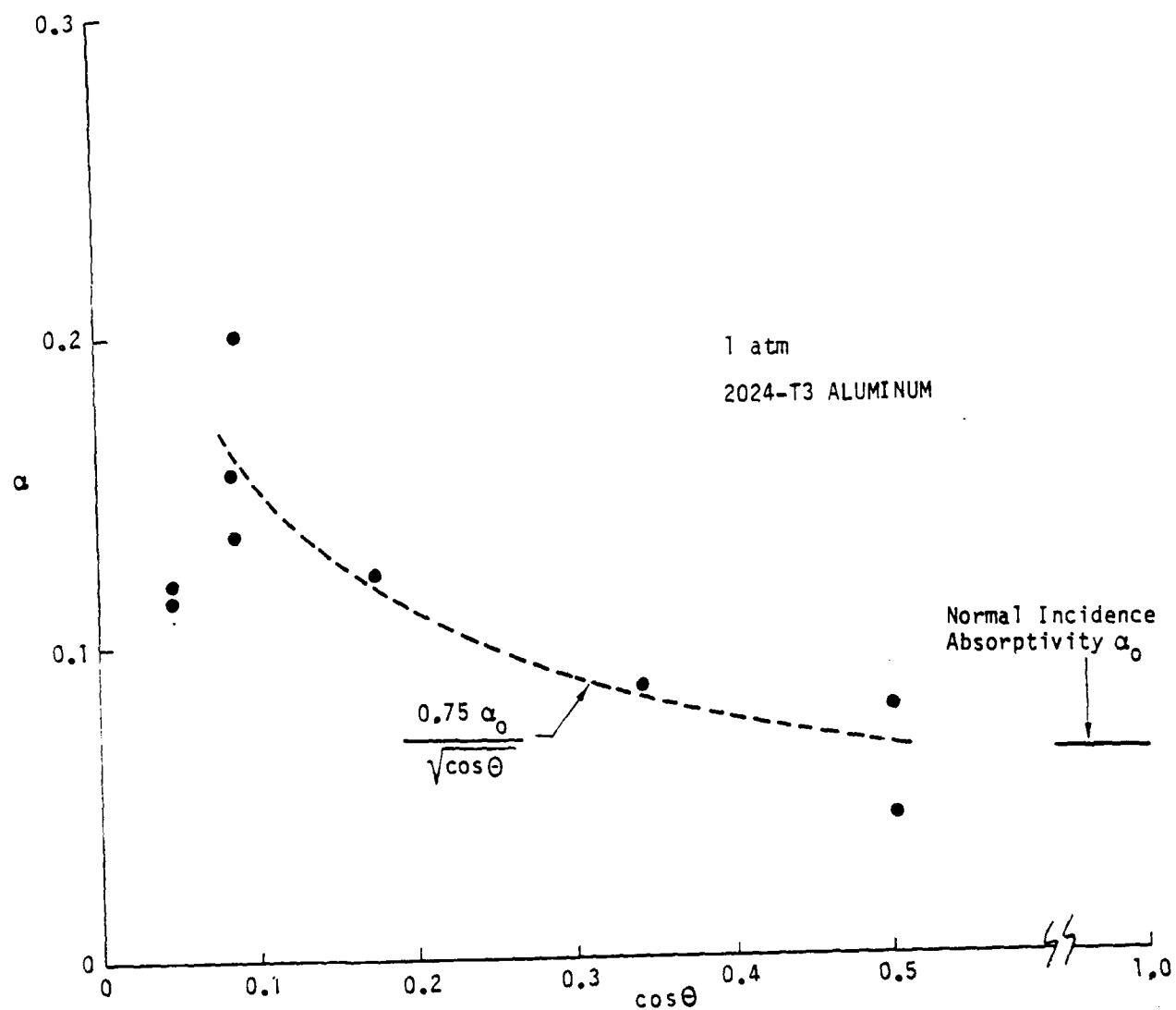
Figure 26. Coupling coefficient α versus Cos θ
for oblique 2024-T3 aluminum targets.

52

dimensions on the target as can be seen in Figure 27. These patchy plasmas apparently ignite at local laminae where the incident irradiance is high enough to cause vaporization.

3.5 SPATIAL DISTRIBUTION OF ABSORBED FLUENCE

Because both the incident fluence and plasma ignition are never completely uniform it is of great interest to determine the variation of absorbed fluence over the laser spot. The previously presented data were always taken at the geometrical center of the focal spot. To define this variation, arrays of 5 thermocouples were spot welded on the backs of 2024-T3 aluminum targets. These thermocouples were located at the center and one each at vertical and horizontal positions at a given distance from the center. In two different arrangements, this distance was either 1 or 2 cm.

These individual thermocouples can influence each other so a cross-talk test was made. This was done by masking the target so that only the area immediately above one thermocouple was exposed to the beam. By observing the response of the remaining thermocouples it was deduced that this cross-talk, at worst, amounts to 25%. That is, the next closest thermocouple had 0.25 as much signal as the exposed thermocouple. This results from plasma spreading. In general, however, less than 9% cross-talk was observed under all combinations of measured and exposed thermocouples.

The actual data observed when all of the target area above the array was exposed to laser beams at three different intensity levels are shown in Figure 28. These data are normalized to the coupled fluence measured by the central thermocouple. Compared to the beam profiles, the coupled fluences are extremely smooth. The normal scatter in thermal coupling is

60°

1 cm
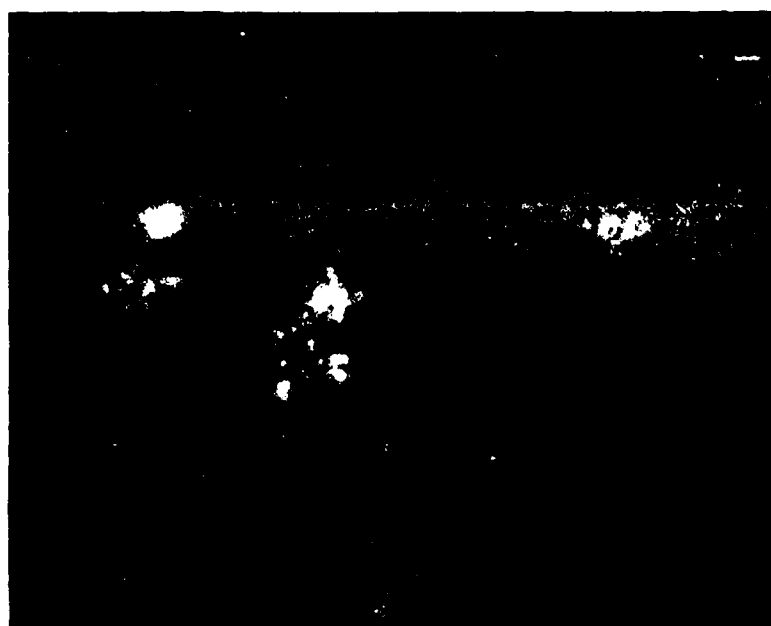
85°

1 cm

Figure 27. Photographic records of plasmas at oblique incidence.
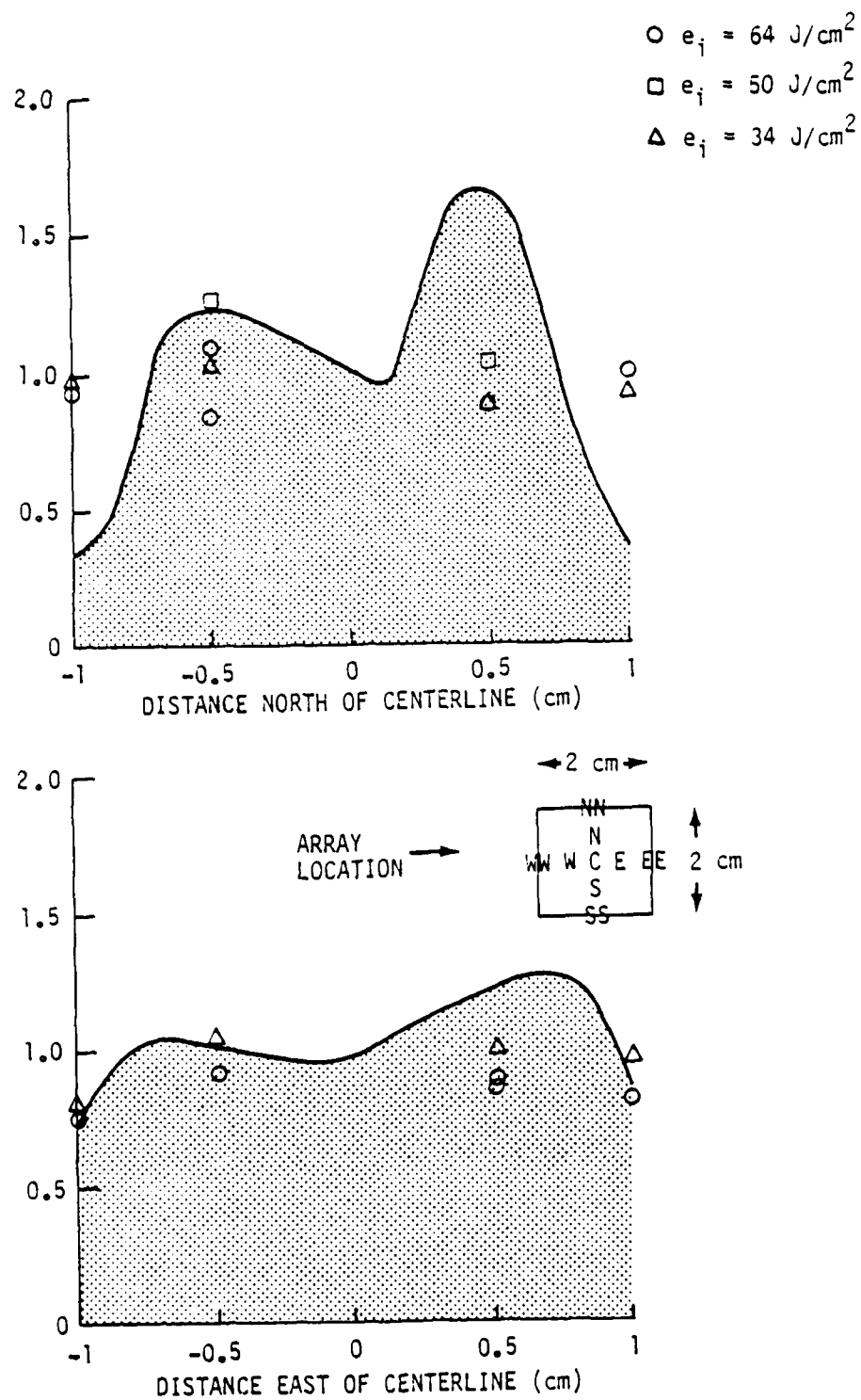
Figure 28. Spatial profiles of thermal coupling compared with beam profiles.

larger than the spatial variations that are seen here. It appears that the absorbed fluence determined from a central thermocouple was indicative of coupled fluence over the whole spot.

3.6 IMPULSE PRODUCTION

The ballistic pendulum apparatus described in the Appendix was used for measuring impulse with 2024-T3 aluminum. The large spot (2 cm dia.) resulting from the 5.25 m focal length optics provided a $\hat{r}$ = 2.4 situation which was nearly one-dimensional. The targets were made of 2024-T3 aluminum and had not been exposed previously. The best evaluation of the specific impulse for the PHOCL-50 far-field beam profile must use $\overline{E}$ = 0.56 E which is the high intensity central fraction of the total incident energy as discussed in Section 2. At an incident fluence of 57 J/cm^2, the average measured specific impulse was

$$\frac{I}{E} = 7.7 \text{ dyn-s/J} \tag{13}$$

where $\overline{E}$ = 0.56 E is the high intensity central fraction of the total incident energy as discussed in Section II. This value was chosen for computing the specific impulse because the lower intensity part of the energy doesn't maintain laser-supported combustion waves which produce the impulsive pressure. Comparing the above large-spot (2-cm diam) result with various work (Ref. 4) with a smaller spot size (0.94 cm diam) shows that the specific impulse has increased by a factor 1.28. This is due to the larger spot area which maintains a high plasma pressure for a relatively long time.

---

4. R.B. Hall, W.E. Maher, D.J. Nelson, and D.B. Nichols, High Power Laser Coupling, AFWL-TR-77-34, AFWL, KAFB, New Mex, 1977.

56

3.7 PULSE-LENGTH DEPENDENCE OF SINGLE-PULSE COUPLING

In observing thermal coupling as a function of $\hat{\tau} = ct_p/r$, there are significant advantages in comparing results from the same laser, so that device-related features are unchanged. In this section, the value of $\hat{\tau}$ was varied by changing the pulse length t_p. In addition to measuring the coupled fluence, the fractions of incident pulse fluence occurring before and after plasma ignition were also determined.

The laser pulses were truncated in time to generate pulses of two lengths, but with an unchanged characteristic leading edge and rise time. The use of fixed laser conditions also minimized variations in other beam properties, including the content and time dependence of beam spectral components.

Thermal coupling analysis is complicated by the fact that plasma ignition occurs at various times during the incident pulse, depending on both the incident irradiance and the incident fluence (Ref. 2). These measurements were intended to clarify that analysis by the measurement of both the plasma ignition time and the thermal coupling for two different pulse lengths.

The experimental arrangement is shown in Figure 29. As in Section 3.1, the incident PHOCL-50 DF laser beam was sampled by a CaF_2 wedge to provide energy monitoring and fast-detector time profiling. The beam was brought to a focus beyond the wedge and then recollimated. At the focus a spark gap with variable delay allowed the initiation of a laser-supported absorption wave at an arbitrary time during the laser pulse, blocking the latter part of the incident pulse. After passing through this cutoff assembly the beam was focused on the target by a 2.9 m focal length mirror. The 0.127-cm thick Al-2024 targets were situated in the mirror focal plane at three degrees from
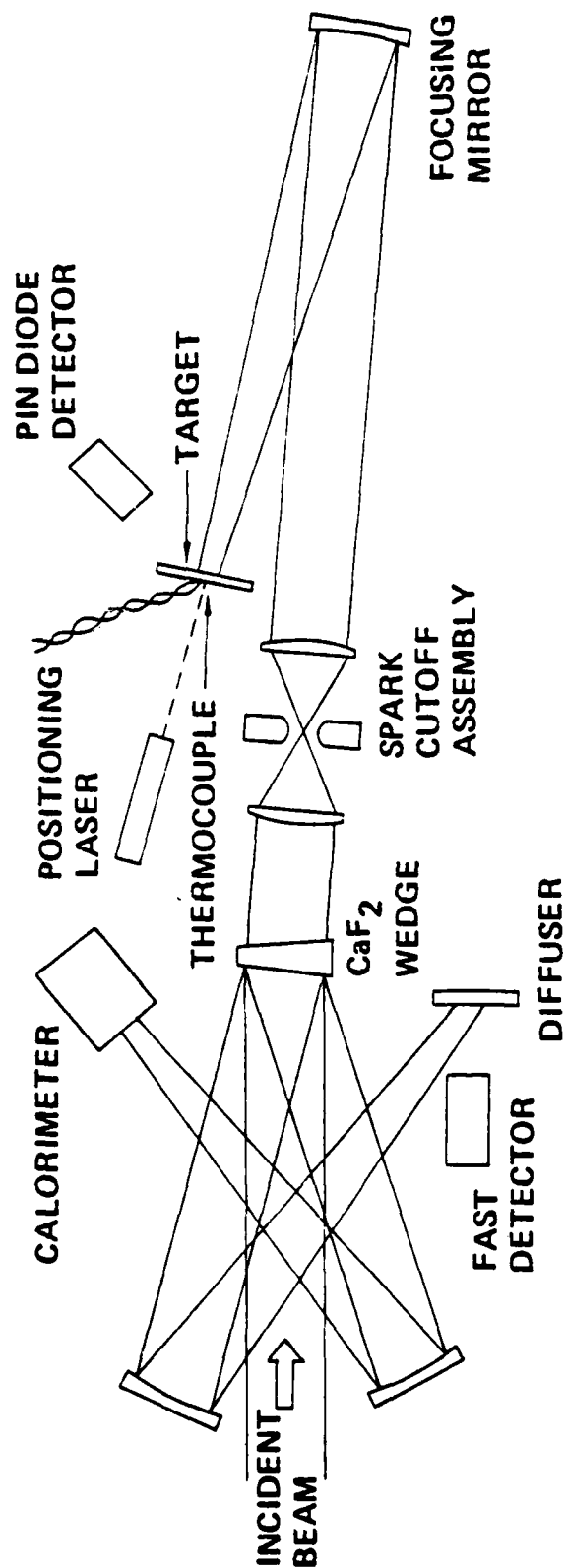
Figure 29. Experimental arrangement for variable pulse length DF laser coupling.

normal incidence to prevent the return of the incident beam to the optical train. Each target was instrumented with a chromel-alumel thermocouple on the back at target center. A new target was used for each shot in this study, and the targets were located from the rear by a positioning laser. During each shot the time of initiation of a target surface plasma was measured by a fast PIN diode visible-light detector. The coincidence of the photodiode signal and the plasma initiation was demonstrated by simultaneously observing the cutoff of incident DF laser radiation transmitted through a 0.07-cm pinhole in the target.

The distribution of DF laser radiation in the focal plane of the 2.9-m focal length mirror was measured with the spark cutoff assembly in place. At a beam position after the spark cutoff assembly the beam was attenuated by a factor of 33 by reflection from a second CaF_2 wedge to give focal plane intensities observable by burn patterns on unexposed, developed, photographic paper. Standard Teflon attenuators at the PHOCL-50 laser provided variation in total laser energy per shot. The resulting relative spatial profile is similar to that shown in Figure 11. With this focal length (2.9 m), an effective area S = 1.69 cm^2 converts total incident beam energy E to peak fluence e_i = E/S. The average laser pulse length is 2 μs with a pulse shape as indicated for one example in Figure 30.

Local thermal coupling for each laser shot was derived from the peak of the curve of rear-thermocouple temperature versus time. Axial diffusion time for the targets was 6 ms; thermocouple peak times were tabulated for each measurement, and occurred at about 50 ms.

Figure 30 shows the variation in coupled fluence for cutoff pulses with 2.0μs FWHM and having about 55% of the long-pulse energy. The truncated and
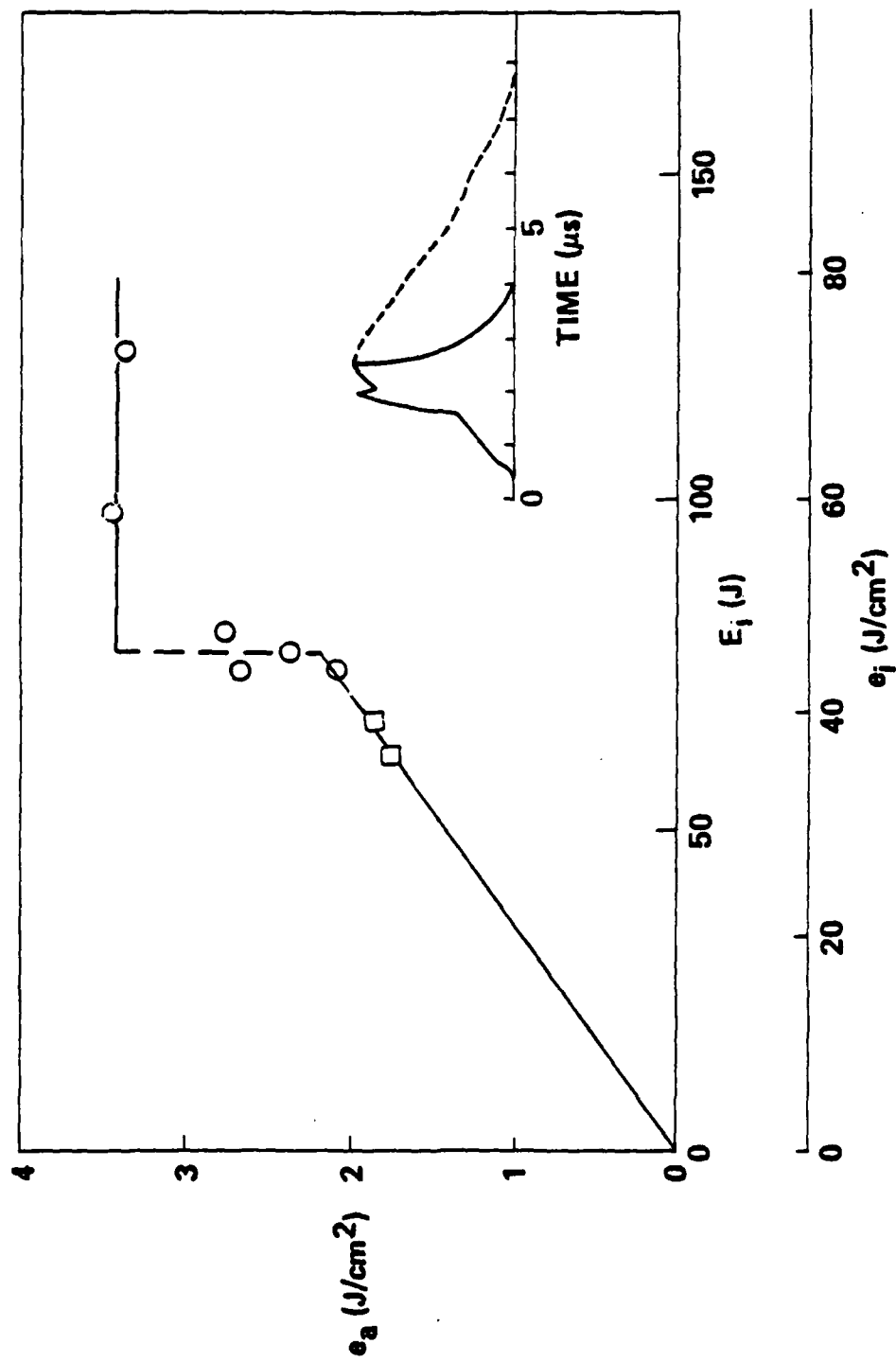
Figure 30. Thermal coupling measured for the short, 2.0 μsec FWHM, pulse. Example indicated by the inset. Surface plasmas were observed in the measurements given by circles.

full-length pulse shapes are shown in the inset. Lines are given for the measured intrinsic coupling of 0.048 below threshold, and a constant e_a = 3.4 J/cm^2 above threshold. For comparison purposes, the full-pulse-width coupled fluence variation is seen for τ = 2.4 and 4.2 in Figure 13. The τ for this cutoff-pulse experiment would be 2.4.

This cutoff-pulse data appears to have an intrinsic coupling that is considerably lower than the 7% indicated by the data in Figures 12 and 13. The ignition threshold with the cutoff pulse occurs at a fluence level which is 40 percent higher than with the long focal length results given in Section 3.1. It is believed that modifications in the spatial profile caused by lens aberrations explains this difference. Above the plasma ignition threshold the constant 3.4 J/cm^2 value for absorbed fluence corresponds well with the 4 J/cm^2 seen in Figure 13.

IV. MULTIPLE-PULSE LASER COUPLING

Previous laser effects experiments at 10.6 μm wavelength showed that repeated exposures of a given target led to variations in the ignition of plasmas. More reliable experimental conditions were sought and it then became standard practice in single-pulse experiments to make only one laser exposure on a single target. This was important for absorbing targets such as titanium and stainless steel but was less important for polished (or as-received) aluminum. In fact, at 10.6 μm wavelength, no essential difference between repetitively-pulsed and single-pulsed coupling occurs with aluminum targets.

In contrast, with the results of coupling experiments at 10.6 μm wavelength, the interaction of the shorter wavelength DF radiation with aluminum targets leads to significant surface damage. Typically, single-pulse DF pulses above the plasma ignition threshold cause melting and vaporization. This results in a roughened surface which has been found to considerably modify the coupling of subsequent laser pulses to the target.

4.1 MULTIPLE-PULSE EXPERIMENTS ON ALUMINUM

In Figure 31 the repeated pulse effect data at 1 atm are shown. Three separate sets of data with three targets are superimposed. The variation of coupled fluence versus shot number varies somewhat, dependent on the target itself, but the overall trend shows that after about 10 pulses coupled fluence per pulse has more than doubled but then ceases to increase. No CO_2 thermal coupling, either single or repetitively pulsed, has exceeded 3 J/cm^2 at these pulse energies. The coupled fluence shown on Figure 31 is the per-pulse fluence (and not the cumulative) delivered fluence.

62
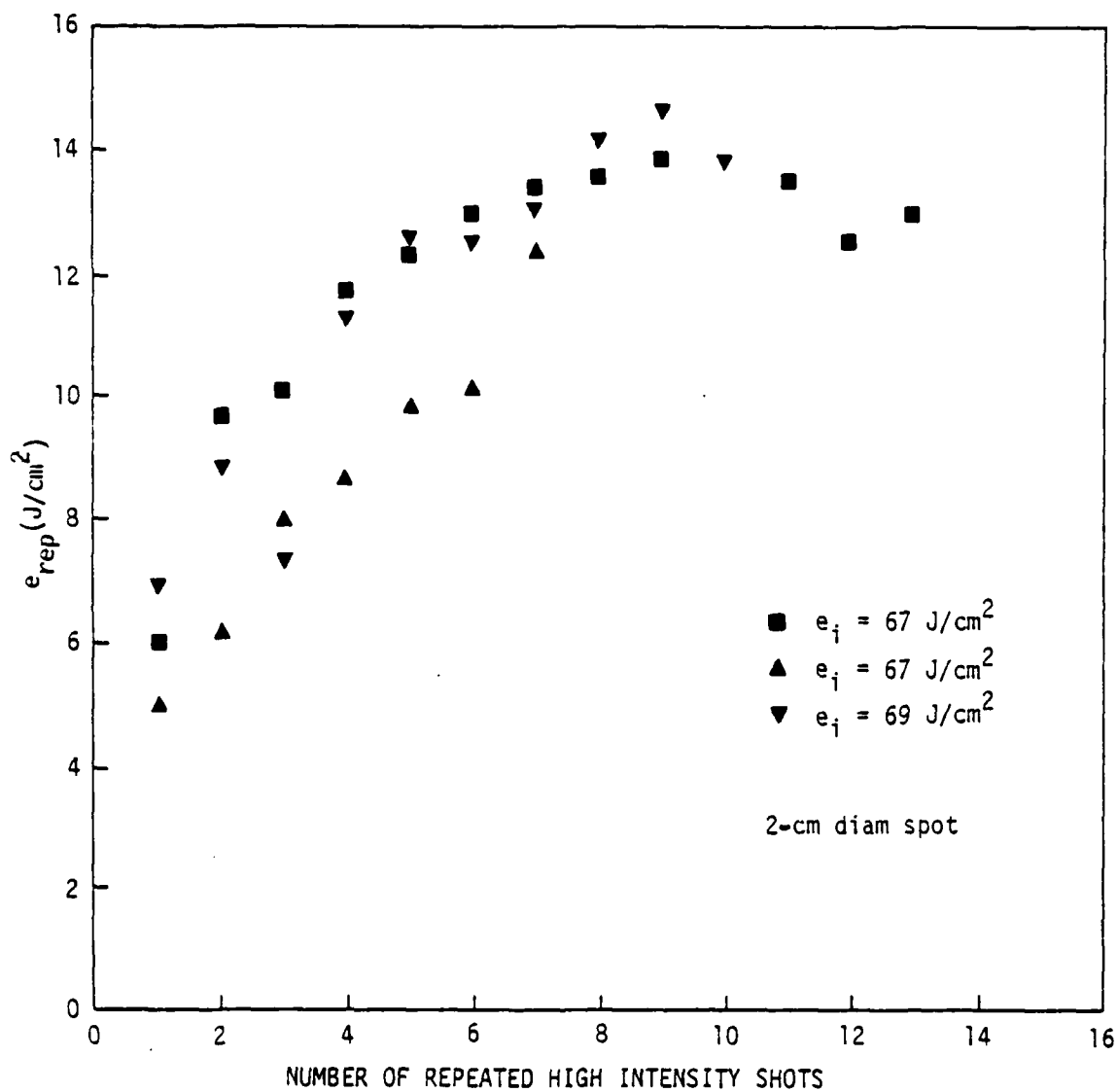
Figure 31. Repeated DF pulse thermal coupling on 2024–T3 aluminum at 1 atm.

The surface condition after multiple DF pulse exposures has been examined by scanning electron microscopy (SEM) which shows that severe surface modification has taken place. Additional energy deposition on the target after 10 pulses may rearrange the surface locally, but a characteristic highly absorptive surface is already formed. The average coupled fluence of 13.5 J/cm^2 for e_i at 68 J/cm^2 indicates a high itensity coupling coefficient of about 20%.

Figure 32 compares as-received surface features with an aluminum 2024-T3 target after it has been exposed to 10 high intensity DF laser pulses. This photograph does not reveal the actual spongelike formations. The texture that the target surface develops has a complex three-dimensional form. There are many crevices and tendrils whose size is about the same size as the 3.8 μm laser beam wavelength. It is not known if this surface condition after multiple exposures to a pulsed DF laser beam is unique to 2024-T3 aluminum. The roughened surface may be caused by the interaction of the plasma gas flow with the molten and vaporizing surface. Alternatively, hydrogen gas absorbed interstitially in the crystalline structure may be released under laser heating to form bubbles which break at the melted surface followed by rapid cooling to freeze surface features.

The multiple-pulse data of Figure 31 were taken at an incident fluence whose magnitude was about twice the plasma ignition value. Figure 33 shows the variation of coupled fluence when the incident fluence was just above plasma threshold. According to the current understanding of enhanced coupling, maximum heating occurs near the ignition threshold which was observed in the single-pulse results of Figure 12. However, there is no evidence near the plasma threshold for any repeated pulse effect even though the single-pulse coupling is somewhat greater under these conditions. Measurements were also

64
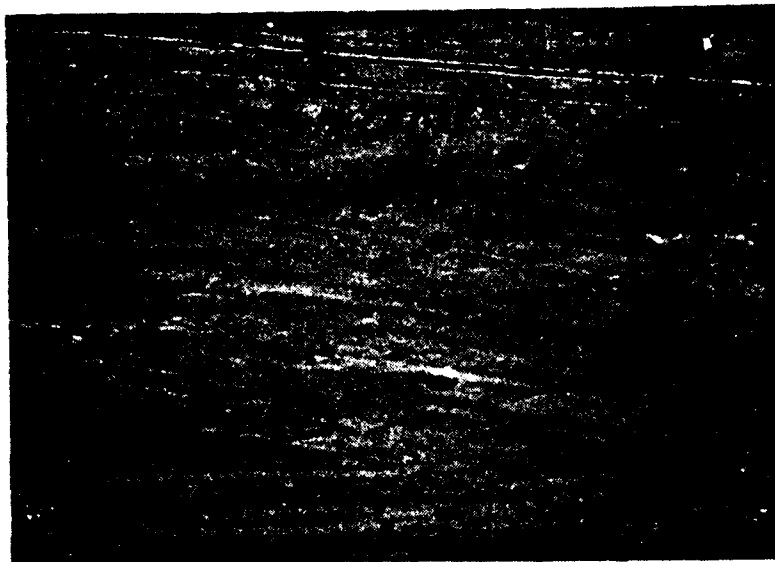
CLEANED ONLY
MAGNIFICATION 700X
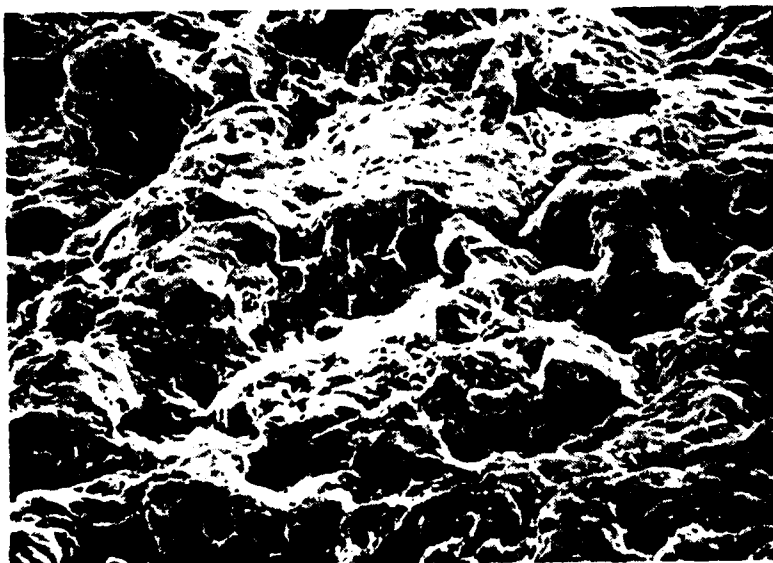
EXPOSED
MAGNIFICATION 700X

Figure 32. SEM of laser-roughened target.

65
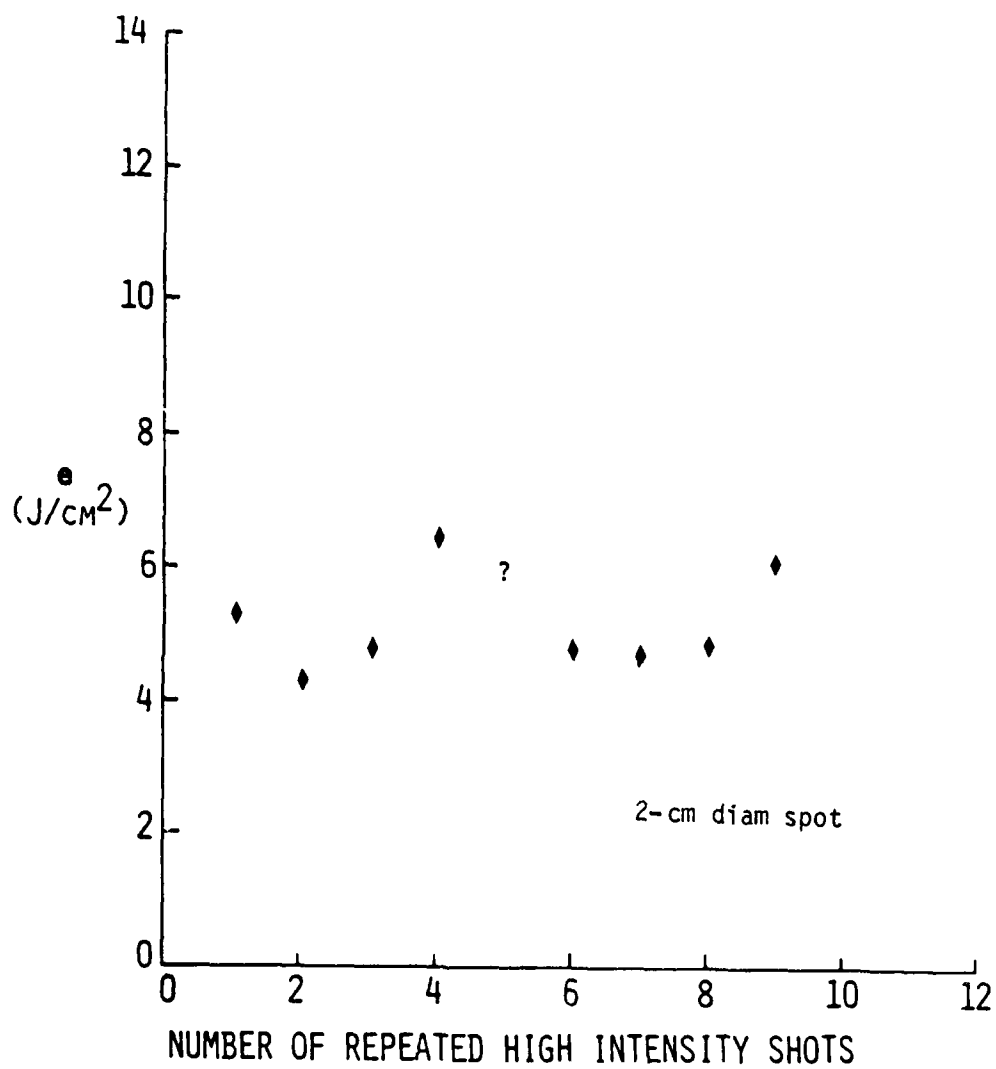
Figure 33. Repeated DF pulse thermal coupling at 1 atm on 2024-T3 aluminum near plasma threshold.

made at an incident fluence of $e_i = 134$ J/cm^2 with the results shown in Figure 34. At this high incident fluence, a smaller focal spot was used, so $\hat{r}$ is larger. Again the multiple-pulse effect occurs but appears to be only about 75% of the value found at lower intensity. Because of the smaller spot size with this higher irradiance experiment, it is not clear at this time what the optimum incident intensity should be to obtain maximum multiple-pulse damage. There obviously is an optimum irradiance to find multiple-pulse interactions since single pulse coupling decreases at both high and low irradiances.

Since the observed surface roughness is dependent on plasma ignition, and the resulting interaction with the surface, measurements of coupled fluence were made at 0.25 atm. The results shown in Figure 35 are nearly identical to the one atmosphere case of Figure 31 at comparable incident fluence values. At a pressure of 100 μm of Hg and a high incident fluence of 152 J/cm^2 the coupled fluence increases very slowly with the number of pulses as shown in Figure 36. Coupled fluence magnitudes of 9 J/cm^2 are consistent with the previous single-pulse data of Figure 18.

The single-pulse intrinsic coupling (i.e., coupling in the absence of plasma) of the 2024-T3 aluminum targets was previously shown to be about 7% in Figure 12. One target (denoted by ▲ in Figure 31) was taken after completing the repeated exposures and its absorptivity at 3.8 μm was measured in a Hohlraum reflectometer. Although the measurement geometry is somewhat different from a laser exposure, the measured absorptance of 19% indicates that the target's surface is permanently modified.
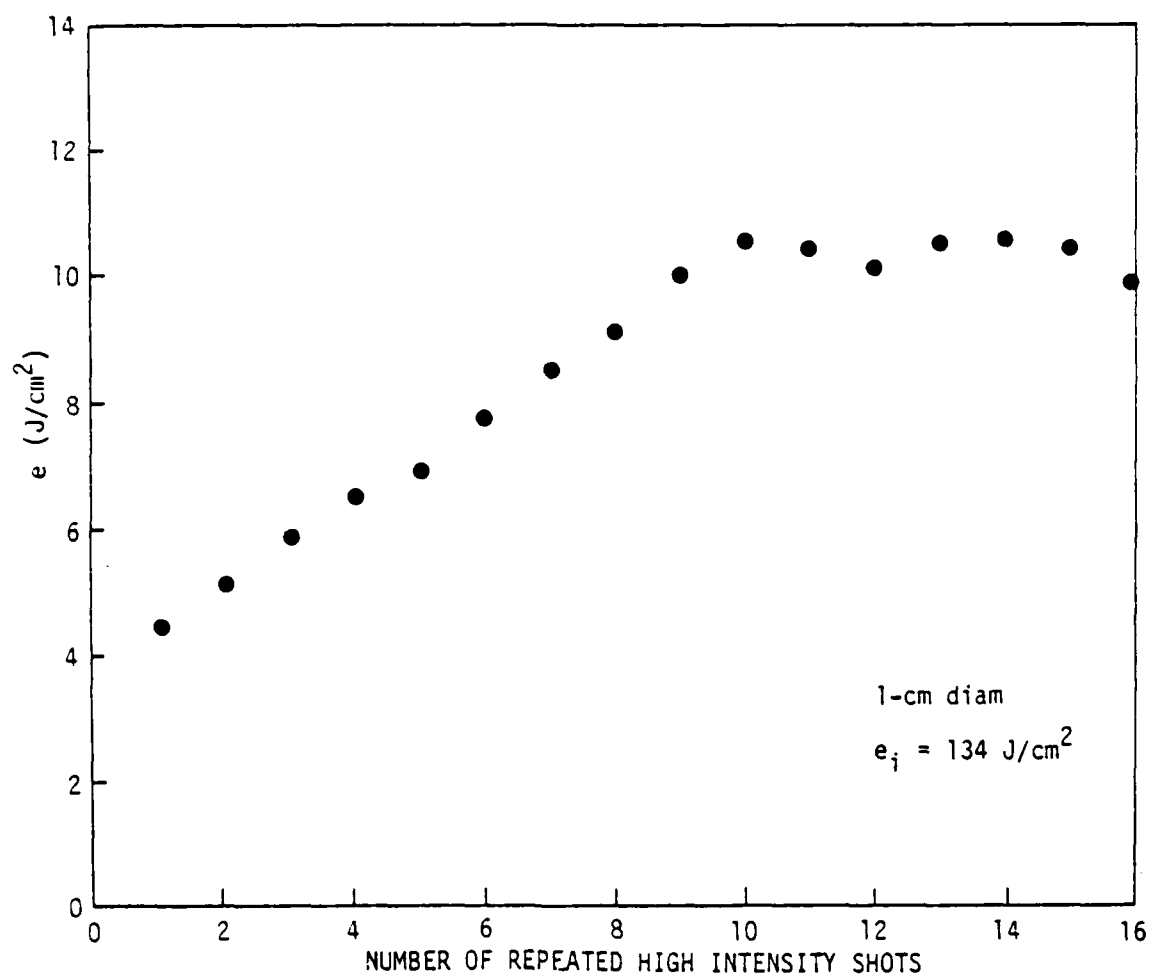
Figure 34. Repeated DF pulse thermal coupling at 1 atm on 2024-T3 aluminum at high intensity.
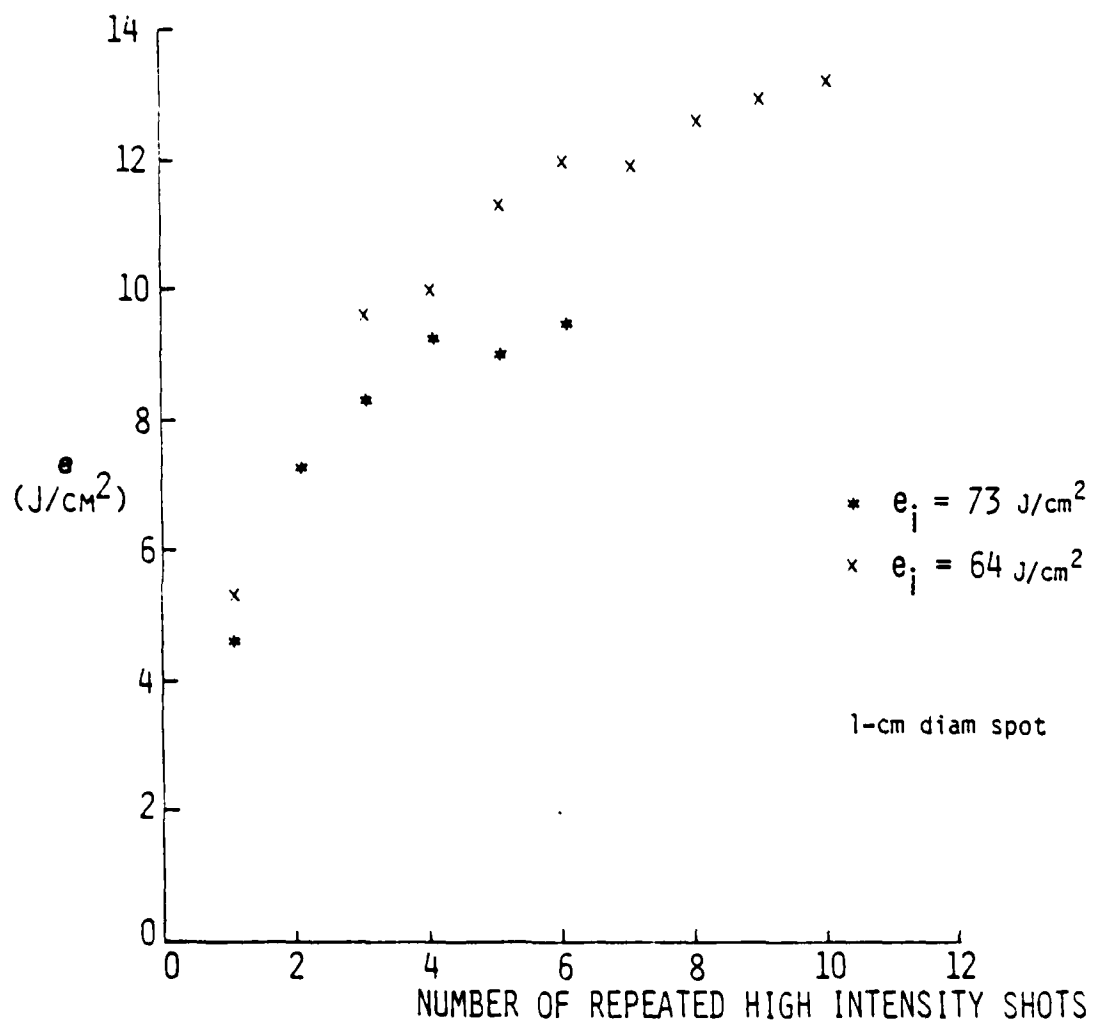
Figure 35. Repeated DF pulse thermal coupling on 2024-T3 aluminum at 0.25 atm.
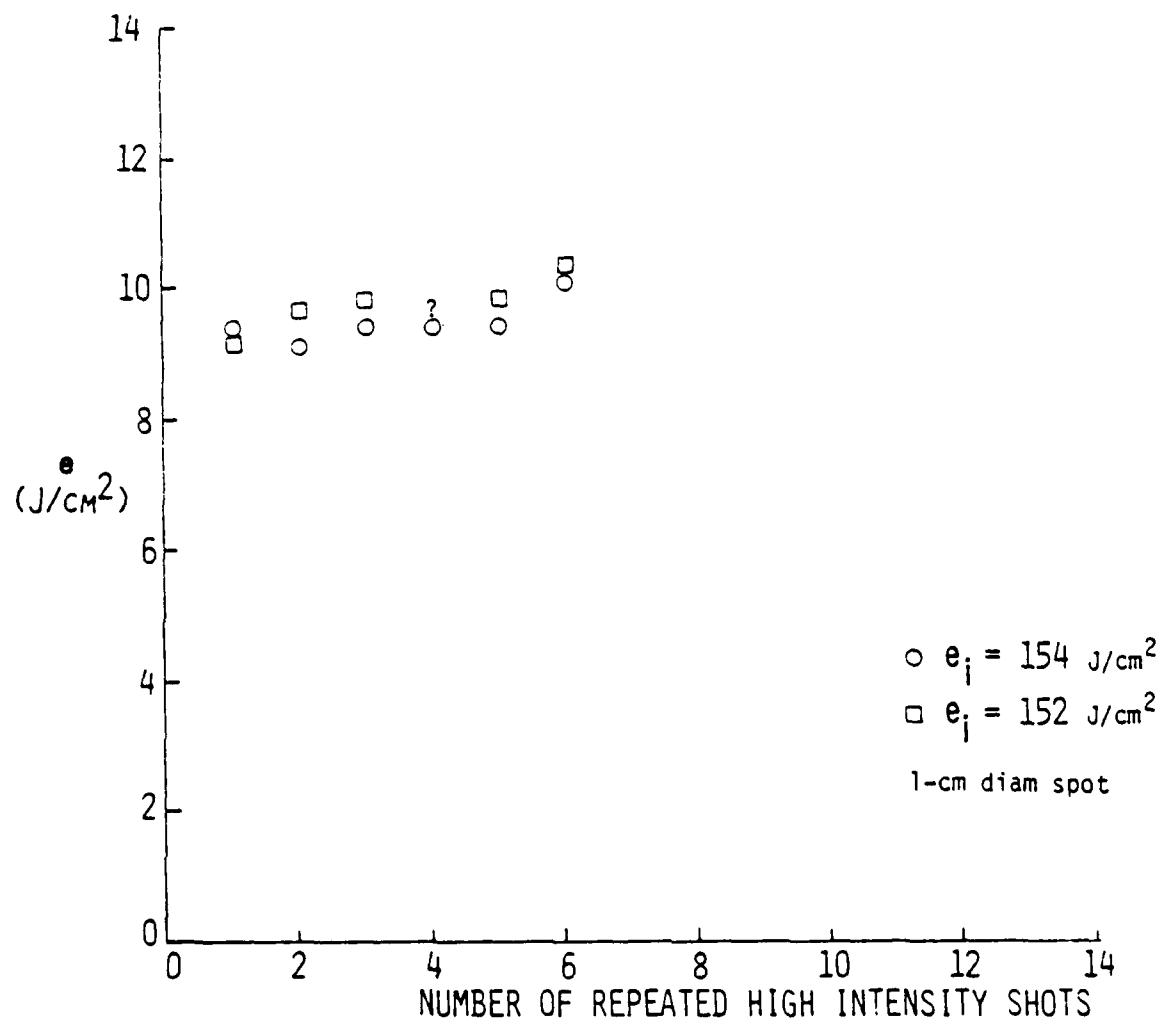
Figure 36. Repeated DF pulse thermal coupling at 0.1 torr pressure on 2024-T3 aluminum in vacuum.

By attenuating the incident laser beam well below the plasma ignition
threshold one can also determine the intrinsic absorptivity of a laser-
roughened surface. After 13 shots were accumulated on the target labeled ■
in Figure 31, the intrinsic absorptivity was determined to be 0.28 with an
incident fluence of 15 J/cm^2 (approximately half the ignition value). This
datum is indicated on Figure 37 by the point labeled ✿. Figure 37 also
indicates how the intrinsic absorptivity of a laser-roughened surface depends
on the number of accumulated shots. This measurement was carried out by first
firing a high intensity laser shot followed by a low intensity shot. Since
the low intensity shot is below the plasma ignition threshold, the intrinsic
absorptivity of the laser-damaged surface is determined. This process (on
the same target) is repeated N times. In this way, one determines the varia-
tion of the intrinsic absorptivity with N. In particular, the run labeled ▼
in Figure 31 was carried out in this manner. The values of intrinsic
absorptance obtained range from 7% after one high-intensity shot to about 30%
after 10 shots. After only these 10 shots, no clear experimental indication
of saturation of the absorptivity with shot number is apparent. However, it
is expected that a more extensive series of experiments would show such a
limitation on the intrinsic absorptivity.

4.2 MULTIPLE-PULSE OPTIMIZATION

The optimization of a multiple pulse high intensity laser system for
deposition of energy in targets can be done in several ways. To obtain
the minimum time, the multiple pulse effect described in Section IV suggests
that the laser be operated at constant high average power. An incident
fluence of about 68 J/cm^2 most rapidly leads to high absorbed fluence per
shot and to the most rapid accumulation of the total absorbed fluence
required to affect the target. This strategy of depositing maximum energy in
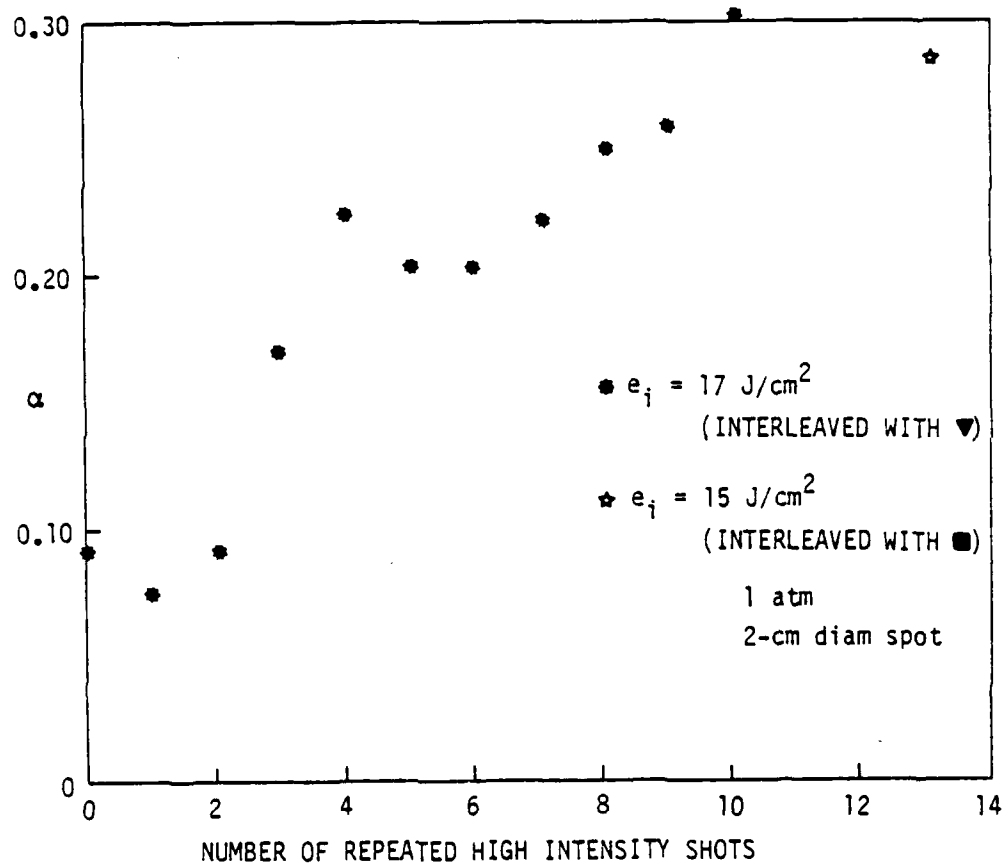
Figure 37. Intrinsic (no plasma) absorptivity of 2024-T3 aluminum as a function of the number of high intensity laser shots.

72

minimum time is often required. In order to maximize the total number of targets that can be engaged by a single laser in a battle, however, it is of interest to consider a possible strategy which may minimize the laser fuel required to damage a target. This section is an example of this optimization in which minimum total laser energy is required.

It is of interest to note that the enhanced (high intensity) coupling coefficient is only two-thirds as great as the low-intensity coefficient after only 10 laser shots on an aluminum target. This may indicate that an optimum strategy in damaging a real target in the sense that the required laser energy will be minimized may be to first emit a burst of about 10 (or less) high power laser pulses which serve to roughen the surface. After damaging the surface in this way (and increasing its absorptivity) the laser power could be reduced and a high coupling efficiency to the surface maintained. The requirement for a minimum encounter time is not a feature of this analysis.

As indicated above, both the plasma-enhanced coupling and the intrinsic absorptivity of a target are dependent on the number of previous pulses and on the intensity of the laser pulse. Since we have performed only a limited number of experiments on multiple-pulse interactions, this problem cannot yet be modeled with general validity. However, in this section, we will indicate some of the considerations that are required to optimize a repetitively pulsed laser engagement. Since sufficient data have been obtained at only one intensity and pulse length, the problem considered here is to determine the optimum combination of high intensity and low intensity laser shots to damage a target. The more general uptimization problem including variable irradiance, spot size, and pulse length can be carried out following more data acquisition. For the present, the results will be applicable to an incident laser fluence of 67 J/cm^2 which

73

correspond to the results of Figure 31.

Under these conditions (at one atmosphere pressure), the absorbed fluence per pulse e_N can be written approximately as

$$e_N = 6 + 7 \left[1 - \exp\left(- \frac{N-1}{4}\right)\right] \text{ J/cm}^2 \qquad (14)$$

In Equation 14, e_N is the absorbed fluence at an aluminum target at the Nth high intensity pulse. The various constants in Equation 14 are specific to an incident irradiance of 67 J/cm^2 but were chosen to match the experimental results. For example, when N is large, the absorbed fluence reaches a saturated value of 13 J/cm^2.

The total fluence e_{PT} absorbed by the target is obtained by summing Equation 14 over N pulses.

$$e_{PT} = \sum_n e_n = 13 \, N - 7 \sum_{n=0}^{N-1} \exp(-n/4) \qquad (15)$$

The total incident fluence is

$$e_{iT} = 67 \, N. \qquad (16)$$

From Equation 14 it is evident that, for the situation with plasma, the enhanced coupling coefficient per pulse as a function of pulse number is

$$\alpha_p = \frac{13}{67} - \frac{7}{67} \left[\exp \left(- \frac{N-1}{4}\right)\right] \qquad (17)$$

On the other hand, one sees from the data of Figure 37, for the low intensity situation (with no plasma), that the intrinsic absorptivity of the laser-roughened surface increases approximately as

$$\alpha_I = 0.07 + 0.23 \left[1 - \exp \left(- \frac{N-1}{4}\right)\right] \qquad (18)$$

74
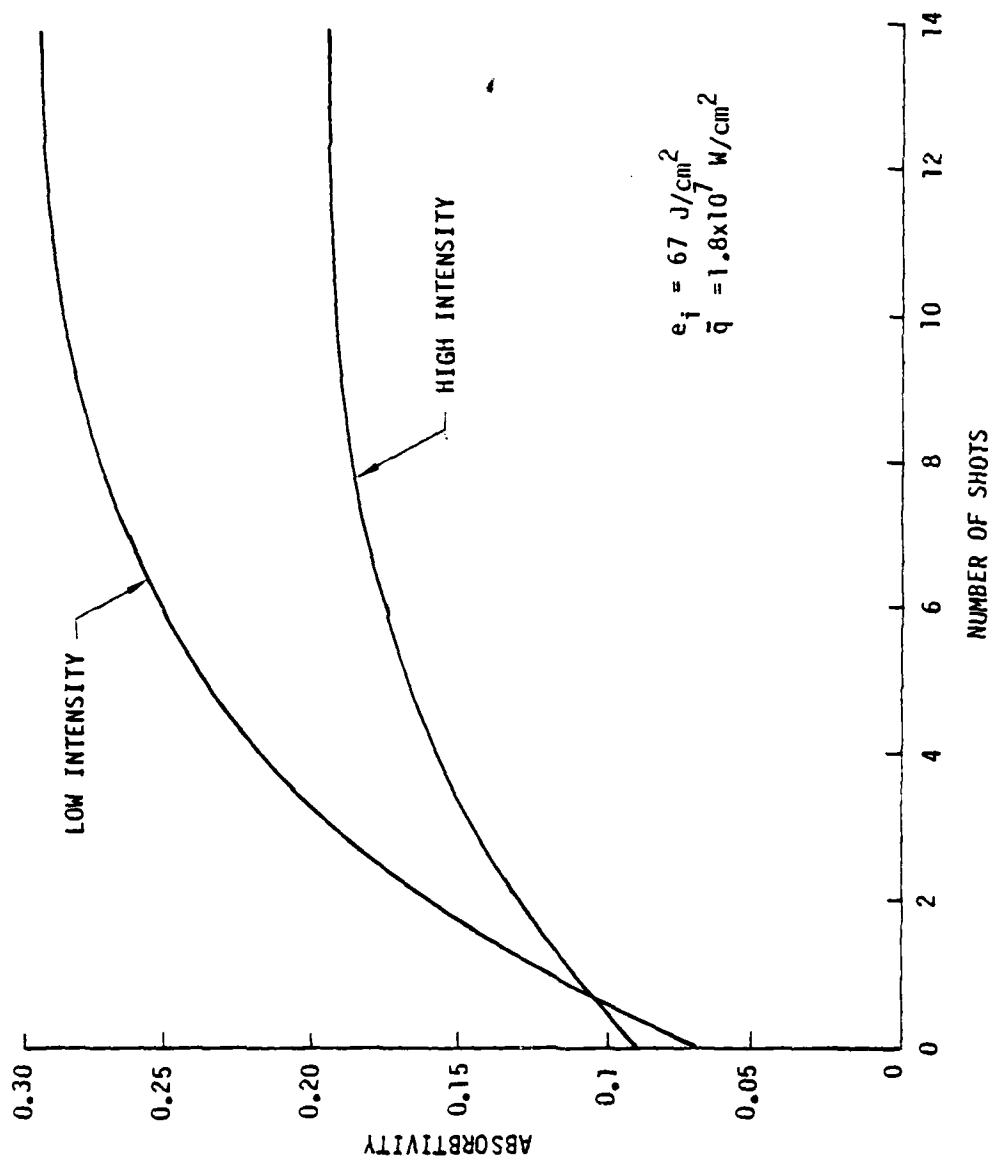
Figure 38. Variations of both the low intensity and high intensity absorptivity with the number of high intensity shots.

The intrinsic absorptivity α_I starts at an initial value of 0.07 and increases to 0.30 after a large number of pulses. These intrinsic and enhanced coupling absorptivities are plotted in Figure 38. It should be emphasized that these curves are valid under the given experimental conditions (pressure = 1 atm, 2024-T3 aluminum target material, λ = 3.8 μm, spot diameter = 2.1 cm, pulse length = 3.4 μs, and incident fluence = 67 J/cm^2). In general, the descriptions of the single and multiple-pulse coupling are dependent on all these parameters. However, at the present time, only a limited amount of data has been collected.

As noted earlier, because of the high intrinsic absorptivity of the laser-roughened target in the absence of plasmas, it may be a good strategy to first deliver N_0 high intensity pulses followed by an additional N_2 low intensity (sub-threshold) pulses. These N_2 low intensity pulses would have an incident irradiance and fluence below the plasma ignition threshold value. Under these conditions, the total absorbed fluence is

$$e_{AT} = e_{PT} \, (N_0) + e_L \, N_2 \, \alpha_I \, (N_0) \tag{19}$$

where e_{PT} and α_I are defined by Equations 15 and 18, respectively. In Equation 19 e_L is the fluence incident on the target during each of the N_2 low intensity pulses.

The results of evaluating Equation 19 are shown in Figure 39 for values of N_0 = 3, 5, and 11 and for e_L = 20 J/cm^2. In this case, the total number of delivered pulses is the sum $N_0 + N_2$. The results of Figure 39 do not show the advantages of combined low and high intensity pulses to maximum advantage. Under certain conditions, depending on the plasma ignition

76
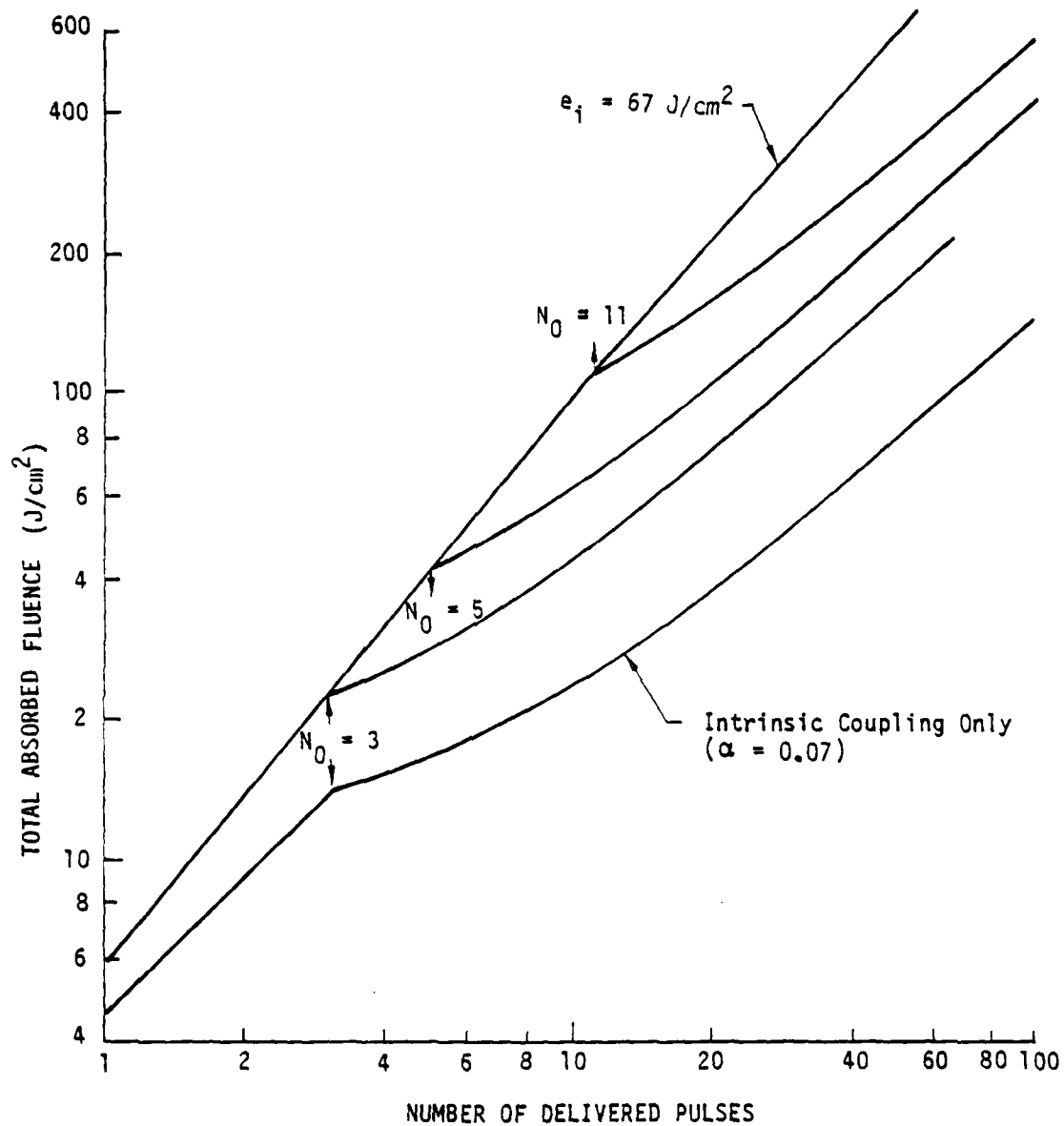
Figure 39. Total absorbed fluence vs the number of delivered pulses. The incident fluence is $e_i (= 67 \text{ J/cm}^2)$ for N_0 pulses and then drops to 20 J/cm^2.

77

threshold, reducing the incident laser intensity leads to an increase in the average absorbed power above that obtained with high intensity pulses only. Although the total absorbed fluence increases at a lower rate when the fluence is reduced to only 0.3 times its high intensity value, the actual efficiency of energy delivery can increase. Figure 40 shows the ratio β of total absorbed fluence (see Equation 14) divided by the total incident fluence for this situation with both high and low intensity pulses. The total incident fluence is the sum of e_{iT} (from Equation 16) and the incident fluence contributed by all the N_2 low intensity pulses. The total incident fluence is thus,

$$e_{iT} = 67 \ N_o + e_L \ N_2 \qquad (20)$$

Figure 40 clearly indicates that the efficiency with which a target can be heated can be increased if enough high intensity pulses are first used to roughen the target surface. In the case shown by Figure 40, 3 pulses are too few while 11 high intensity pulses yield a higher energy transfer efficiency than with only enhanced coupling.

This analysis is to minimize the total incident laser power for a fixed (or required) level of absorbed fluence. With the level of understanding that we now have of the DF multiple-pulse effect, this complete optimization problem cannot be undertaken. This occurs because both single and multiple-pulsed coupling are intensity, spot size, pulse length, pressure, and material dependent. Determining the number of high intensity pulses N_o is required to minimize the total incident fluence with the constraint that a required (fixed) level of absorbed fluence e_{AT} be reached. From Equation 19 one finds

78
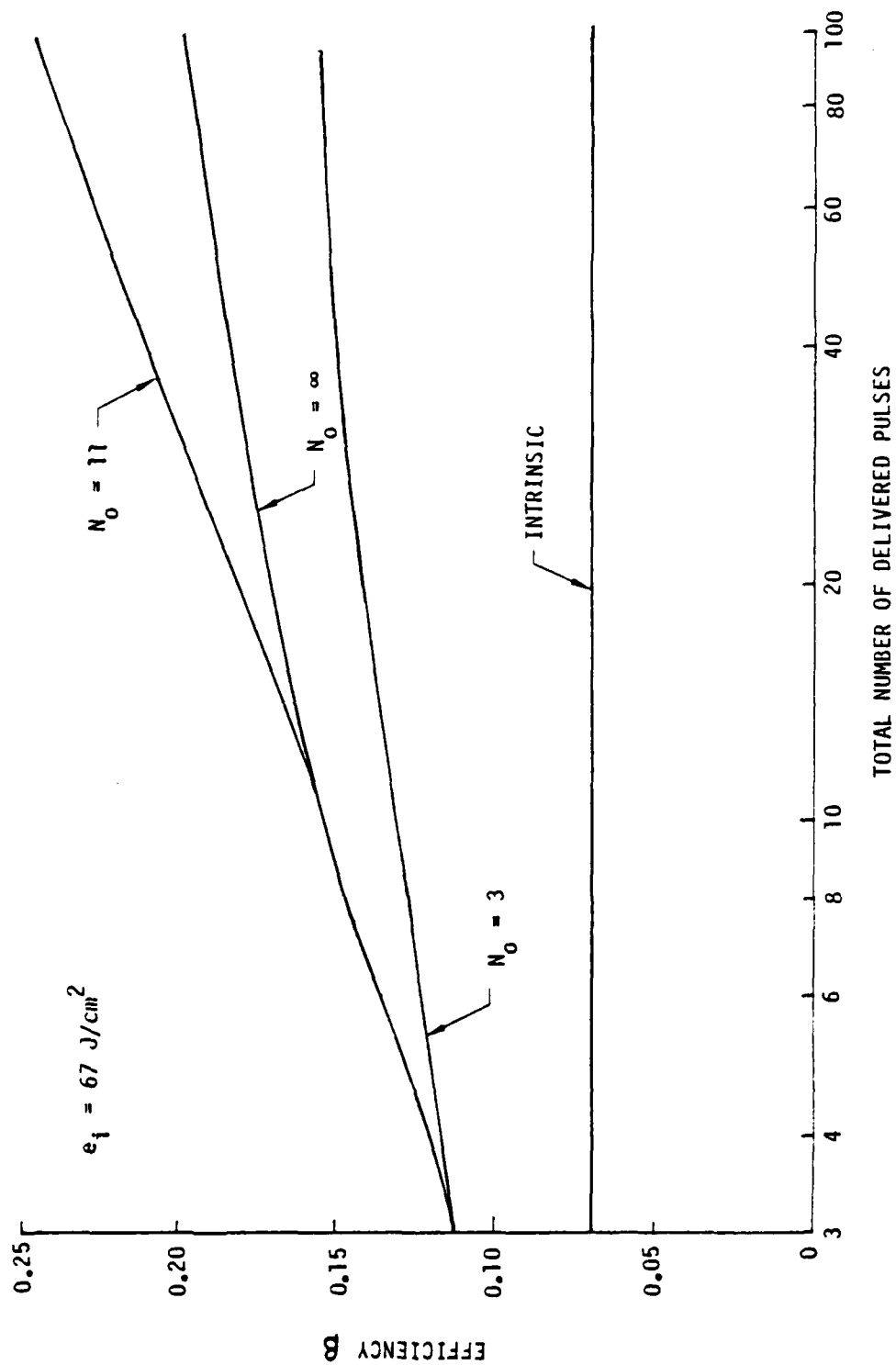
Figure 40. Efficiency of energy delivery as dependent on the total number of delivered pulses. After N_0 pulses, the incident fluence reduces to 20 J/cm^2.

$$e_L \ N_2 = \frac{e_{AT} - e_{PT}(N_0)}{\alpha_I \ (N_0)} \qquad (21)$$

If Equation 21 is then substituted into Equation 20 the total incident fluence becomes

$$e_{IT} = 67 \ N_0 + \frac{e_{AT} - e_{PT}(N_0)}{\alpha_I \ (N_0)} \qquad (22)$$

Since both the fluence $e_{PT}(N_0)$ absorbed during the N_0 pulses that produce plasma and the intrinsic-coupling fluence are defined functions of N_0, Equation 22 can be differentiated to find the optimum operating conditions. This differentiation is aided by noting that Equation 15 can be rewritten as:

$$e_{PT} = 13 \ N - 7 \left[\frac{1-\exp(-\frac{N}{4})}{1-\exp(-\frac{1}{4})} \right] \qquad (23)$$

Differentiating Equation 22 and setting it equal to zero yields a curve of the number of high intensity pulses that minimize the total incident fluence under the constraint that a required fluence is absorbed on the target. The results of this operation are shown in Figure 41 where, for example, in order to absorb 215 J/cm^2 one should utilize 7 high intensity shots followed by the delivery of 580 J/cm^2 of sub-threshold pulses. The low intensity pulses need to be delivered where the only constraint is that the product $e_L N_2$ is fixed. In these cases, for example, the peak incident irradiance must be reduced below the plasma threshold value. This could be accomplished, for example, by stretching the pulse length by a factor of 2 to 5 and keeping
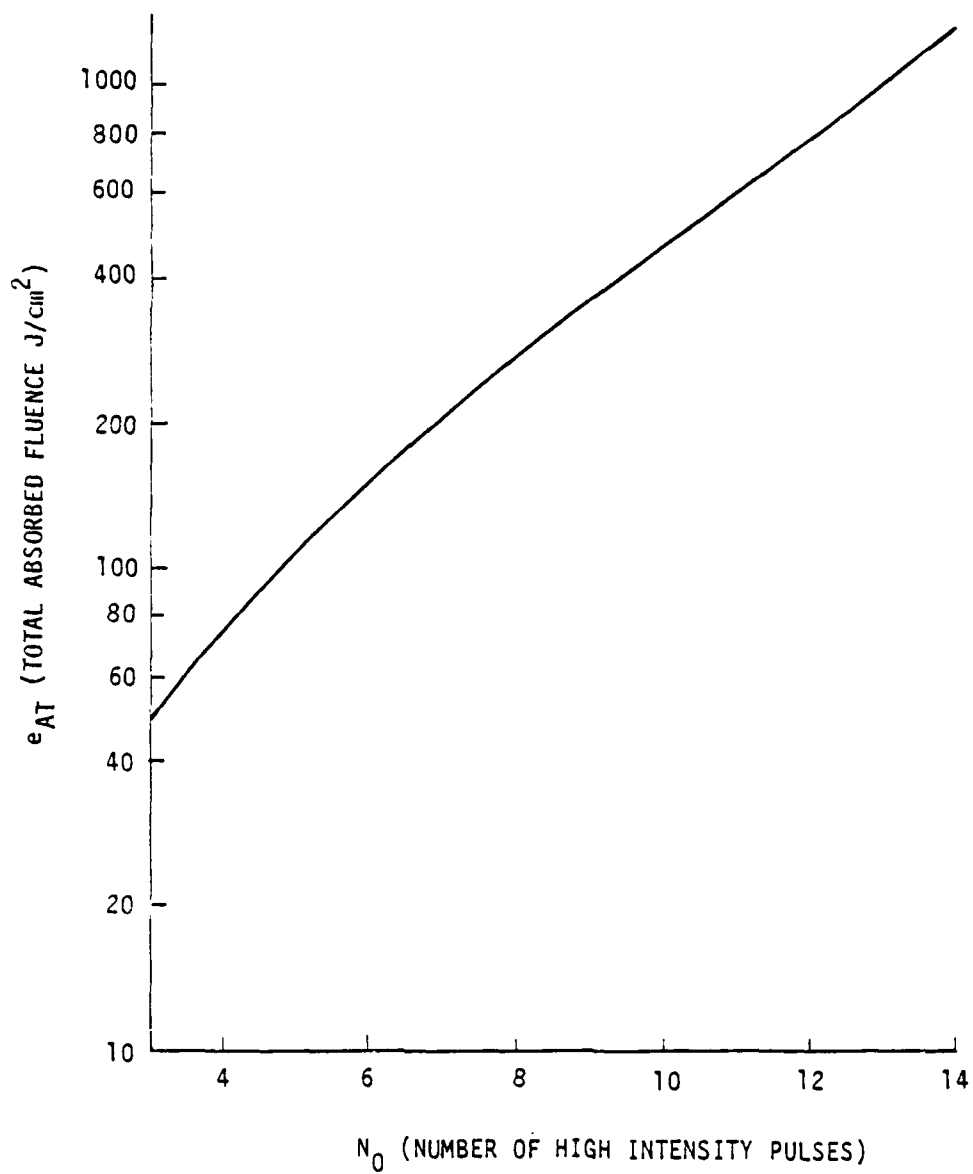
Figure 41. Number of high intensity pulses in order to absorb total fluence e_T for a minimum incident fluence.

the irradiance per pulse relatively high. The resulting division of fluence
between low and high intensity pulses is shown in Figure 42. The analytically-
determined optimum operating conditions shown in Figures 41 and 42 result from
the minimum of curves of incident fluence as a function of N_0 for fixed e_{AT}
as seen in Figure 43. It can be seen that, as long as enough high irradiance
pulses have been utilized, that the total incident fluence is nearly in-
sensitive to the pulse number N_0.

Figure 44 compares the total incident fluence required for pulsed
coupling under several conditions. The upper two curves assume that the
plasma ignition threshold condition is not met and that only intrinsic
coupling occurs. For aluminum surfaces the corresponding absorptivities
are 0.03 and 0.07, respectively for CO_2 and DF wavelengths. As pointed out
previously, when the incident irradiance is large enough, DF radiation leads
to the multiple-pulse effect. Using the data of Figure 31 and the analytical
approximations already described, the curve labeled enhanced multiple-pulse DF
coupling is obtained. At large required fluence, the multiple pulse effect
thus gains greater than a factor-of-two saving in total energy if the total
coupling were limited to a simple summation of single pulses.

The lowest curve in Figure 44 illustrates the potential savings in total
incident energy if the strategy of combining high and low intensity pulses
is utilized. It should be pointed out that all the multiple-pulse effects
optimization models described so far have been based on data acquired at a
single intensity, pulse length, and spot size. As described earlier, all the
multiple-pulse parameters are dependent on these variables as well as the
air pressure, target material, etc. Accordingly, the calculations are pre-
sented only to demonstrate potential advantages and optimizations that one

82
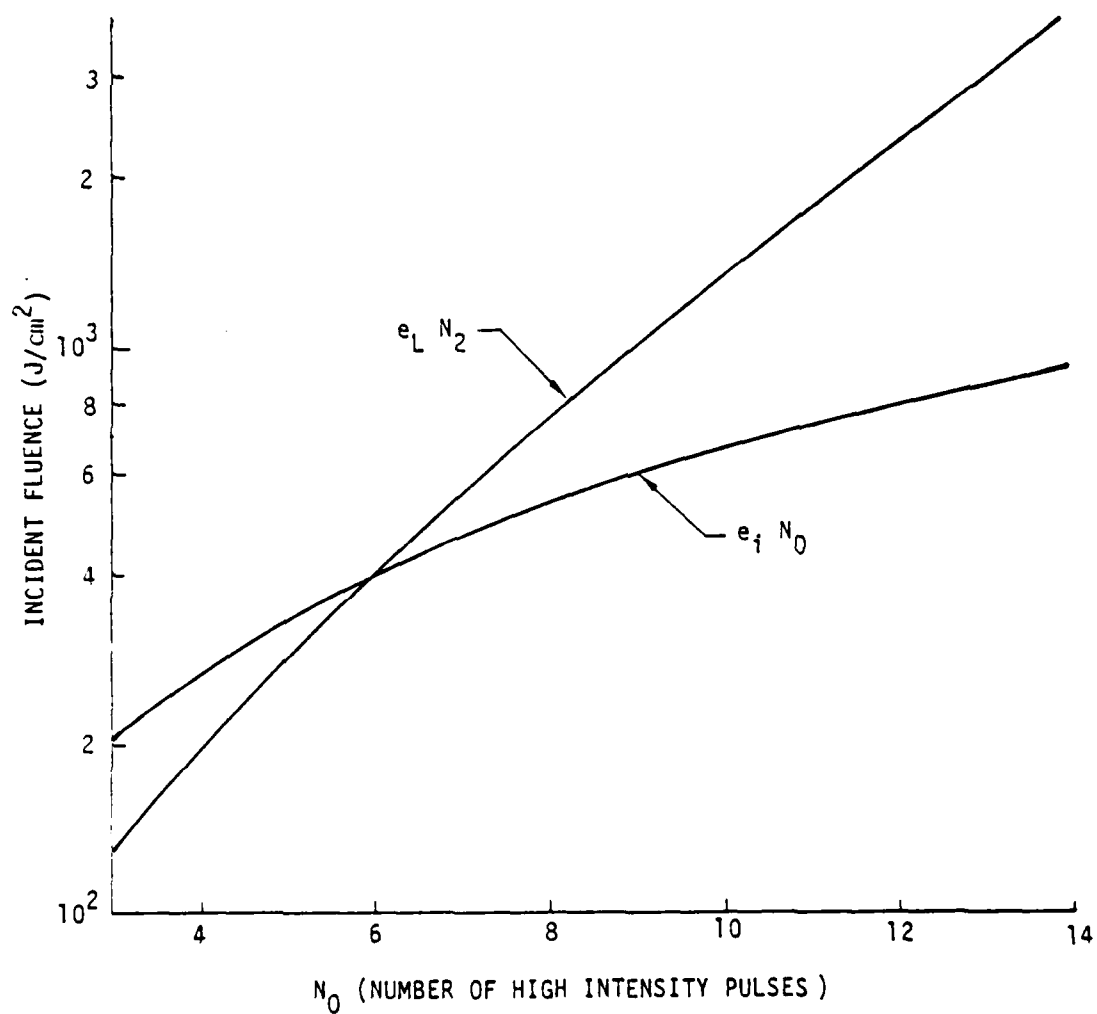
Figure 42. Relationship between incident high and low intensity fluences necessary to minimize the total incident fluence.
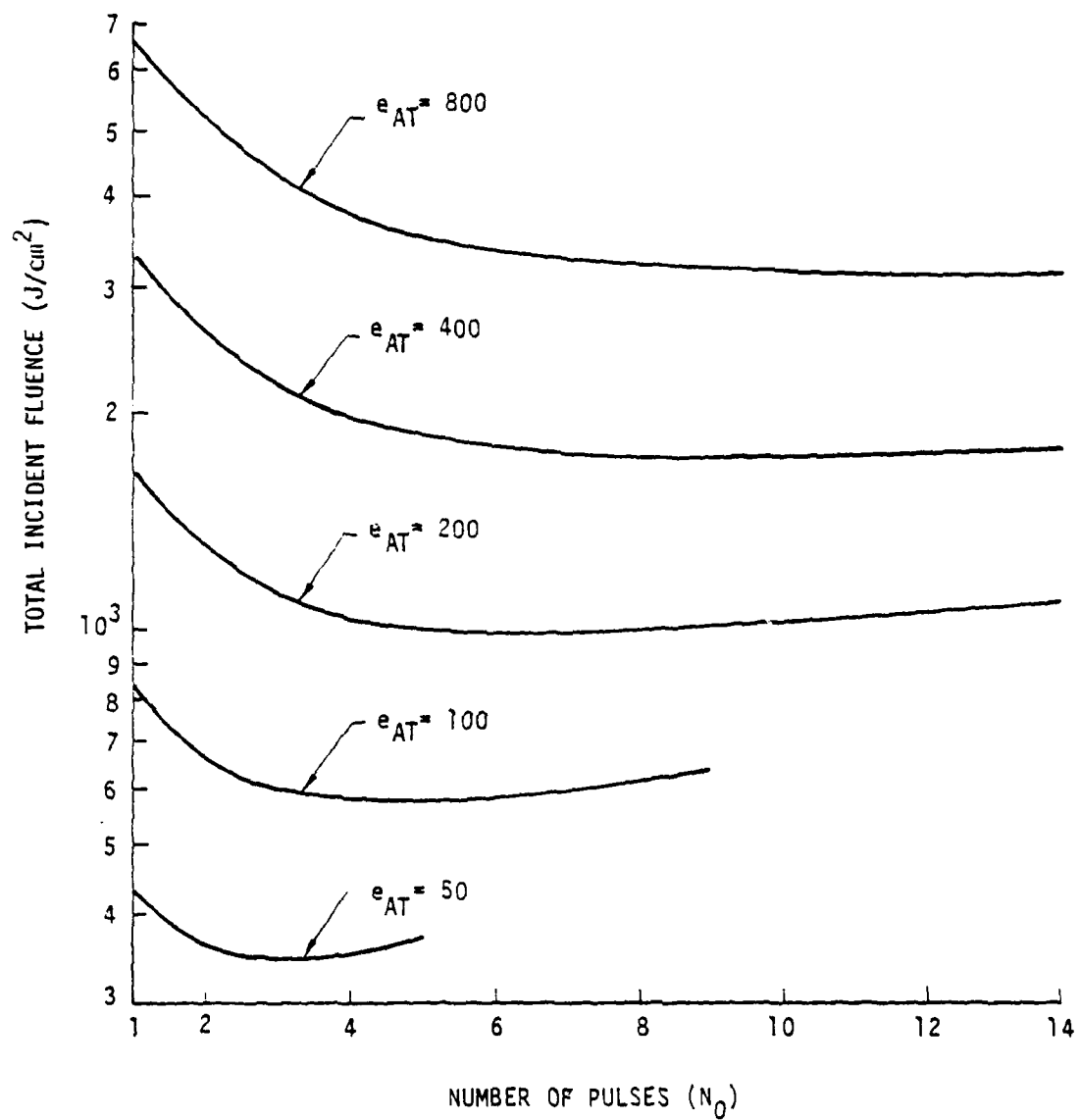
Figure 43. Total incident fluence required for fixed values of absorbed fluence as a function of the number N_0 of high intensity pulses.

84
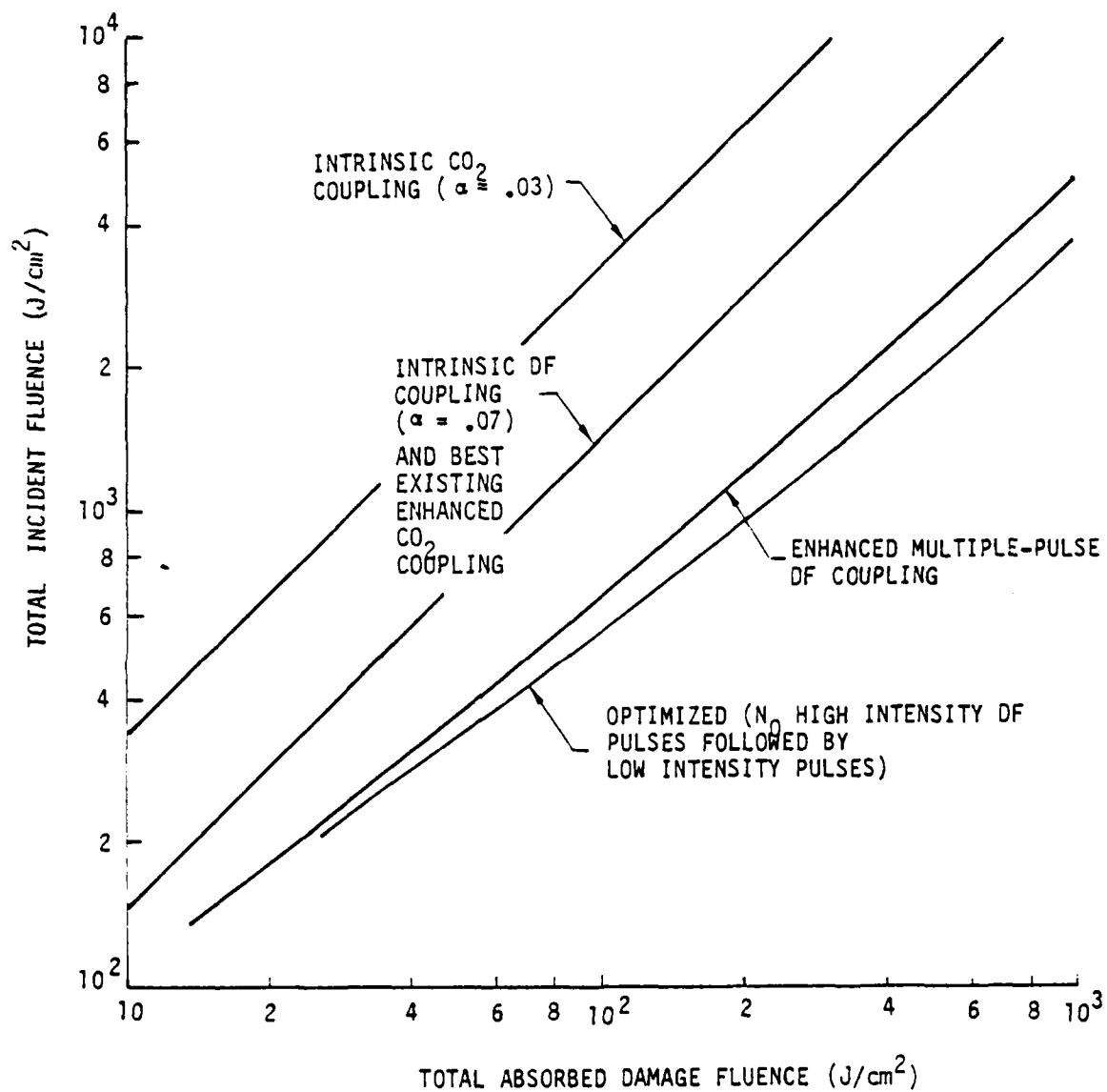
Figure 44. Total incident fluence required to obtain a given absorbed fluence.

85

would utilize when the necessary data base is available. It is possible that a larger total laser energy saving is possible when a more completely optimized multiple-pulse scenario is considered.

V. SINGLE-PULSE OPTIMIZATION WITH
DIFFERENT WAVELENGTHS AND PULSE LENGTHS

As noted earlier, enhanced coupling of pulsed lasers is dependent on intensity, pulse length, and spot size. For single pulse coupling this description is well developed for CO_2 lasers and the first data have now been obtained at DF wavelengths. On the other hand, the multiple pulse DF coupling effect discussed previously is not considered at all in this section.

The data that have become available from repeated and single pulse CO_2 and DF laser effects experiments can be represented by a number of analytical functions. There is considerable scatter in the data in many cases and some parameters have not been explored over much of their ranges. When particular functional forms are utilized to describe the phenomena, it must be noted that extrapolation of these beyond the regions with available data should be treated with caution. In particular, the results of this section should not be extended to pulse lengths much shorter than 3.0 microseconds or pulse intensities greater than 10^8 watts/cm^2.

With these qualifications in mind the approach that will be taken here is to describe the enhanced coupling coefficient for single pulses by

$$\alpha = \alpha_0 \ f(\hat{\tau}) \ \exp(-q/q_*) \qquad (24)$$

where α_0 is the value at zero incident fluence extrapolated linearly from data above plasma threshold, and $\alpha_0 = 0.23$ at $\lambda = 10.6$ μm, and $\alpha_0 = 0.40$ at $\lambda = 3.8$ μm. Equation 24 is not the only analytical function that can represent the available experiments. Future work is needed to either verify of modify this format since there are important systems applications considerations which result. The single-pulse DF experiments reported in Section 3, however, are consistent with a total coupled fluence that decreases as the

87

incident irradiance becomes large. The function $f(\hat{\tau})$ describes the decrease with pulse length of the plasma coupling coefficient and is given by

$$f(\hat{\tau})\bigg|_{\hat{\tau}<1} = \frac{2}{\hat{\tau}} \ln(1 + \frac{\hat{\tau}}{2})$$

$$f(\hat{\tau})\bigg|_{\tau>1} = \frac{0.81}{\hat{\tau}} (2.4-1.4/\sqrt{\hat{\tau}}) \tag{25}$$

The parameter $\hat{\tau} = ct_p/r$ describes, in a qualitative way, the cooling effect of hydrodynamic expansion in reducing plasma temperature. In the enhanced coupling regime, energy transfer to the target surface is dominated by UV radiation. Since the plasma radiation intensity is strongly dependent on the temperature, any cooling is important. In the definition of $\hat{\tau}$, the plasma sound speed $c = 6.6 \times 10^5$ cm/sec, t_p is the laser pulse length, and r is laser beam radius.

The analytical model of Equation 24 agrees with CO_2 coupling experiments accomplished both at AVCO and the MIRADCOM CCEBL laser. The intensity parameter q_* in Equation 24 is given by

$$q_* = 10 \left(\frac{10.6}{\lambda}\right)^{1/2} \frac{1}{r^{1/4}} \text{ MW/cm}^2 \tag{26}$$

The format of Equation 24 was inferred from CO_2 and DF experimental results and with modeling results given by Boni (Ref. 5).

---

5. A.A. Boni and F.Y. Su (SAI), and P.D. Thomas and H.M. Musal (Lockheed), Theoretical Study of Laser-Target Interactions, SAI 77-567LJ, 1977.

Although the coupling coefficient itself is maximum both for small q and t_p, this is not a satisfactory operating situation since the fluence delivered is

$$e = q \, t_p \; J/cm^2 \qquad (27)$$

Since one must deliver a finite fluence per pulse in order to damage real targets one must consider realistic irradiances and pulse lengths. Equation 27 shows that there is a maximum fluence that can be delivered to a target at a fixed pulse length and spot size. This maximum fluence e_{max} is (at λ = 10.6 μm)

$$e_{max} = 0.085 \, t_p \, q_* \, f(\hat{\tau}) \; J/cm^2 \qquad (28)$$

At 3.8 μm the numerical coefficient in Equation 28 is approximately a factor of 1.7 times larger. For equal pulse lengths and spot sizes one notes from Equation 28 that a pulsed laser at 3.8 μm can couple 2.9 times as much fluence to reflective targets as does one operating at 10.6 μm. It should also be noted that a 10.6 μm laser operating at t_p = 15 μs can never couple more than 5.8 J/cm^2. This occurs because of the LSC-LSD transition. The maximization calculation gives this when $\hat{\tau}$ = 1 and q = q_* using Equations 24, 25, 26, and 28.

To look at coupling as dependent on wavelength, the required laser incident energy E is compared with pulse length (E = πr_b^2 x q t_p). Figure 45 shows contours of constant absorbed fluence at a spot diameter of 2 cm for a wavelength of 10.6 μm. Similar contour plots can be generated for any wavelength and laser spot size based on these equations. As noted previously, these curves show that a given absorbed fluence can either be obtained at
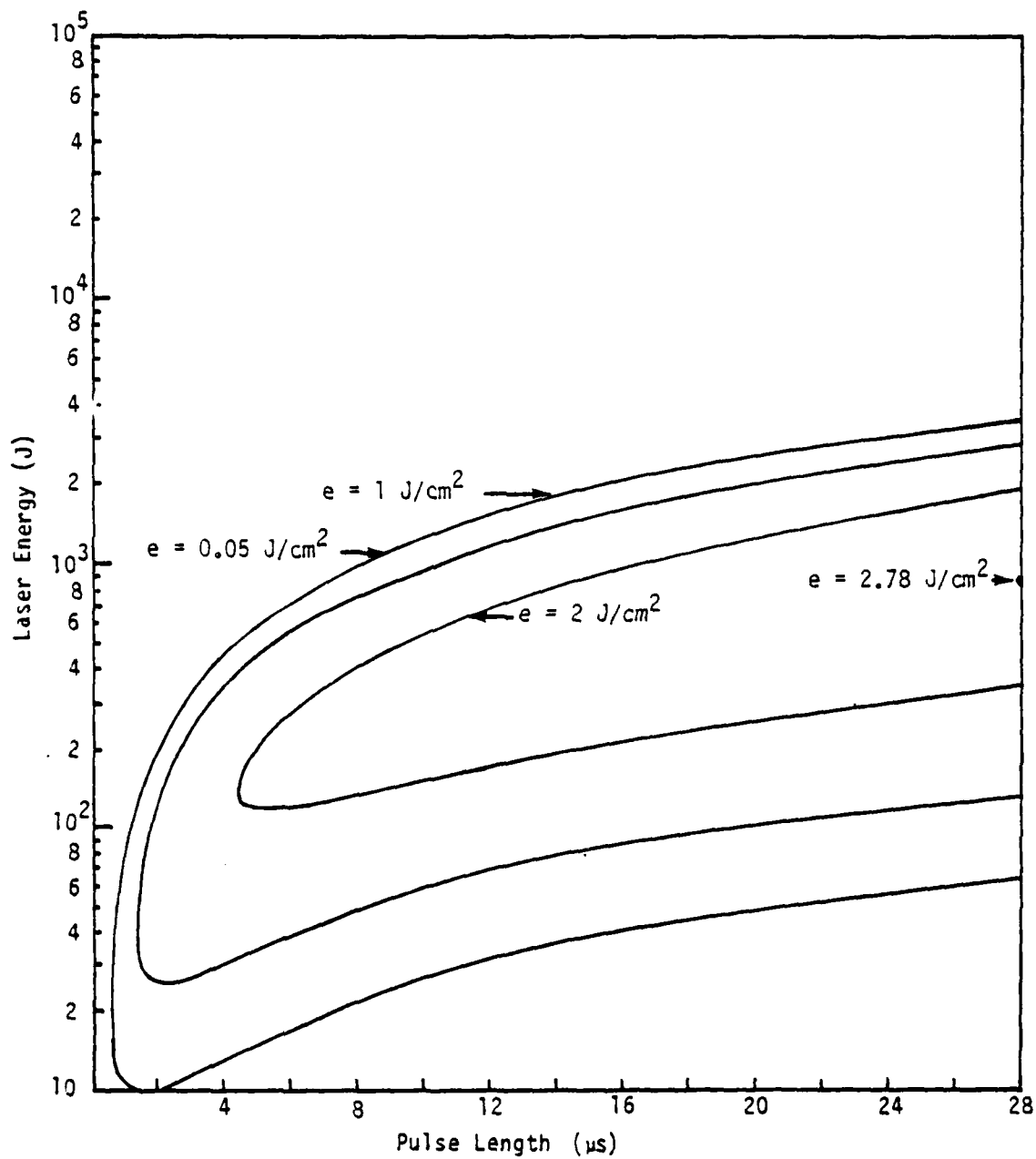
Figure 45. Contours of absorbed fluence as dependent on laser energy and pulse length.. $D_S = 2$ cm, $\lambda = 10.6$ μm.

low or high irradiance. In addition, one notes that for a given pulse length there is always a maximum fluence that can be absorbed. Thus, from Figure 43 (λ = 10.6 μm) for t_p = 4.5 μs, e_{max} = 2 J/cm^2.

At low irradiances, where low absorbed fluence are obtained, little wavelength dependence occurs. When relatively high fluences are required, however, one obtains a large advantage (in reduced laser energy requirement) in operating at shorter wavelengths. This potential importance of high absorbed fluences per pulse can be determined by taking a hypothetical but realistic damage model. Assume that the laser weapon under consideration operates at 50 Hz and must commit significant thermomechanical damage in 1 s. If this is the case, one can determine absorbed fluence requirements (per pulse) in order to damage a given metallic plate.

For aluminum alloy, one obtains the required single pulse absorbed fluence e for a fixed number of pulses of 50 to be

$$e = 19.4 \text{ h } J/cm^2 \tag{29}$$

where h is the target thickness in cm. Thus, for h = 0.18 cm, e = 4.3 J/cm^2.

It should be reemphasized that the results of this section do not take into account the very important multiple-pulse effect described in Section 4.1. Thus, while CO_2 results described here are realistic, the possible laser energy advantages using a DF laser will be considerably greater than discussed here.

The results given here are useful in determining laser energy requirements for certain combinations of pulse length and spot size. It is also interesting

to determine the best conditions of spot size and pulse length which minimize laser energy requirements in order to obtain a given absorbed fluence. A minimization of total engagement time is not addressed here.

From Equation 24 and from $E = \pi r_b^2 \, t_p \, q$ one can write

$$e = a \, x \, e^{-x} \, \hat{\tau} \, f \, r^{3/4} \ \text{J/cm}^2 \tag{30a}$$

$$E = b \, x \, \hat{\tau} \, r^{11/4} \ \text{J} \tag{30b}$$

where

$$x = q/q_*$$

$$b = 10 \, \pi/c \ \sqrt{\frac{10.6}{\lambda}}$$

$$a = \frac{\alpha_0 b}{\pi} \tag{31}$$

Substituting Equation 30a into Equation 30b yields

$$\frac{E}{e^{11/3}} = \pi \alpha_0^{-11/3} \left(\frac{c}{10}\right)^{8/3} \left(\frac{\lambda}{10.6}\right)^{4/3} \left[x^{-8/3} \, e^{(11/3)x}\right] \hat{\tau}^{-8/3} \, f^{-11/3} \tag{32}$$

It is evident that the functions of x and τ in Equation 32 minimize E for specific values of x and $\hat{\tau}$. Performing the required differentiations yields

$$\hat{\tau}_{opt} = 2.73$$

$$x = 8/11 \tag{33}$$

Substituting Equation 33 yields the minimum possible laser energy in order to obtain the absorbed fluence e.

$$E_{min} = 39.6 \times \pi\alpha_0^{-11/3} \left(\frac{c}{10}\right)^{8/3} \left(\frac{\lambda}{10.6}\right)^{4/3} e^{11/3} \text{ J} \qquad (34)$$

From Equation 34 one observes that a 3.8 μm wavelength laser requires much less energy to do a given level of damage (fixed e) than a 10.6 μm laser. It should be recalled, of course, that this result is only valid when the conditions of Equation 33 are met. This leads to

$$r(opt) = 2.97 \left(\frac{10\alpha_0}{c}\right)^{-4/3} \left(\frac{\lambda}{10.6}\right)^{2/3} e^{4/3} \text{ cm}$$

$$t_p(opt) = 5.46 \text{ r μs} \qquad (35)$$

It should be noted that the required minimum laser energy to obtain a given absorbed fluence varies as the (11/3) power of e. Thus, to double e the incident laser energy must always increase by at least a factor of 12.7 (the spot size and pulse length each increasing by a factor of 2.5).

The above results and comparison with experiments at both 10.6 and 3.8 μm are shown in Figure 46. In all cases it can be seen that the actual laser energy required to obtain a given coupled fluence is greater than the minimums indicated by the dark lines. This occurs because the pulse width and spot size in the experiments were not chosen in the "optimum" way indicated by Equation 35. The above optimization procedure specifically did not consider constraints imposed by laser device performance or by limitations imposed by rep-pulsed propagation. The intent of this section was to give examples of the considerations which must be considered a laser weapon application. The DF optimization condition cannot be extrapolated far beyond the set of existing data. More data is needed to make believable laser systems comparisons.
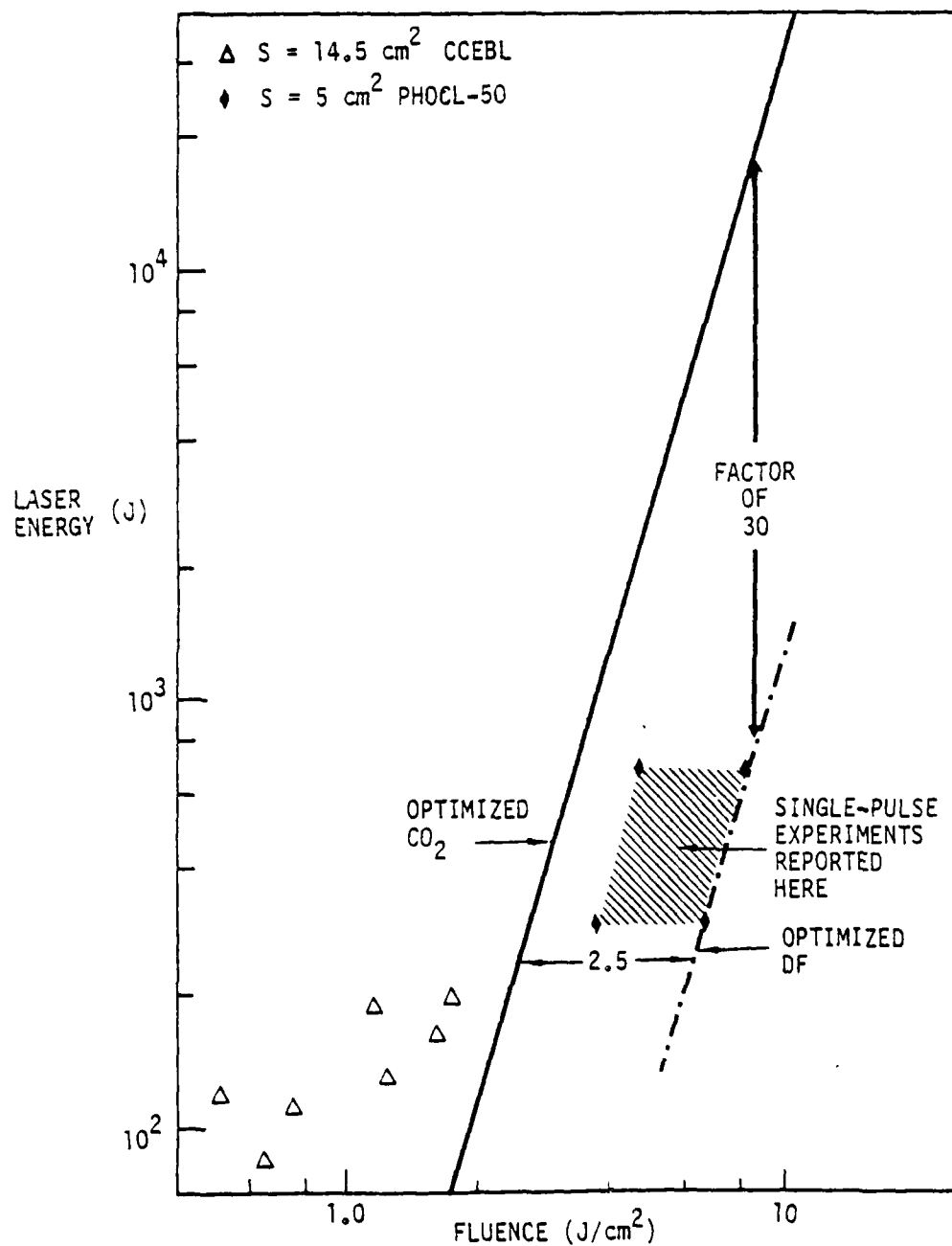
Figure 46. Coupled fluence for 10.6 and 3.8 μm and comparison with optimized condition.

VI. CONCLUSIONS

Pulsed DF radiation has shown unusual capabilities to damage metallic targets, for both single pulse and multiple-pulse interactions.

When examining single-pulse coupling phenomena it has been shown (see Section V) that much higher coupled fluences can be obtained at DF wavelength compared to CO_2 wavelength. This occurs because of the longer absorption length in the laser-produced plasma which leads to a more uniform heating of the plasma. The resulting higher temperature leads to greater UV radiation which, in turn, leads to larger amounts of coupled energy to the target surface. Under identical plasma electron densities, the absorption length at 10.6 μm is only one-eighth that with DF lasers. This difference means that a higher transition irradiance must be reached for DF laser beams before the absorption waves reach supersonic velocities. Under these conditions, a smaller fraction of the incident DF laser beam energy is transferred to the kinetic energy of the plasma wave and more contributes to increasing its temperature.

Section V shows, from a single-pulse coupling basis only, that potentially very large energy reductions can be realized if a DF instead of a CO_2 laser is used. This occurs because of the nonlinear plasma enhanced coupling coefficient. This absorptivity depends on irradiance, pulse length, and spot size. Thus when computing the deliverable fluence for a given sized laser (energy), a much larger fluence is possible with a DF laser. The results show that the required laser energy must increase as the (11/3) power of the absorbed fluence per pulse.

95

In a realistic scenario, there are always a large number of required pulses to cause thermal damage to a real target. Thus, the multiple-pulse results of Section IV are particularly of interest. As an example, the per pulse coupled fluence to an aluminum target has been measured to more than double after about 10 high intensity pulses have been accumulated on the same spot. The fluence was shown to increase from 6 to more than 13 J/cm^2. This factor of two is extremely important because of the scaling mentioned above. Thus to increase the coupled fluence by such a factor of two requires a laser with about 12 times as much energy if only single-pulse coupling were applicable. This multiple-pulse effect has never been observed at CO_2 wavelength.

The multiple-pulse effect results from a greatly-increased roughness of the target surface. Measurements described in Section IV show that the intrinsic (below plasma threshold) absorptivity of this rough surface can reach at least 30%. With this factor in mind, an analysis (see Section IV) shows that the overall required incident laser energy can be reduced if a sequence of both high and low intensity pulses are used in order to damage a given target. Thus, for example, 10 high intensity pulses serve to roughen the surface while a sequence of subthreshold pulses can serve to supply most of the required energy in order to melt the target. In this case, the sub-threshold pulses can be absorbed with about 30% efficiency.

The work described herein is incomplete since only a limited range of spot sizes, pulse lengths, and irradiances have been examined. A wider range of parameters should be investigated to assess the potential application of pulsed DF lasers to realistic scenarios. This in turn should lead to the development of equations which more accurately model both single and multiple-pulse phenomena.

96

APPENDIX

DIELECTRIC TARGET RESPONSE

Two sets of experiments were performed with dielectric targets. In the initial set of experiments only fiberglass targets, some previously unexposed, and some others previously exposed to a repetitively pulsed CO_2 laser (Driver at Avco Everett Research Laboratories), were used to compare specific mass removal for those two different initial conditions. Both specific impulse and specific mass loss were measured.

The fiberglass material used in these tests was Cordopreg, supplied by the U. S. Army Materials Research and Technology Center, Watertown, MA. This material was made into large two-ply sheets from specially prepared separate fiberglass/resin plies.

Tests with this material using an oven showed that even at low temperatures volatile components could be removed quite quickly. A two-ply sample lost 52 mg mass in the 28 s it took for it to reach 300°C in a preheated 300°C oven, which represents 0.5% of the original mass. Actual mass losses during laser irradiation of a 4 cm^2 focal spot area resulted in a larger mass loss per unit area. A long term oven test (1 h at 300°) on a 10 x 10-cm Cordopreg sample produced a mass loss of 500 mg and also turned that sample color from yellow to black.

Preexposed Targets (Mass-Loss)

The preexposed Cordopreg samples to be tested had a relatively uniform black charred surface which covered a square about 6.5 cm on a side. The PHOCL-50 beam area of 2 x 2 cm was centered within the charred area. The specific mass loss of 10 KJ/g for preexposed targets was one-fourth that found for fresh specimens when the incident fluence was 60 J/cm^2.

97

Mass Loss and Impulse of Fresh Targets

A ballistic pendulum, shown in Figure A1, was built in order to determine the impulse of large targets. The Cordopreg targets were initially rinsed with methanol and left to dry before exposure to the laser beam. Following laser exposure, no further cleaning was done. Typically, these targets had a somewhat charred surface. These Cordopreg samples were found to be somewhat hygroscopic after exposure to the laser beam, i.e., their mass was changing by nearly 0.1% during the intervals between repeated mass measurements.

The ballistic pendulum was constructed to hold 10 x 10-cm sheet samples at its center. The moving element of the pendulum is an open structure of balsa-wood segments weighting 32.6 g and is hung from fine nylon monofilaments with an effective arm length of 43 cm. A precision photographic picket-fence graticule allowed the motion of the pendulum to be measured as a function of time because it chopped an HeNe laser beam. The detector output was recorded on a visicorder showing the oscillations for several cycles, and the time per cycle extrapolated to zero time allowed the impulse to be determined.

Spot sizes of 1 and 2 cm dia were used in these experiments. The single shot specific impulse obtained with fresh Cordopreg is shown versus incident fluence in Figure A2. For both the small and large spots, the maximum I/E is 5.5 dyne-sec J^{-1}. The impulse threshold, for both spot sizes, occurs at approximately 16 J/cm^2.

Similarly, the mass loss occurring in these single pulse experiments using the two different spot sizes are plotted versus incident fluence in Figure A3. The lowest specific mass loss for a spot size of 2 cm is $Q^* = 22$ KJ/g and occurs

PENDULUM SUPPORTS

LASER BEAM SPOT

PENDULUM

VISIBLE LASER BEAM DIRECTION

VISIBLE DETECTOR

PICKET FENCE RETICLE
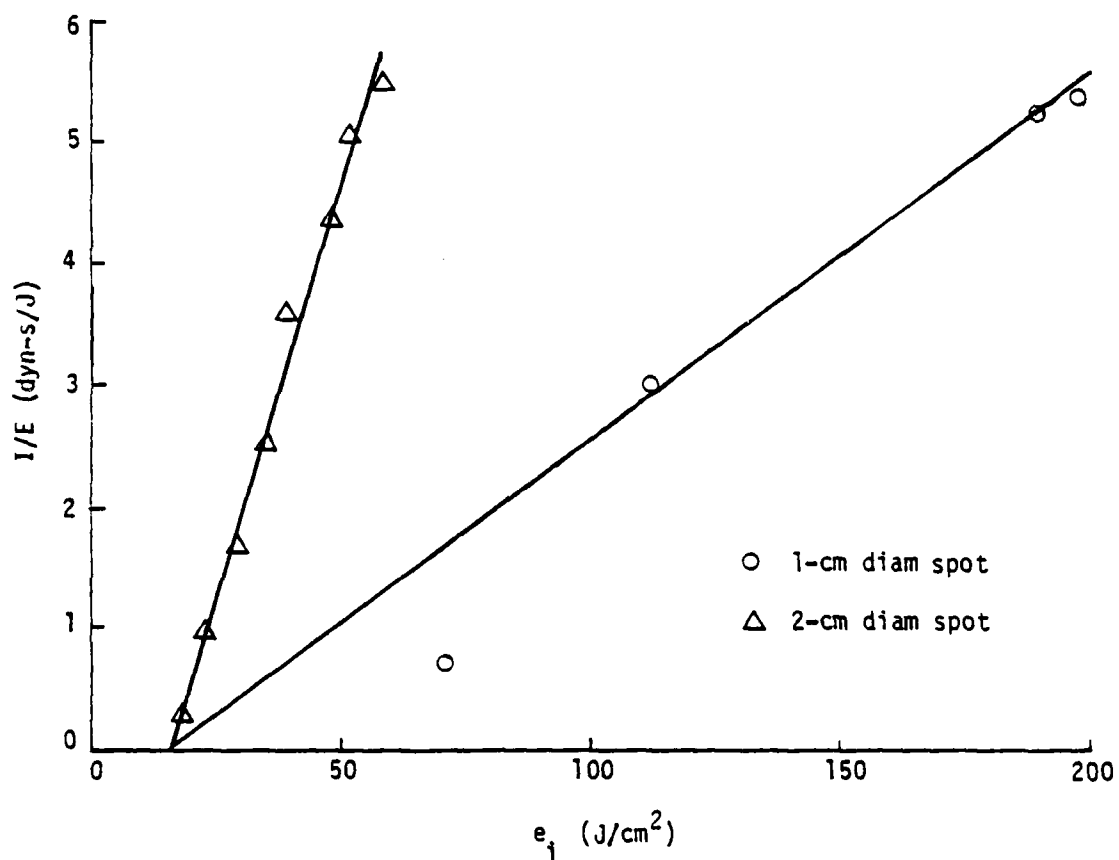
Figure A1. Ballistic pendulum.

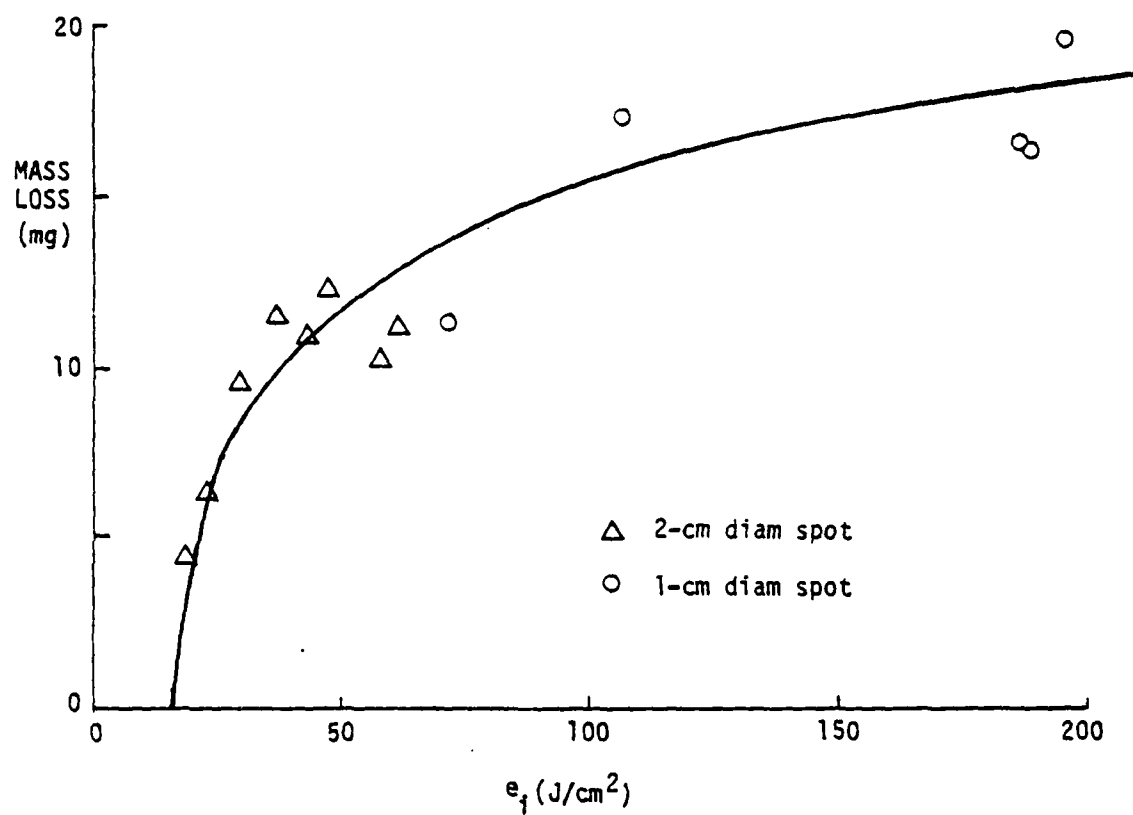Figure A2. Specific impulse data on previously unexposed Cordopreg versus
incident fluence.

Figure A3. Mass loss data on previously unexposed Cordopreg versus incident
fluence.

at an incident fluence of 35.6 J/cm^2. This specific mass loss is about half the value found for preexposed targets at a higher fluence.

Multiple-Pulse Response of Cordopreg Targets

The response of Cordopreg targets to a series of pulses was measured. Since PHOCL-50 can be fired only once every 5 min, this type experiment does not fully simulate a repetitively-pulsed laser firing at 50 Hz. This is particularly true of Cordopreg fiberglass targets because the effects of average heating do not occur.

Measurements of mass loss as a function of the number of pulses already incident on the Cordopreg surface required that the targets be removed from the ballistic pendulum after each shot, reweighed, and replaced in a manner which didn't affect their masses. Each target was weighed several times before any exposure and several times after each exposure to obtain a valid average weight. However, when these repeatedly exposed targets were weighed several times between two exposures, relatively large variations in mass were observed compared to that found with nonexposed targets. This indicates that once the outside gel coating is removed these targets become hygroscopic. These surfaces appear fuzzy after laser exposure which results in a large surface area to absorb water vapor.

Multiple pulse exposures of Cordopreg produced increases in I/E. The data obtained with two different spot sizes are shown in Figure A4. Mass loss measurements were made during these same experiments. However, no significant effect was seen in that during seven laser shots on the same spot. Mass loss for each of seven successive shots made with either the 1 cm or 2 cm diameter laser spots never varied far from the average of 0.01 g per shot.
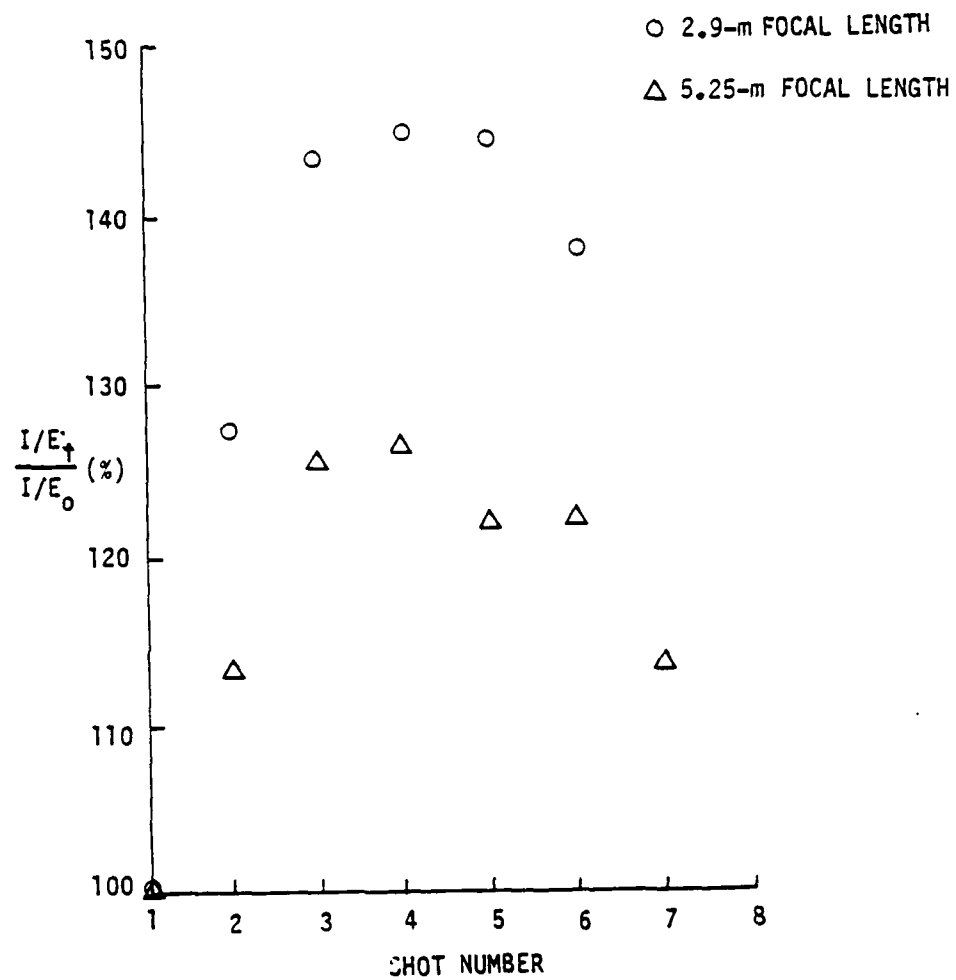
Figure A4. Specific impulse data for Cordopreg exposed to multiple pulses.

full-length pulse shapes are shown in the inset. Lines are given for the measured intrinsic coupling of 0.048 below threshold, and a constant e_a = 3.4 J/cm^2 above threshold. For comparison purposes, the full-pulse-width coupled fluence variation is seen for $\hat{\tau}$ = 2.4 and 4.2 in Figure 13. The $\hat{\tau}$ for this cutoff-pulse experiment would be 2.4.

These cutoff-pulse data appear to have an intrinsic coupling that is considerably lower than the 7% indicated by the data in Figures 12 and 13. The ignition threshold is at a higher fluence value for the cutoff pulse data, too, so there is a possible 40% discrepancy in the determination of fluence values between these two experimental setups. A sensitivity of these phenomena to modifications in the spatial profile details may also explain this difference. Above the plasma ignition threshold the constant 3.4 J/cm^2 value for abosrbed fluence corresponds reasonably well with the 4 J/cm^2 seen in Figure 13. Overall, the data for the shorter effective pulse width show the same behavior as the longer pulse data do.

DAT FILM